2019

Point Cloud Technology for Analysis of Existing Structures

Jacob Cano
University of Central Florida

POINT CLOUD TECHNOLOGY FOR ANALYSIS OF EXISTING STRUCTURES

by

JACOB ANTHONY CANO
B.S. Florida International University, 2015

A thesis submitted in partial fulfillment of the requirements
for the degree of Master of Science
in the Department of Civil, Environmental and Construction Engineering
in the College of Engineering and Computer Science
at the University of Central Florida
Orlando, Florida

Spring Term
2019

Major Professor: F. Necati Catbas

ABSTRACT

For this thesis, a study was completed on two different structures on the UCF Orlando campus through the use of both structural plans and point cloud technology. The results sought to understand the viability of point cloud technology as an accurate tool for the static and dynamic modal analysis of existing structures. For static analysis, a portion of the framing of Spectrum Stadium was rendered, modeled, analyzed and compared to a previous case study. The results emphasized how different users can render dissimilar member sizes and lengths due to human judgment on point cloud visuals. The study also found that structural plans cannot always be relied upon as the most accurate source for analysis as the new point cloud produced more accurate results than the structural plans when compared to the control model. For the pedestrian bridge, the structure was scanned, rendered and modeled for both static and dynamic modal analysis. The point cloud produced from scanning the bridge was modified twice in order to have three distinct point clouds with varying densities: fine, medium and coarse. These three cases were compared to structural plans in a static analysis. The fine point cloud produced the most accurate displacement results with an accuracy above 96%. The data sources were also compared to experimental data under dynamic modal analysis to discover how lessening the density of point clouds affect the accuracy of results. The analysis showed that point cloud technology can give you an accuracy of 88% and above for frequency while also producing MAC values exceeding 0.9 consistently. Also, changes in density were found to change the accuracy of results but the numeric values stayed within close proximity by not differing more than 10%. This thesis shines a light on the accuracy point cloud technology can ascertain and the potential it has within engineering.

I dedicate this thesis to my parents, Natalia Vergara and Luis Cano, and my loving girlfriend Natalie Varela.

ACKNOWLEDGMENTS

Firstly, I would like to share my infinite thanks to my thesis advisor and professor Dr. F. Necati Catbas, P.E. whose guidance throughout this extended process was vital to the completion of this work. I would also like to extend my thanks to the members of my thesis committee: Dr. Georgios Apostolakis, Dr. Ricardo Zaurin and Dr. Lori Walters. Their input, expertise and feedback helped me have a greater understanding for the subject matter within this thesis. My thanks are also extended to Rob Michlowitz for his essential input in point cloud registration. I would also like to express my gratitude to three of my fellow classmates: Paulo Dos Santos, Samantha Weiser and Pruthviraj Thakor for their invaluable assistance and friendship.

I want to thank my parents whom without their love and support none of this would have been possible. I am forever indebted to them for giving me a life surrounded by a belief in me and my ability to excel. I love you guys and I am blessed to have two loving parents. Lastly, I would like to thank my wonderful girlfriend Natalie Varela. Her love, support and patience were what ultimately motivated me to achieve this goal. I love you more than anything in this world and I thank you for always being by my side.

TABLE OF CONTENTS

LIST OF FIGURES

LIST OF TABLES

CHAPTER 1 – INTRODUCTION

In today's growing construction era, developing more efficient and effective products of high quality is paramount; therefore, there is a need for more modern technologies such as finite element analysis (FEA) software and three-dimensional laser scanning. These modern technologies play a big role in the applications of civil infrastructure design, maintenance, operation and as-built construction verification. Advancements in possible analysis alternatives, such as point cloud data collection, have become of great interest to engineering practice and research due to the potential this technology possesses.

1.1 Objectives

Structural plans are the standard source of data for FEA modeling within the realm of engineering. This report intends to evaluate the plausibility of point cloud technology as a tool that provides accurate results when analyzing existing structures. The static behavior of a section of a steel-reinforced football stadium and the static and dynamic properties of a pedestrian bridge, both located on the University of Central Florida (UCF) campus, will be studied. By using a 3D laser scanner, point cloud data will be obtained and stitched together to create a 3D image capable of being imported into an FEA program.

Moreover, the stadium results will be compared to a previous study that provides the structural plans and the point cloud data. To understand the accuracy point cloud technology can deliver, the new study will compare results found by different users, structural plans and actual on-site measurements. The bridge will also have a comparative analysis using the original

structural plans versus three levels of point cloud densities: Fine, Medium and Coarse. The results, consisting of displacements and reactions for static analysis and mode shapes, periods, frequencies and eigenvalues for dynamic modal analysis, will be determined through FEA software. The Modal Assurance Criterion (MAC) will also be utilized so as to compare the four data sources of the pedestrian bridge against actual experimental data gathered in the field. The results will give readers an indication of the ability point cloud technology has, whether it is feasible to use and how density affects results.

1.2 Scope

Using the data collected via the sources mentioned in Section 1.1, the respective computer models of each data source will be created in order to complete analyses by the FEA program. Several programs are needed to complete the project and are listed as follows: Autodesk Recap, Autodesk Inventor, AutoCAD, SAP2000 and MATLAB. Using the same structures when comparing two different sets of data sources allows for a fair comparison of results, both static and dynamic. The analysis of the stadium and bridge will be simplified by solely including their steel framing. The concrete footings for Spectrum Stadium are represented as pinned supports and the concrete abutments for the pedestrian bridge are represented as fixed supports.

1.3 Description of Scanned Structures

1.3.1 Spectrum Stadium

Spectrum Stadium is located at the northeast of the UCF campus alongside North Orion Boulevard. The stadium is a predominately steel structure capable of holding over 45,000 people. The stadium is mainly supported through a system of wide flanged beams and columns that is arranged around the entire structure. The purpose of this structure is to operate as the location of home games for the UCF football team. Refer to Figure 1.1 for a photo of Spectrum Stadium.

Figure 1.1: Spectrum Stadium on UCF campus
Source: UCF Facilities
http://ucfknights.com/ViewArticle.dbml?DB_OEM_ID=34100&ATCLID=211735275

1.3.2 Pedestrian Bridge

Parking Garage VI – H Pedestrian Bridge is located near the CFE Arena on Gemini Boulevard North on the UCF Campus. This pedestrian bridge is a steel truss bridge with a reinforced concrete deck. It is 177 feet long by 12 feet wide and comprised of three spans. The bridge mainly facilitates the movement of pedestrians and small utility vehicles. Essential steel components of this bridge are comprised of HSS and W-sections. Refer to Figure 1.2 for a photo of the pedestrian bridge.

Figure 1.2: Parking Garage VI – H Pedestrian Bridge on UCF campus

CHAPTER 2 – LITERATURE REVIEW

2.1 Point Cloud Technology

A point cloud is a set of data points in space. Point clouds are generally produced by 3D Light Detection and Ranging (LiDAR) scanners, which measure numerous points on the external surfaces of objects around them [1]. Each of these points in space provide an individual 3D coordinate by supplying their X, Y and Z position values. Point clouds can be used as a reference to recreate existing structures or insert additional models [2]. Attaching a point cloud into a compatible software allows it to be used as a guide for drawing, display changes or color stylization that can demonstrate different features of the structure [2].

There are several methods of point cloud data collection that can be utilized via the use of laser scanners: stationary 2D and 3D, phased-based, time of flight, mobile and airborne [3]. Point clouds have numerous purposes including creating 3D CAD models for manufactured parts, metrology, quality inspection, visualization, animation, rendering and mass customization application [4]. Having used a 3D laser scanner in this study, the pros and cons that accompany the tool becomes crucial before determining its appropriateness for a project. Once a user recognizes the capabilities and limitations of this powerful tool, an educated decision can be made regarding the suitability of the scanner. The following pros and cons are just some of the traits that come with using a LiDAR scanner:

Pros:

- Faster data capture times when compared to typical structural measuring techniques

- Effective data collection reducing the amount of on-site visits
- Unobtrusive data collection method, eliminating the need for hands-on or invasive techniques
- Highly precise and accurate measurements
- Leads to a lower transfer cost due to small number of resources for data acquisition thus leading to higher productivity
- Illustrates the structural space in 3D as opposed to the normal 2D display of measurements in structural plans

Cons:

- High initial investment
- Requirement of purchase and training of the new software to be used for the creation of point clouds
- High-end and sophisticated hardware for data processing
- Susceptible to technical errors that could delay projects

2.2 Leica Scanner

The device used for the pedestrian bridge scan was a Leica ScanStation P-Series 3D laser scanner. The scanner has impressive capabilities including being operated for a variety of uses such as capturing 3D geometry of civil infrastructure, 3D data integration for Building Information Modelling (BIM) and re-constructing crime scenes [5]. The instrument is able to scan at a rate of 1 million points per second and has the capability to capture surfaces from a distance up to 270 m away [5]. It is durable enough to function in temperatures ranging from -20°C to +50°C, compliant

with the IP54 ratings for dust and water resistance, demonstrates survey grade dual axis compensation and delivers low range noise [5]. The advantages of this system are its high speed, precision and range for challenging projects.

2.2.1 Basic Principle of Laser Scanning

The scanner works by emitting a light signal (laser) through a transmitter and receiving the return signal by a receiver [6]. Today, there are two typical scanner types used which are defined by the technique they use for their distance calculation [6]. The first scanner type is known as ‘Time of Flight’ which uses a distance calculating technique based on the time elapsed between the emission of the laser and the reception of the return signal [6]. The second scanner type is the ‘Phase-Based’ which calculates distance by comparing the phases of the output signal and the return signal [6]. Overall, time of flight scanners tend to scan slower than phase-based scanners but can scan farther while phased based scanners tend to scan faster but are limited in scanning range [7]. Figure 2.1 gives an illustration of the difference between the two techniques.

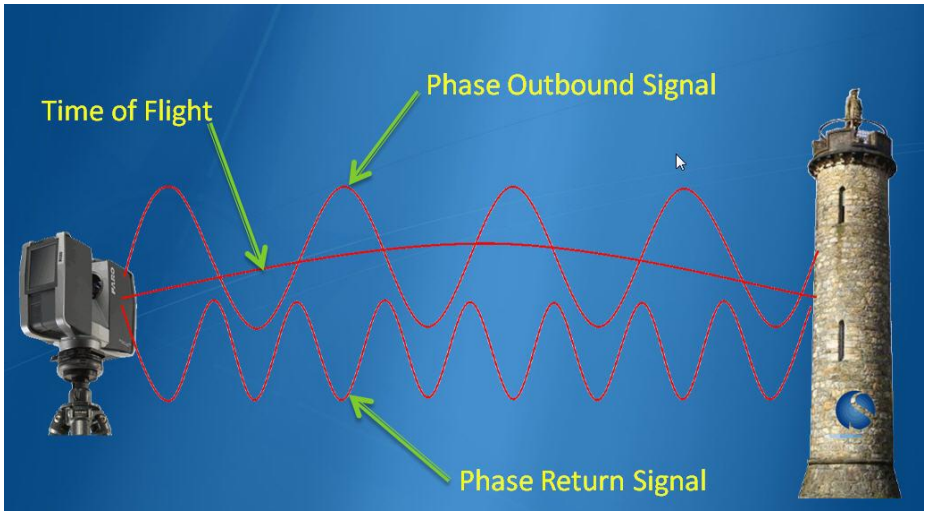

Figure 2.1: Scanner Distance Calculation Techniques: Time of Flight vs. Phased-Shift Based
Source: SurvTech Solutions
http://floridalaserscanning.com/3d-laser-scanning/how-does-laser-scanning-work/

Figure 2.2 shows a diagram of a typical laser scanner. The emitter is seated on the body while he body rotates around the axis vertically which also consists of a horizontally rotating mirror [6]. This mirror reflects the laser and directs it towards a detected surface point [6]. These movements occur at extremely high speed which then lead to accelerated data acquisition [6]. This ability entices the use of these tools since they can collect both millions of data points in seconds while also providing powerful accuracy.

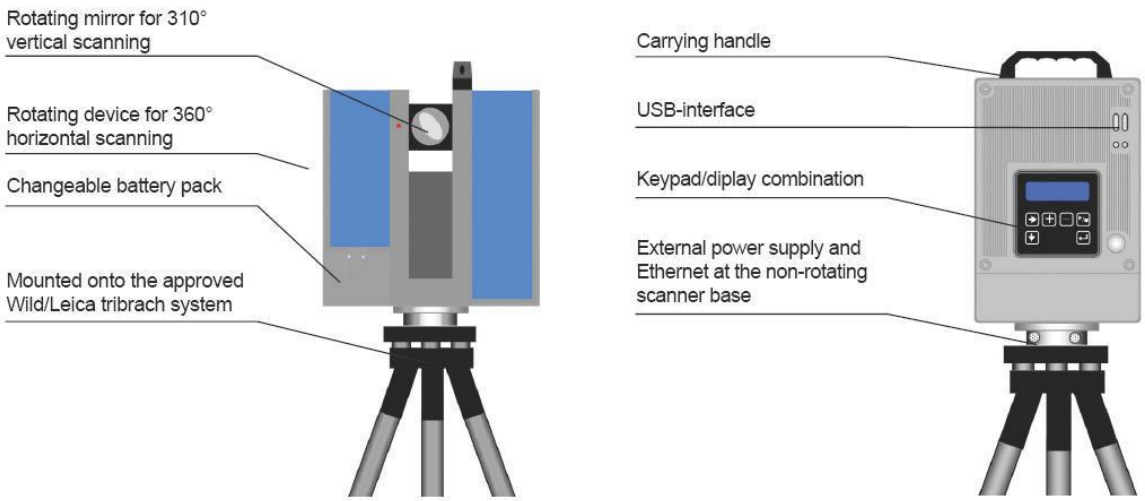

Figure 2.2: Anatomy of a 3D laser scanner
Source: 3DSCAN
http://www.3dscan.it/en/blog/how-does-it-work-a-3d-laser-scanner/

2.2.2 Image Acquisition and Parameters

The resolution of a scan can be established by the speed and pitch of rotations given by the user [6]. The slower a scanner rotates, the denser the point cloud becomes due to the amount of grid points acquired. The denser a point cloud is, the better the quality of data collected. The computed distance, vertical angles and horizontal angles are based on the position of the mirror and body for each measured point [6]. The value of reflectance of surface is also acquired and is usually higher when the surface is white [6]. Reflectance can at times become a hindrance when scanning highly reflective materials such as windows or mirrors. This issue with shiny surfaces is what is known as ‘noise’ [8].

These parameters can be affected by several settings input by the user. An example of a simple parameter input by the user is deciding between scanning a small angle wedge or 360°.

Parameters can also differ depending on the type of LiDAR system a user is equipped with; for example, if dealing with an airborne scanner the scanning pattern becomes a factor that is not present when using a stationary 3D laser scanner [9]. An example of these scanning patterns can be seen in Figure 2.3.

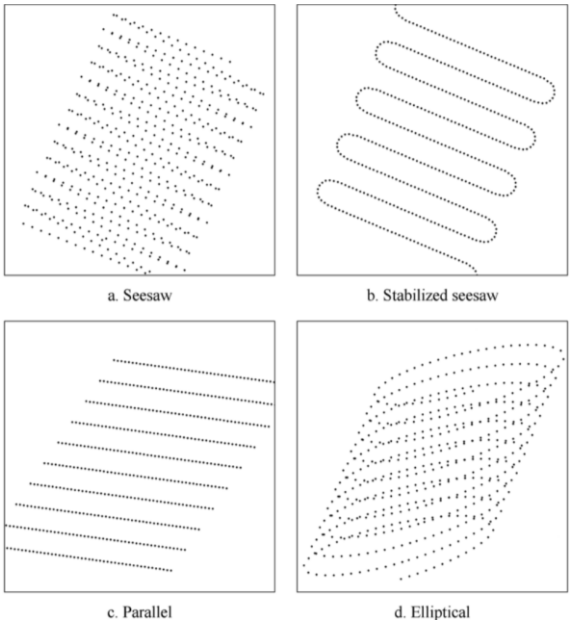

Figure 2.3: Scanning patterns for airborne LiDAR
Source: USDA – Forest Service
https://www.fs.fed.us/pnw/pubs/pnw_gtr768.pdf

A digital camera is integrated within the laser scanner in order to collect images of the areas scanned [6]. The purpose of these cameras is to allow a user to use the color collected through the images captured and input them into the point cloud [6]. This option is ideal for the archiving of structures since it allows the point cloud to have a greater photo-realistic look. Once all these capabilities have been applied by a user, depending on their goal, they can use the point cloud to output 2D and 3D deliverables [6].

2.3 Modal Dynamic Analysis

2.3.1 General Overview

The dynamic analysis of a structure produces several results such as natural frequency, displacements, time history outputs and modal shapes [10]. In the real world, every structure undergoes dynamic loading [10]. The internal stresses of structures and their resulting deflection, due to this loading, are time dependent or dynamic in nature since load application and removal varies with time [11]. Modal dynamics, specifically, determines the frequencies and mode shapes of a structure and depend on the mass, damping and stiffness distribution of the system [10]. Anything that possesses mass and elasticity is inclined to vibration and therefore behaves in an oscillatory nature [11].

2.3.2 Types of Vibrations

Generally, the types of vibrations fall within two categories: free and forced. Free vibration occurs when a structure is disturbed from its static equilibrium and allowed to vibrate without an external force being applied [12]. Free vibration is the type of vibration that was considered for the study described in Chapter 5. A structure that undergoes free vibration will vibrate at one or more of its natural frequencies depending on the mode that is being studied [11]. The equation of motion for free vibration is shown in Equation 1. The variables in Equation 1 are listed as follows: [m] = mass matrix, [c] = damping matrix, [k] = stiffness matrix, { $\ddot{u}$ } = acceleration, { $\dot{u}$ } = velocity and { u } = displacement. If the system has n degrees of freedom, the size of [m], [c], and [k] is [n x n]. If a system has anything more than one degree of freedom, it is considered a

multiple degree of freedom system [10]. When no damping is present, the [c] has no value therefore rendering it negligible. The equation of motion for an undamped system can be written as shown in Equation 2.

$$[\, m \,]\{\, \ddot{u} \,\} + [\, c \,]\{\, \dot{u} \,\} + [\, k \,]\{\, u \,\} = \{\, 0 \,\} \quad (1)$$

$$[\, m \,]\{\, \ddot{u} \,\} + [\, k \,]\{\, u \,\} = \{\, 0 \,\} \quad (2)$$

The second type of vibration occurs under the influence of external forces and thus named forced vibration [12]. A condition known as resonance occurs when the frequency of the external force matches the natural frequency of the structure [11]. This coinciding of frequencies causes significant deformations for structures which could ultimately lead to critical failure [11]. The equation of motion for forced vibration is shown in Equation 3. The new variable in this equation, when compared to free vibration, is P(t). This variable represents the external force acting on a system and differentiates forced vibration from free vibration. Should damping not be present, it would similarly be neglected as it was in Equation 2.

$$[\, m \,]\{\, \ddot{u} \,\} + [\, c \,]\{\, \dot{u} \,\} + [\, k \,]\{\, u \,\} = P(t) \quad (3)$$

2.4 Prior Work

Research into the feasibility of point cloud technology as a tool for model reconstruction has been and still is being completed. [13] evaluated the accuracy of deformation of a structure

using two point clouds, one with the undeformed shape and the other with its deformed shape. The study concluded that this point cloud comparison gave a measurement accuracy of ± 0.2 mm (95% confidence interval) [13]. Much research has been completed on the accuracy of the scanner itself, its ability to obtain real-life measurements and what factors contribute to the accuracy of the results. [14] explains that decisions made during the 'registration' of a point cloud have a direct impact on the accuracy point cloud dimensions can produce. The topic of point cloud registration is further discussed in section 3.3 of this thesis.

Lastly, studies on digital photogrammetry, such as laser scanning, when compared to traditional measuring techniques have been completed. Research completed by [15] showed the percent differences found when photogrammetry techniques were compared to both typical hand measurements and structural plan designs. The study found that photogrammetry only differed from a range of 0.06% - 1.43% when compared to hand measurements and 0.23% - 8.00% when compared to structural plan dimensions [15]. Similarly, dimensional comparisons where completed for the structures mentioned in this thesis to further understand the uncertainty expected when using this technology.

CHAPTER 3 – METHODOLOGY

According to the American Society of Engineering Education, one of the basic objectives within engineering is the detailed comprehension of the engineering method and an elementary aptitude in its application [16]. The methodology of this study focuses on a need and problem point cloud technology could potentially serve. Through this narrowed emphasis, an essential question was framed: could point cloud modeling be used as an alternative to structural plans? The need for such a substitute was explored in-depth by defining potential issues point cloud technology could help mitigate. The main issue examined, regarding engineering, is what to do should structural plans not be available in time-sensitive cases or if the as-built structure differed from what was shown in the structural plans.

Time-sensitive cases are highlighted in situations such as post-disaster structural integrity assessments. For these assessments, time plays an essential role for engineers in determining whether structures are on the brink of critical failure and are a risk to public safety. The use of point cloud technology is already utilized in post-disaster assessments by the Federal Emergency Management Agency (FEMA) due to the large-scale areas LiDAR scanners can map out [17]. This real-world application emphasizes the need for such technology in the ability to assess structures within engineering.

With the goal of this study aiming to assess the viability of point cloud technology, a quantitative approach was undertaken as the appropriate course of action. This approach was chosen due to the need for engineers to quantify the integrity of structures through numeric measurements and calculations. As mentioned in Section 2.2, a LiDAR scanner was used for this

study but its sole purpose was to collect the points that make up the point cloud data. The other essential tools used for this study are computer programs such as Cyclone Register 360, Autodesk Recap, AutoCAD, SAP2000 and MATLAB. Of all the programs, Cyclone Register 360 is the only program capable of registering the point cloud data collected by the scanner since it is made by the same company that manufactures the laser scanner.

3.1 Surface Reconstruction and Modeling

The goal of using a laser scanner is to regenerate structures seen in the field to a point cloud model with surfaces that are tangible enough for software to read. In order to reconstruct these surfaces, a set of sample points is collected by the laser near a structure's surface and recreated as closely as possible within the software [18]. It is impossible to obtain 100% accurate regeneration considering only a finite set of sample points can be collected by a laser, but the greater amount of data points collected the higher the accuracy [18]. The more points collected, the denser a point cloud becomes which allows for better recreation of the real-life structure [18].

The best collection of data points a user can have is when the essential areas are given high density while the featureless areas are limited in data point collection [18]. A multitude of factors can affect the collection of these data points which in turn, affect the quality of model generation. These factors can be things such as scan time for density, type of surfaces, noise level and obstructions. Since these factors play a role in accuracy, it is important that the appropriate algorithm program be used for the reconstruction method [18]. Once such a program is chosen, a user will be able to garner the correct geometry, features and topology through the sample data points collected [18].

3.2 Classification of the Reconstruction Algorithms

The classification of the reconstruction methods is a complex process due to the amount of methods and their respective subcategories. According to [19] and [20], there are five major categories for algorithm reconstruction: spatial subdivision, surface construction with distance functions, surface construction by warping, incremental surface-oriented construction and clustering. Each of the five categories have individual methods within them found through the work of an assortment of researchers.

The first major category, known as spatial division, enlists two subcategories called surface-oriented cell selection and volume-oriented cell selection [20]. This category is the only of the five to also have two subcategories that contain different approaches. The two subcategories have general steps that are followed, respectively, but have been applied with different techniques. An example of a different technique is found in [21], where a distance function was applied within the surface-oriented cell selection approach. This technique is also notable for being able to fall into the second major category: surface construction with distance functions [19]. For the volume-oriented approach, Boissonat's approach is seen throughout research works but is not the only method used; for example, [22] demonstrates an approach that differs from Boissonat's by being able to fill any holes on the surfaces collected. This new technique becomes beneficial, considering Boissonat's approach only works for surfaces that do not have any holes [21]. Figure 3.1 displays the approach detailed in [22] where holes on surfaces are filled in through their algorithm process.

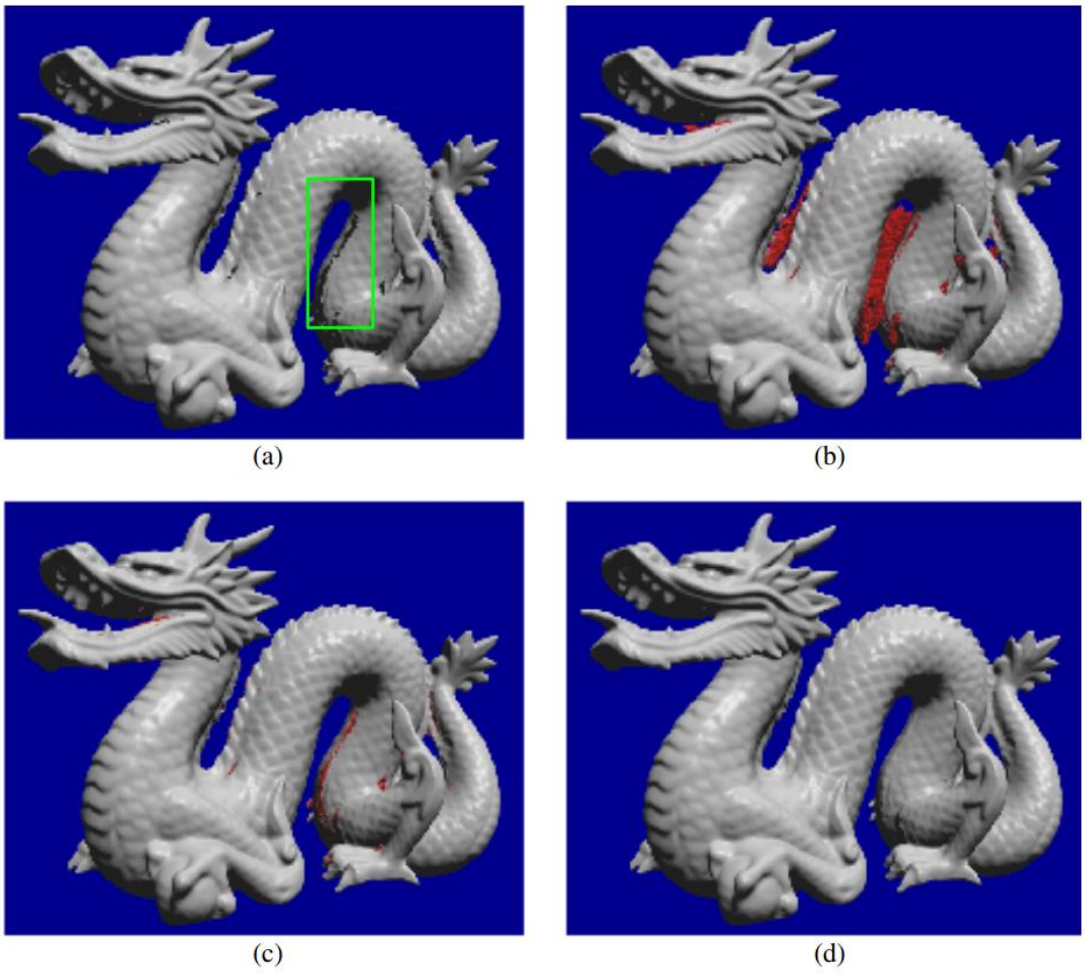

Figure 3.1: Volume-Oriented approach demonstrating holes in surfaces being filled in
Source: Brian Curless and Marc Levoy

Surface construction with distance functions is the second major algorithm category. As mentioned earlier, one of these approaches is also found in [21]. Although it is used within the spatial division category, the approach utilizes distance functions therefore making it applicable to this category as well. These types of category-bending approaches add to the complexity of the classification of these techniques. The third major category is surface construction by warping which, given its name, is self-explanatory. This technique deforms an initial surface in order to

approximate, to the best of one's ability, the given data points collected through scanning [19]. An example of this approach is seen through spatial free form warping which warps the entire space an object is fixed in while simultaneously warping the object congruently [19].

Incremental surface-oriented construction is the fourth major category for algorithm reconstruction. As defined by [20], "the idea of incremental surface–oriented construction is to build up the interpolating or approximating surface directly on surface–oriented properties of the given data points." This approach is illustrated in Figure 3.2. An example of this method is Boissonat's surface approach which adds to the category-bending complexity mentioned in the second major category. This approach uses localized Delaunay triangulation as seen in Figure 3.2 as well [20].

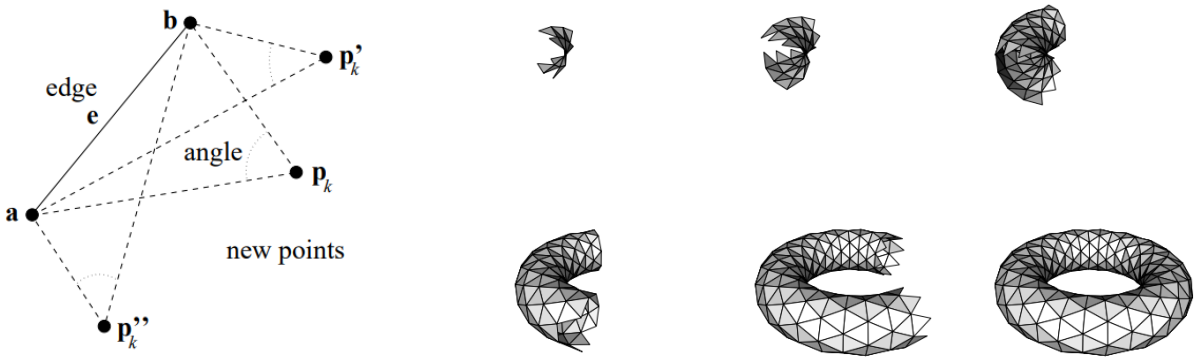

(a) (b)

Figure 3.2: (a) Basic principle of incremental surface-orientation; (b) Boissonat's surface-oriented approach
Source: Robert Mencl

Lastly, the fifth and final major category is known as clustering. This approach is taken when multiple shapes are connected and represented in a set of collected data points [19]. This

method becomes useful as the previous categories are meant more for data representing one shape [20]. In most cases, as in this study, a structure will not be limited to one shape but have several shapes interconnected. Clustering eases this issue by segmenting a set of sample points into a subdivision of points that belong to the same component [20]. Although these five major categories are the standard methods used today, research into new categories and new approaches within the established methods is constant.

3.3 Registration Theory

When attempting to obtain a point cloud from an existing structure, generally, more than one scan shall be necessary for the cloud to be considered suitable. The process known as registration regards the joining or stitching together of individual scans into one comprehensive point cloud [23]. For every scan, the center scan location (0, 0, 0 for x, y, z) is at the mirror embedded within the scanner where the laser beam strikes [23]. If the scanner is moved to different locations, each scan location has its own individual center which has to be aligned in order to properly register the point cloud [23]. To stitch together these scans, the overlapping points have to be matched as perfectly as possible in order to create proper alignment [24].

So as to complete an acceptable registration, [23] states "a minimum of three corresponding points, not on the same line, are required to compute the six rigid-body-transformation parameters needed to translate and rotate a secondary point cloud to a primary one." The more corresponding points you obtain, the more accurate your overall point cloud will be [23]. The goal of these correspondents is to optimize both sets of point cloud scans until they are stitched together with as minimal distortion as possible [23]. Figure 3.3 demonstrates how several scans completed at

different angles are registered into one comprehensive point cloud. The stitching together of two point cloud scans is known as pairwise registration and the steps to complete these steps can be seen in Figure 3.4 [24]. Many factors can affect the accuracy of the registration as concluded in [14]. Decisions in the inclusion of intensity values and/or color features directly affect registration accuracy [14].

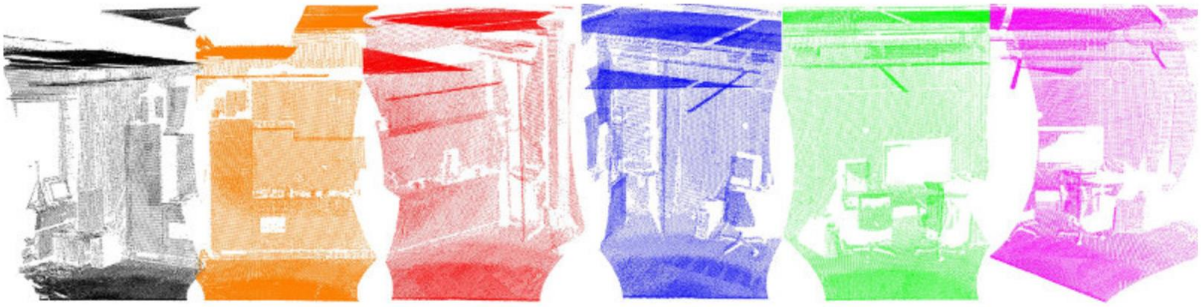

(a)

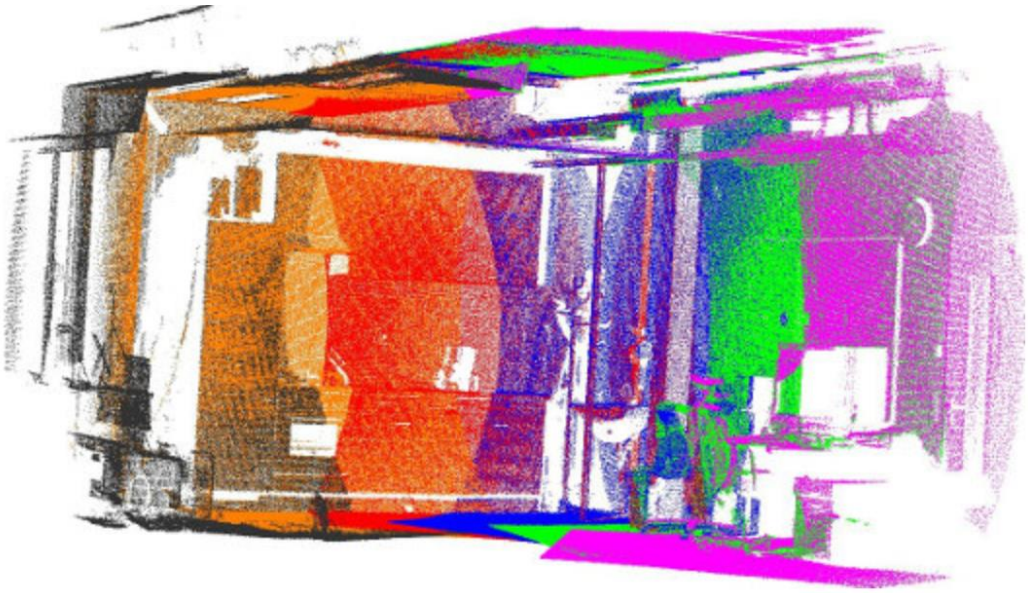

(b)

Figure 3.3: (a) Individual point cloud scans; (b) Stitched together comprehensive point cloud
Source: Point Cloud Library
http://pointclouds.org/documentation/tutorials/registration_api.php

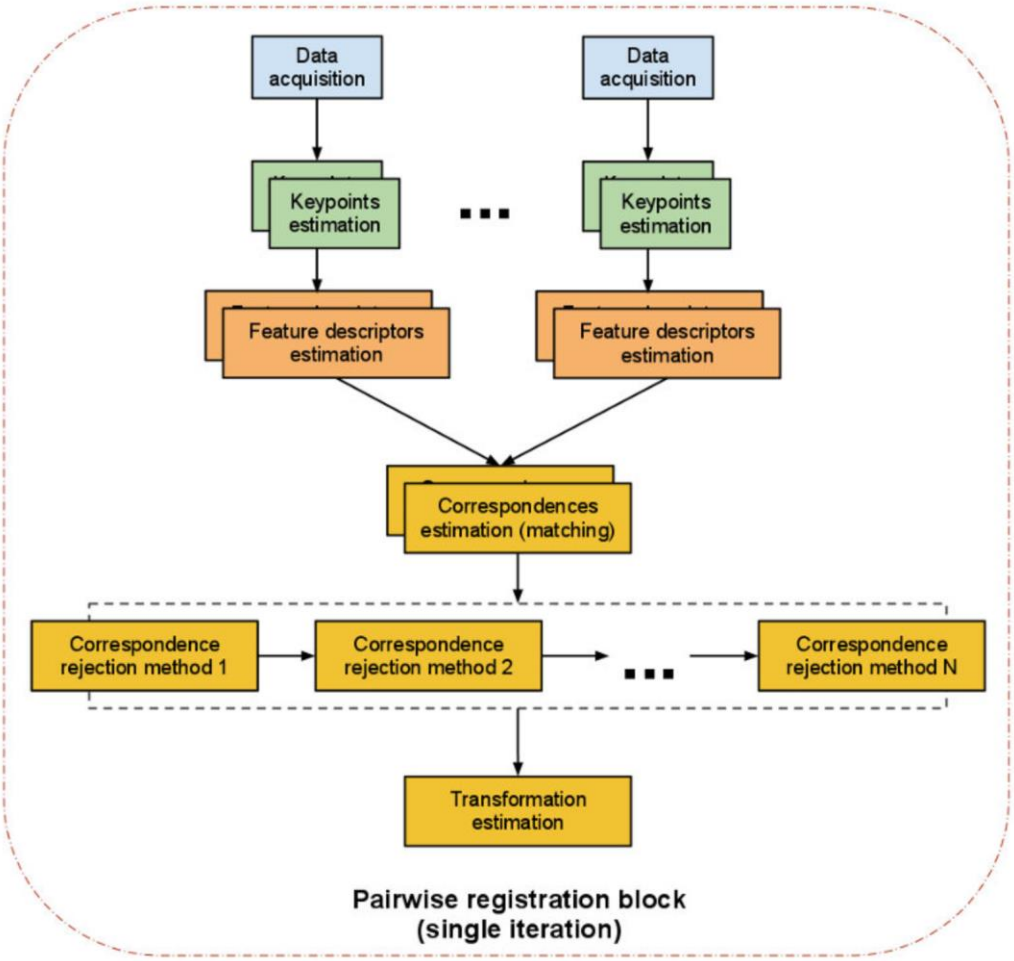

Figure 3.4: Pairwise registration steps flowchart
Source: Point Cloud Library
http://pointclouds.org/documentation/tutorials/registration_api.php

There are two important methods to find the correspondences between the overlapping scanned data: target-based and targetless registration [23]. For target-based registration, artificial targets are the common tool used within the field and it was the tool used for both studies in Chapter 4 and 5. Natural targets can be used but tend to be more challenging and dependent on human judgment [23]. The two main types of artificial targets are highly reflective spheres and black and white planes [23]. The spheres were used for the study done in Chapter 4 and the black

and white planes were used for the study done in Chapter 5. Note that since the targets are placed within the field of view of the scanner, additional time has to be taken during the registration process to remove the points representative of the targets within the point clouds.

For targetless registration, the registration process is divided into two steps: coarse and fine registration [23]. The fact that a single point cloud is capable of containing millions of points, the task of matching two point clouds with millions of points would prove too tedious to be useful [23]. In order to mitigate this issue, two coarse point clouds containing significantly fewer points are matched in order to have a basis for the matching of the fine point cloud containing all the points collected [23]. This method is useful to make the computation of the registration more efficient should targets not be used in the field.

3.4 Data Collection

3.4.1 Spectrum Stadium Data

The point cloud data for Spectrum Stadium was collected by Sofia Baptista and Jacob Solomon with the assistance of the UCF Institute for Simulation and Training (IST). This data was gathered and expanded on in a term paper written by both Ms. Baptista and Mr. Solomon. According to the authors, a FARO Focus3D S120 terrestrial laser scanner was the instrument used to collect the point cloud data [25]. Due to many visual similarities within the support system of the stadium structure, the authors utilized ‘tracking balls,’ shown in Figure 3.5, as artificial targets to help mitigate the issue [25]. The tracking balls work as a reference system for the scanner by helping to ease the registration process within the software once the scans are uploaded. In total,

four 360-degree scans were performed on-site [25]. The location of the stadium section scanned can be seen in Figure 3.6. Figure 3.7 highlights the limits of framing support chosen within that section of the stadium. Once completed, the scans were assembled, processed and imported into Autodesk Recap.

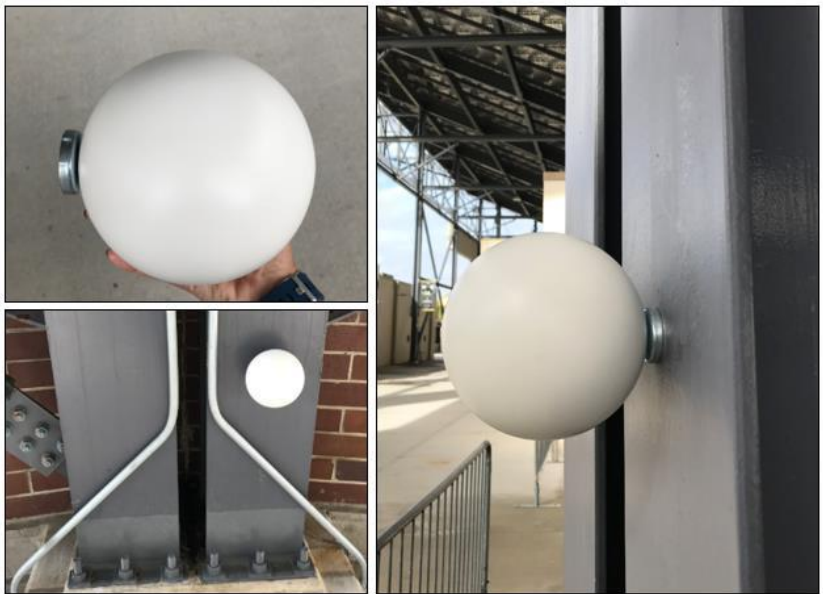

Figure 3.5: Tracking balls used on-site
Source: Sofia Baptista and Jacob Solomon

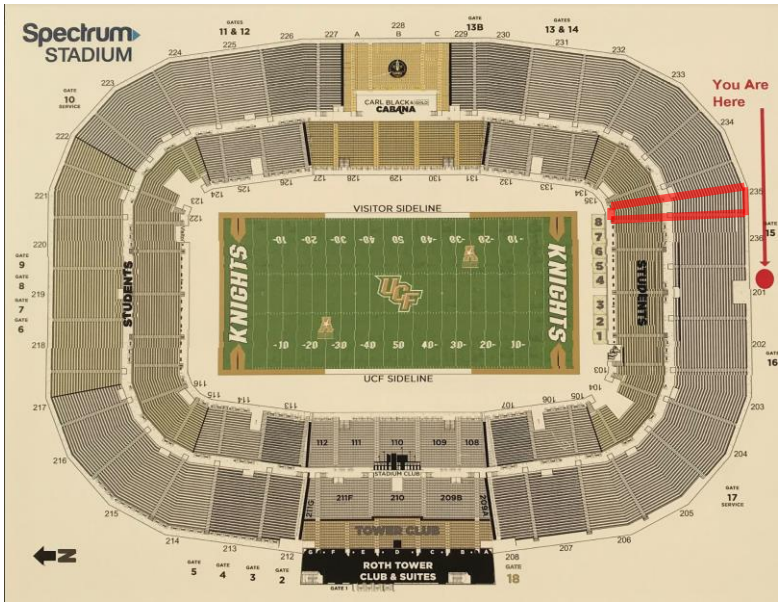

Figure 3.6: Section of Spectrum Stadium scanned shown in red
Source: Sign posted within Spectrum Stadium

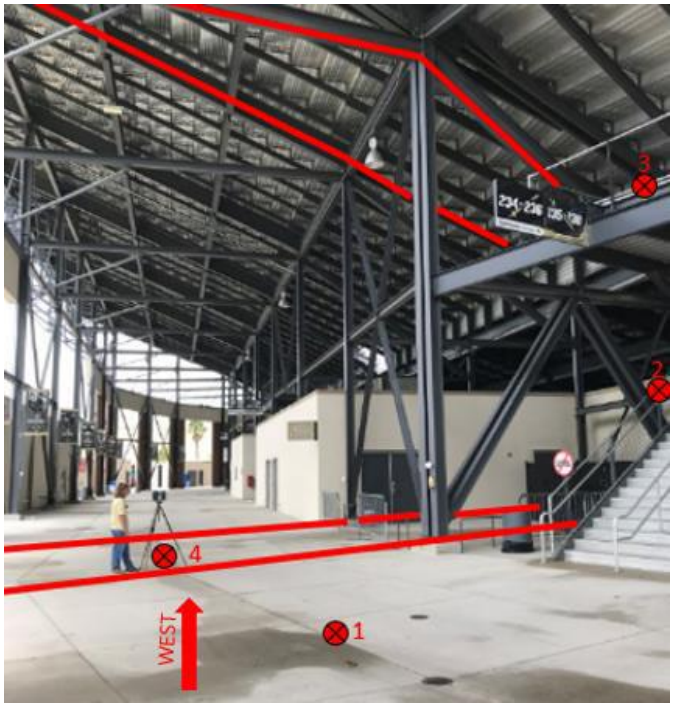

Figure 3.7: Limits of scan area shown by red lines. Marks 1-4 indicate the four scanning locations.
Source: Sofia Baptista and Jacob Solomon

Once the four scans were in Recap, they were combined into a single point cloud to maximize detail to begin rendering section members. The Recap point cloud was then imported into Autodesk Revit to overlay structural elements onto the point cloud visual to the best of the user's ability. The authors stated that the process was too difficult for them to render accurate member sizes so they defaulted to the member sizes given in the structural plans. Once completed, the rendered elements were imported into SAP2000 to complete a static analysis of the structure. The process used by the authors of the original study can be seen in a simplified manner in Figure 3.3. Using the data provided by this term paper, the process to model and analyze the structure via the point cloud files, supplied by Ms. Baptista and Mr. Solomon, was repeated but in a slightly different manner as explained in Chapter 4.

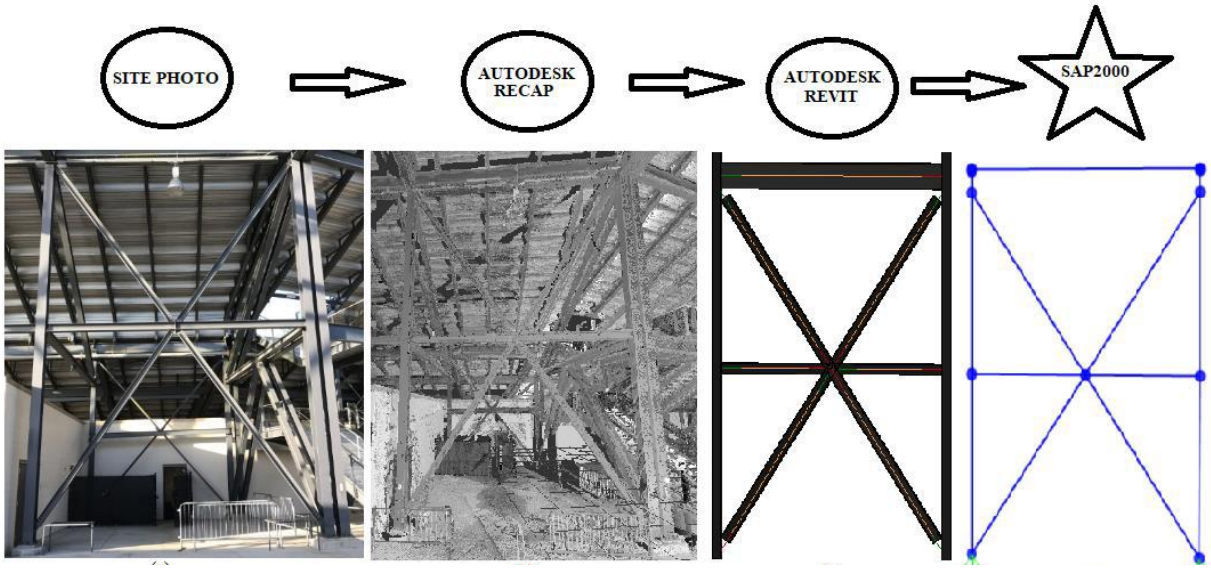

Figure 3.8: Site to model analysis workflow
Source: Sofia Baptista and Jacob Solomon

3.4.2 Pedestrian Bridge Data

Point cloud scanning of Parking Garage VI – H Pedestrian Bridge was completed with the aid of Dr. Lori Walters and Mr. Rob Michlowitz from the UCF IST. Assistance with time scheduling, photo documentation and note-taking were also provided by fellow classmates Paulo Dos Santos, Samantha Weiser and Pruthviraj Thakor. A Leica ScanStation P-Series 3D laser scanner was used for this study and provided by IST. The initial scanning attempt of the bridge was interrupted due to technical difficulties with the laser scanner. Three scans had been completed prior to the scanner's software error but as a result, the scans were forced to be deleted through a software reboot since it was the only way to mitigate the issue. The bridge scan was forced to be postponed and rescheduled due to the issue.

Prior to arriving on-site for the second scanning attempt the following week, the scanner's software was updated and the initial calibration of the scanner was completed to save time. Throughout the second on-site scanning attempt, a scanning time log, shown in Appendix A, was created and includes the overall start time, end time, scanner setup time, scanning time and marking targets. Scanning locations are also detailed on an aerial view of the site shown in Appendix B with corresponding photos.

3.4.2.1 Point Cloud On-Site Procedure

Before commencing the scans, three black and white artificial targets labeled 1, 2 and 3 were set up on the bridge at approximately equal increments. In general, the scanner must be able to see at least two targets at a time. Targets must not be arranged in a straight line so that the

scanner has triangular coordination with the targets. All targets were set at a height of 6.5 feet from the base which was a height chosen at the user's discretion. The height of the targets was chosen to ensure the scanner had a direct line of sight from each scanning location. Figure C.1 in Appendix C shows the target set up process.

The scanner was then set up on the north side of the bridge as that was the designated location for the first scan. When using a stationary laser scanner, it must be leveled on a tripod in order to collect accurate data. The tripod used in this study was a Leica 670223 14ZJP-0000 which was also provided by IST. The tripod was leveled with a smartphone leveling application before attaching the scanner to it. The leveling of the scanner on the tripod itself was fine-tuned with the scanner's digital assistance screen. Appendix C Figure C.2 also displays the process of setting up the scanner on the tripod.

Once the scanner was leveled on the tripod, the scanner was programmed with the name of the project, image resolution required and white balance setting (i.e., sunny, cloudy, etc.). To decrease the amount of time per scan, the scanner was programmed to ignore photo imagery (scan only). This setting limits the scanner to collecting the point cloud data in greyscale because it refrains from capturing photos of each scan view. Finally, the scanner was programmed with the angle range that it should capture. The preceding steps are shown in Appendix C, Figure C.3.

When starting the scan at the first location, the screen of the scanner must be oriented on its right side. For all wedge angle scans (scans that are not 360º scans), the scanner's peephole, shown in Appendix C, Figure C.4, must be placed in the line of sight of the angle's starting point. Once in position, the user manually rotated the scanner using the peephole's line of sight until an end point was determined for the scan. From the pre-programmed resolution and manually set

range, the scanner is able to measure the angle and estimated the amount of time it would take to scan said angle.

After the first scan was complete, targets were located manually and marked within the scanner's screen. The targets must always be captured by the scanner in the same order after each scan. A minimum of two targets must be captured by the scanner per scan but for some of the scans, all three targets were able to be marked allowing for more precision in terms of the scanner's location. Appendix C, Figure C.4 shows how the targets were marked on the scanning screen.

On the north side of the bridge, the scanner was relocated to two more locations. For each scan, the process of leveling the scanner and setting the range was repeated followed by capturing the targets after the scan was completed. At the third location, note that only two targets were captured as opposed to three at the first two locations. This was due to the lack of clarity from interference from a palm tree directly within the line of sight of the target. This issue gave the scanner difficulty in distinguishing where the target ended and the palm tree began. The scanner was then repositioned for one scan at the east end of the bridge, four different scans on the south side of the bridge and one scan at the west end of the bridge. For each scan, the process of leveling the scanner, setting the range, and capturing the targets was repeated.

Finally, the scanner was relocated to two separate locations on the bridge. Prior to the first scan on the bridge, target 1 was relocated to the north side of the bridge. Moving a target is possible if one of the other original targets is left in place and used as a reference point for the newly moved target. For these two scans, manually dictating an angle wedge was unnecessary as the capture range was set to 360 degrees. Overall, the entire process (11 scans total) took place over the course of five hours and forty-five minutes.

3.4.2.2 Point Cloud Registration

After the on-site scanning, the scanner was taken back to the office of Mr. Michlowitz to process the data and form a point cloud. In order to create a composite point cloud, Mr. Michlowitz used the Leica program Cyclone Register 360 which is a 3D laser scanning point cloud registration software. The software is programmed to accept the data collected from the Leica laser scanner and gives users the ability to manipulate, edit and stitch together the scans while also obtaining a registration report. Before any editing, the scans were opened in Cyclone Register 360 and produced the 3D image seen in Figure 3.4. The registration report for the unedited scan can be found in Appendix D.

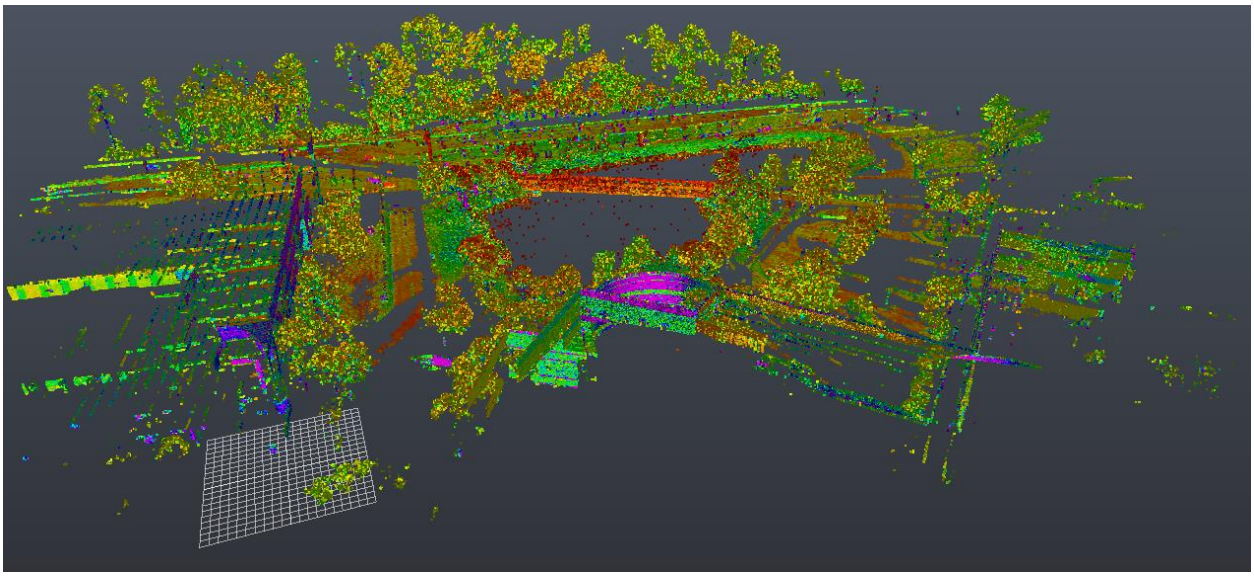

Figure 3.9: Unedited composite point cloud scan in Cyclone Register 360

The stitching together of the 11 scans into one comprehensive point cloud was done via the use of the target locations set up on site which allowed the program to use coordinate triangulation. Dr. Walters noted that the use of targets cut software editing time by approximately

75% although increasing the scanning time on site. Figure 3.5 illustrates the locations the scanner was placed given by the registration report in Cyclone Register 360. The green lines in the figure indicate the strong links between the scanning locations (yellow triangles) which allowed scan overlap, assisting a user in stitching the multiple scans together.

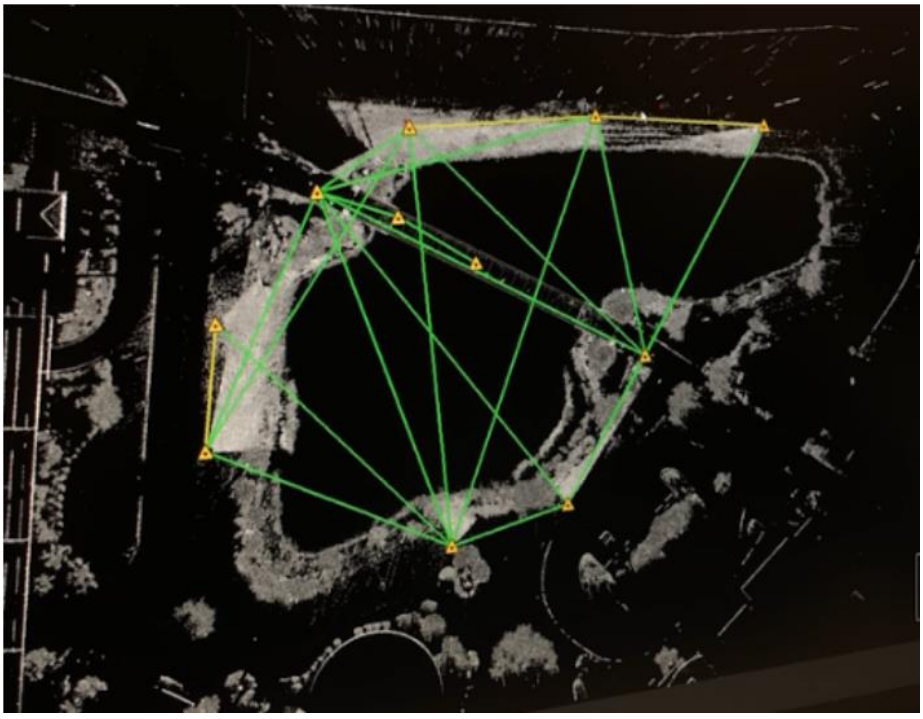

Figure 3.10: Scan locations diagram shown in Cyclone Register 360's Registration Report

The amount of data points collected during the 11 scans included surfaces outside of the bridge, leading to hefty file sizes exceeding over 24 gigabytes in total. These extra points are due to the laser scanner's ability to measure surfaces up to 270 meters away. The amount of points can vary due to numerous factors such as scan angle and resolution choice. In this case, the lowest number of points in a single scan was over 50 million while the higher end of the scans accrued

over 190 million points. In order to eliminate additional points that did not apply to the bridge, Mr. Michlowitz used his expertise with Cyclone Register 360 to edit, trim and register the 11 scans. Some of the elements that had to be trimmed out from the overall composite image are as follows: trees/shrubbery, vehicles, buildings, people, reflection of the pond and the black and white targets.

Due to the amount of shrubbery at the site and its location in reference to the bridge, the complete removal of the shrubbery from the point cloud was not plausible as shown in Figure 3.6. Mr. Michlowitz indicated that the total time it took to register the point cloud was under two hours. Cyclone Register 360 was able to precisely pinpoint the 11 locations the scanner was positioned at to an accuracy of 7/16th of an inch. A zoomed-in image illustrating the density of the fine point cloud can be seen in Figure 3.7. Following the registration, the process of preparing the point cloud for dynamic model analysis began as expanded upon in Section 5.2.

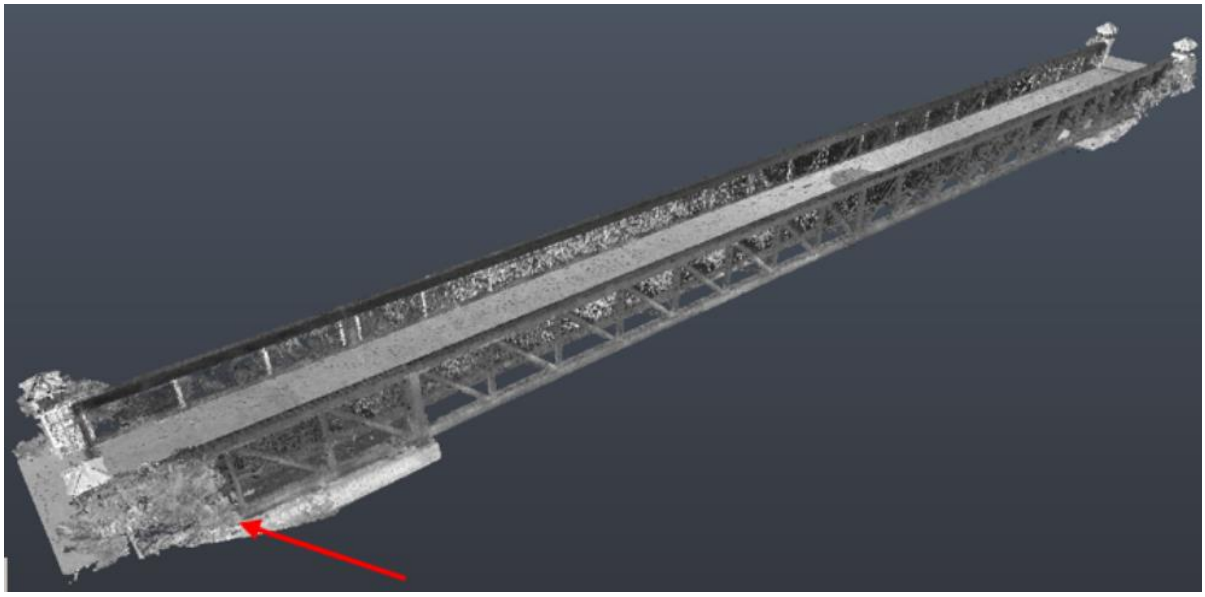

Figure 3.11: Fine point cloud on Autodesk Recap following completed registration. Red arrow indicates leftover shrubbery.

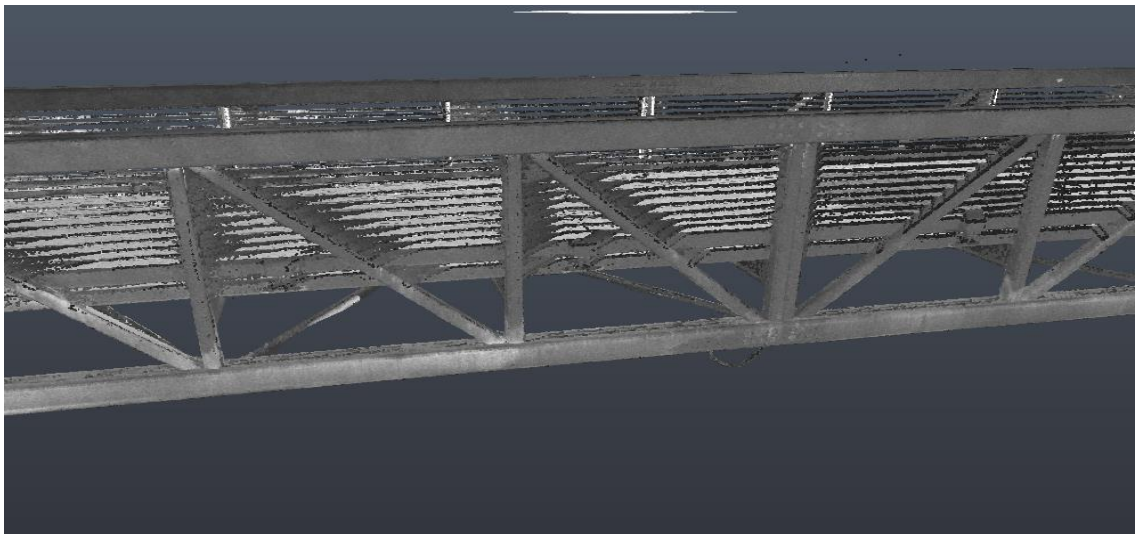

Figure 3.12: Zoomed-in fine point cloud on Autodesk Recap

CHAPTER 4 – SPECTRUM STADIUM STATIC ANALYSIS

4.1 Model Generation Using Point Cloud

As mentioned in Section 3.4.1, the original data collectors of the stadium point cloud data completed a comparative study between the stadium's structural plans and their interpretation of the point cloud. In order to study if any accuracy differential exists when two users use the same point cloud data, the study was repeated similarly with a few differences. The first difference was that a model based on the on-site dimensions was created as a control in addition to the new point cloud model. This was completed to compare the dimensions found by the point clouds as well as those given in the structural plans. The measurements were gathered using a Bosch GLM 80 Lithium-Ion Laser Distance Measurer and a model was created using those measurements alongside the member sizes provided by the structural plans.

Another difference that was noted in this study was the type of FEA program used to render the member sizes. The original data collectors first used Autodesk Recap, then Autodesk Revit and finally SAP2000 to analyze the point cloud. In the case of this study, Autodesk Inventor was used as the FEA program of choice in lieu of Revit. The other programs described, Autodesk Recap and SAP2000, were used in this study as they were in the original. The point cloud of the stadium section used can be seen in Figure 4.1 when opened in Autodesk Recap. Lastly, [25] used the section sizes provided by the structural plans due to difficulty rendering in Revit using the point cloud. For this study, member sizes were rendered using the point cloud directly rather than defaulting to the structural plans in order to see the uncertainty that might exist.

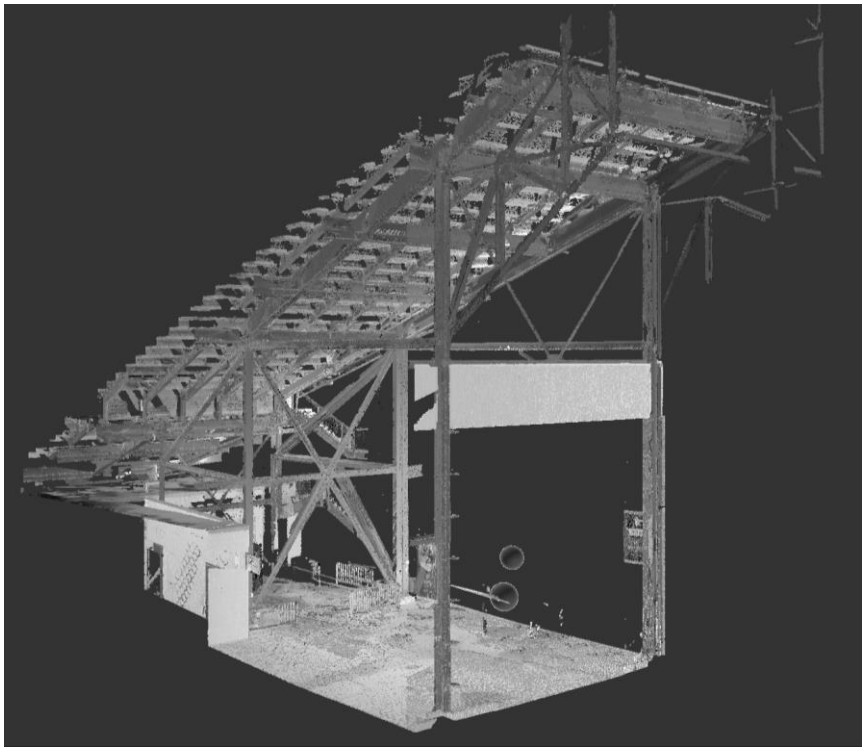

Figure 4.1: Point cloud of stadium section within Autodesk Recap

Inventor has similar capability to Revit in that it is used to render member sizes as closely as possible to the point cloud visual that was imported. The following steps show a brief summary of the procedure taken to render sections onto the point cloud visual within Inventor (Figures of these steps can be seen in Appendix E):

1. Import Recap file into an Inventor “Assembly” file
2. Create a “Part” within the Assembly in order to create a 2D sketch on the sides of point cloud
3. Insert a “Work Plane” on a flat surface of the users choosing to begin the 2D sketch

4. Using the point cloud as reference, create a center-to-center sketch by lining up the sketch lines with the visible sections
5. Once the sketch is completed, insert frames and offset accordingly to match the sections seen in the point cloud as best as possible. Users will have to take a trial-and-error approach to determine the section size that they deem most similar to the shape seen in the point cloud
6. Repeat the process for all applicable sides and sections of the structure

Once the sections were chosen and the point cloud had a fully rendered representation in Inventor, the sketches were imported into AutoCAD. This step was necessary so that the sketch could be input into SAP2000 since AutoCAD dxf files are compatible with SAP2000. Once the sketches were in AutoCAD, the sketch was appropriately lined up ensuring that the frame lines were connected and that there were no misalignments. The member sizes and length values are entirely at the discretion of the user since they are dictated solely on a user's judgment. For example, if a sketch was measured in AutoCAD as having a length of 1200.34 inches, it is possible for a user to assume that the member line had a length of 1200 inches. After completing this process in AutoCAD, the dxf file was imported into SAP2000 for static analysis.

Once the frame drawing was transferred from AutoCAD to SAP2000, as seen in Figure 4.2, the program automatically labels each frame as a W18x35 member. Each frame had to be manually changed and labeled to the appropriate member size as dictated by the rendering created in Inventor. Once completed, seven equally spaced loads of 1.5 kips were placed on the horizontal members seen in Figure 4.2. These applied loads acted as the static load on the structure to complete the analysis for an output of deformations and reactions. These loads were chosen to

fully repeat the study completed by [25] and give a fair comparison without changing any of the circumstances. The results of these load placements are seen in Section 4.2.

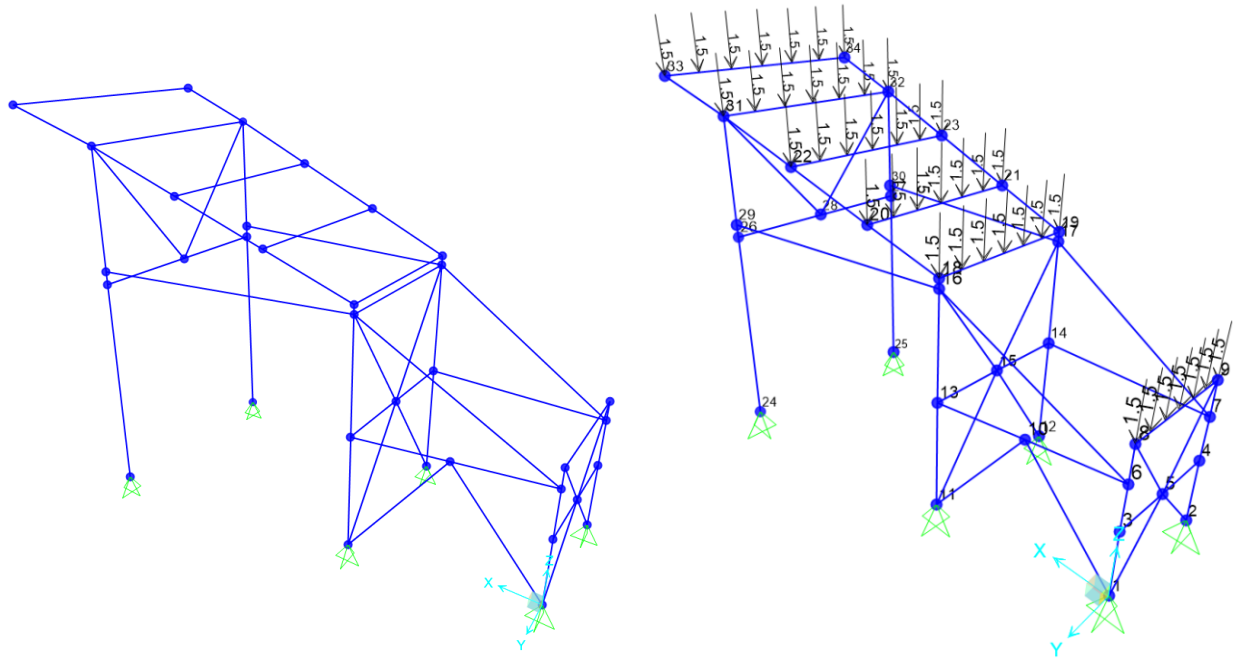

Figure 4.2: Images from SAP2000: (a) Undeformed frame shape; (b) Applied static loads on horizontal members

4.2 Point Cloud Static Analysis Results

At the conclusion of the static analysis executed on the point cloud of a section of Spectrum Stadium, the displacements of critical joints were obtained as well as the reactions at the pinned joints. Prior to obtaining these outcomes, the lengths and widths of the pinned base joints were found after completing the rendering of member sections in the point cloud. These base joint distances were dimensioned to be compared to the previous case study with the elevations of the

structure also being compared. The base dimensions of the structure found through the new point cloud can be seen in Figure 4.3 and the elevations in Figure 4.4.

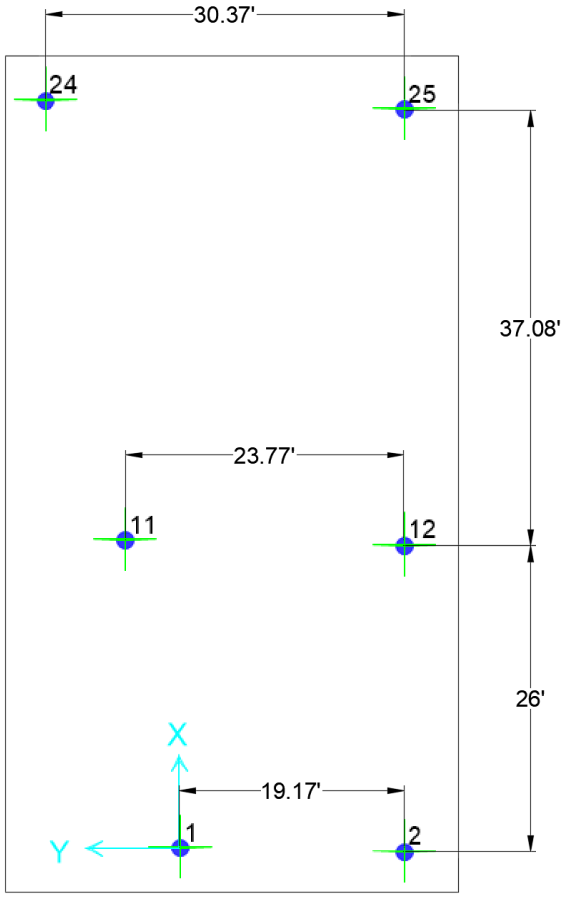

Figure 4.3: Plan view of structure's base points with accompanying dimensions based on the new point cloud model

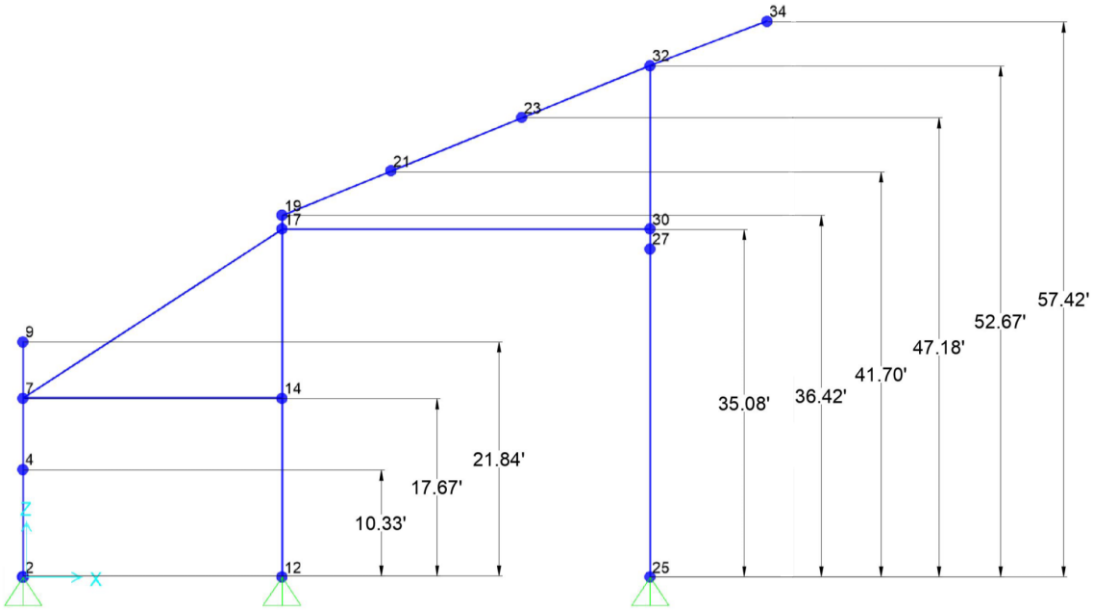

Figure 4.4: Elevation view of new point cloud model with accompanying dimensions

Once analyzed in SAP2000, the framing structure produced a deformed shape showing the points of deflection as shown in Figure 4.5. The deformed shape is an exaggeration of the deformation of the members as to emphasize where displacement occurs. In Figure 4.6, the image establishes the joint labeling for referencing displacement to a respective node. The corresponding deformations for said nodes can be seen in Table 4.1 while the base reactions are shown in Table 4.2. Both the displacements and reactions calculated are compared to the results found in both the original study and the on-site measurements in Section 4.4. For both sets of tables, only the values in the Z-direction were taken into account as was the case in the original study.

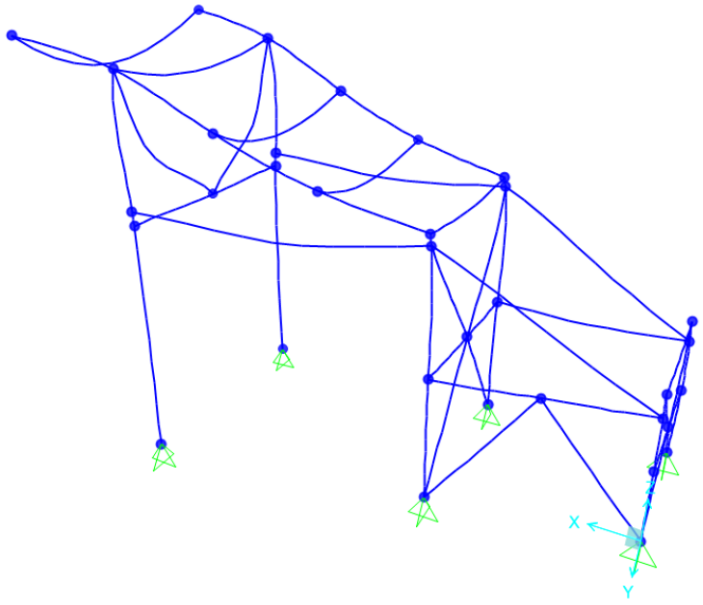

Figure 4.5: Deformed shape of new point cloud model after applying static load

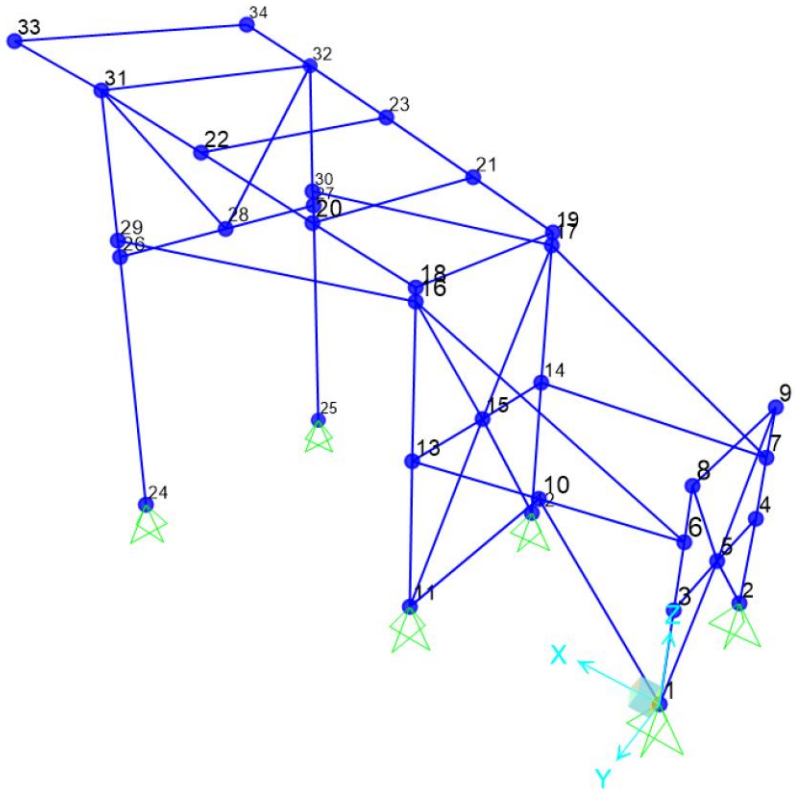

Figure 4.6: Joint labeling via numbered nodes

Table 4.1: New Point Cloud Joint Displacements in Z-direction

Joint Number	**Displacement, U_3 (in)**
8	-0.006
9	-0.006
18	-0.013
19	-0.013
20	-0.117
21	-0.110
31	-0.027
32	-0.027

Table 4.2: New Point Cloud Joint Reactions in Z-direction

Joint Number	**Reactions, R_3 (kip)**
1	8.09
2	7.37
11	18.38
12	17.68
24	28.38
25	28.18

4.3 On-Site Measurements Static Analysis Results

In the case of the model created by the on-site measurements, no rendering was needed as the sections labeled within the structural plans were used in combination with the dimensions found. The model was drawn directly in AutoCAD with the dimensions obtained and then imported into SAP2000. As was shown for the point cloud model, the base joint dimensions and the elevations of the structure from the on-site measurements are shown in Figure 4.7 and 4.8. There comparative results with the rest of the models are seen in Section 4.4.

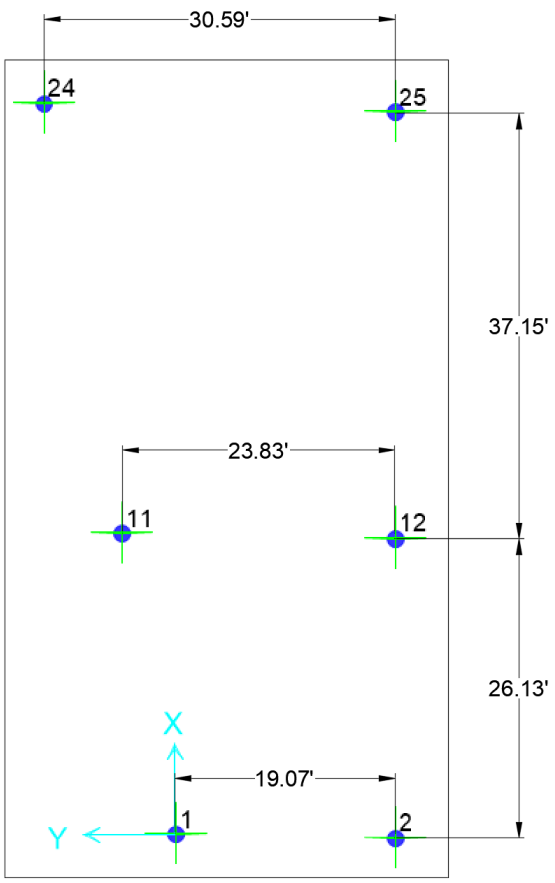

Figure 4.7: Plan view of structure's base points with on-site dimensions

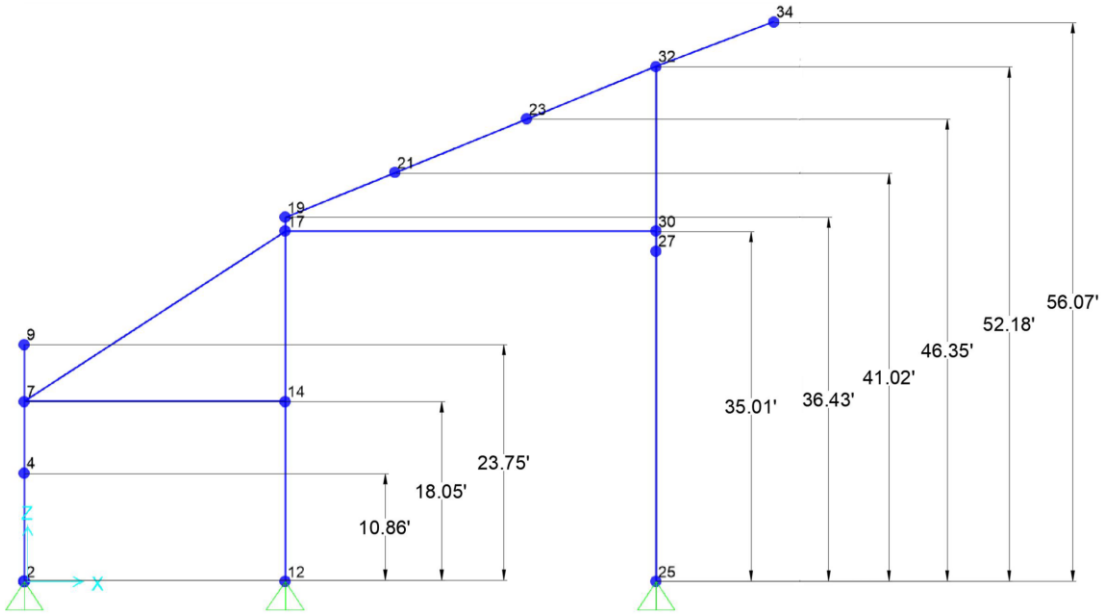

Figure 4.8: Elevation view of on-site measurement dimensions

After being analyzed, the model produced the deformed shape seen in Figure 4.9. Table 4.3 displays the displacements that coincide with the deformed shape and go by the same joint numbering seen for the new point cloud in Figure 4.6. Both the new point cloud and the on-site model results are compared to the original study in the following section.

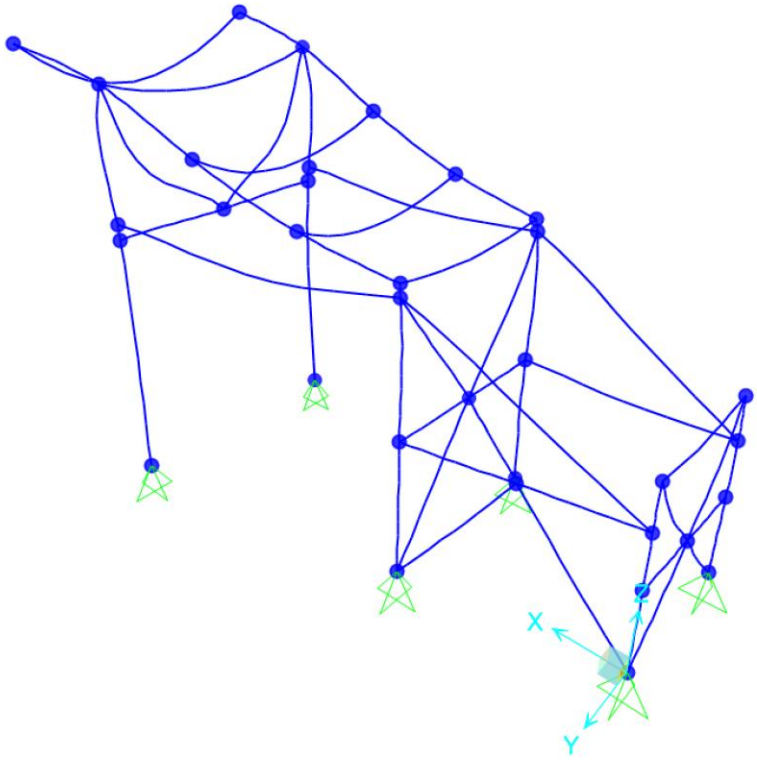

Figure 4.9: On-site measurement model deformed shape

Table 4.3: On-Site Measurement Model Joint Displacements in Z-direction

Joint Number	**Displacement, U_3 (in)**
8	-0.006
9	-0.006
18	-0.014
19	-0.014
20	-0.116
21	-0.106
31	-0.028
32	-0.028

Table 4.4: On-Site Measurement Model Joint Reactions in Z-direction

Joint Number	Reactions, R_3 (kip)
1	8.57
2	7.86
11	18.25
12	17.72
24	27.26
25	26.91

4.4 Comparative Analysis of Stadium Results

4.4.1 Dimension Comparison

The results founded in this study varied in outcome when compared to the structural plans of the stadium, the point cloud analysis completed in the original study and the in-field measurements taken at the stadium. The initial comparison between all the model sources involves the dimensions of the structure. Figure 4.10 shows the differences in length and width dimensions between the original point cloud study and the structural plans. Figure 4.11 shows the difference between the new point cloud study and the on-site measurements. Figures 4.12-4.15 show the different elevation obtained through the different data sources. Overall, the percent difference ranges and averages for the dimensions gathered by each data source, when compared to the actual dimensions found on-site, are as follows:

- Original point cloud: Range = 0.5% - 10.0%; Average = 3.3%
- Structural plans: Range = 0.2% - 24.2%; Average = 5.0%
- New point cloud: Ranges = 0.2% - 8.0%; Average = 1.9%

Both point clouds fared far better than the structural plans most likely due to the as-built structure undergoing adjustments during construction and/or renovations done over the years. With the new point cloud averaging a 1.9% difference to the actual dimensions of the structure, point cloud technology shows its ability to gather precise data.

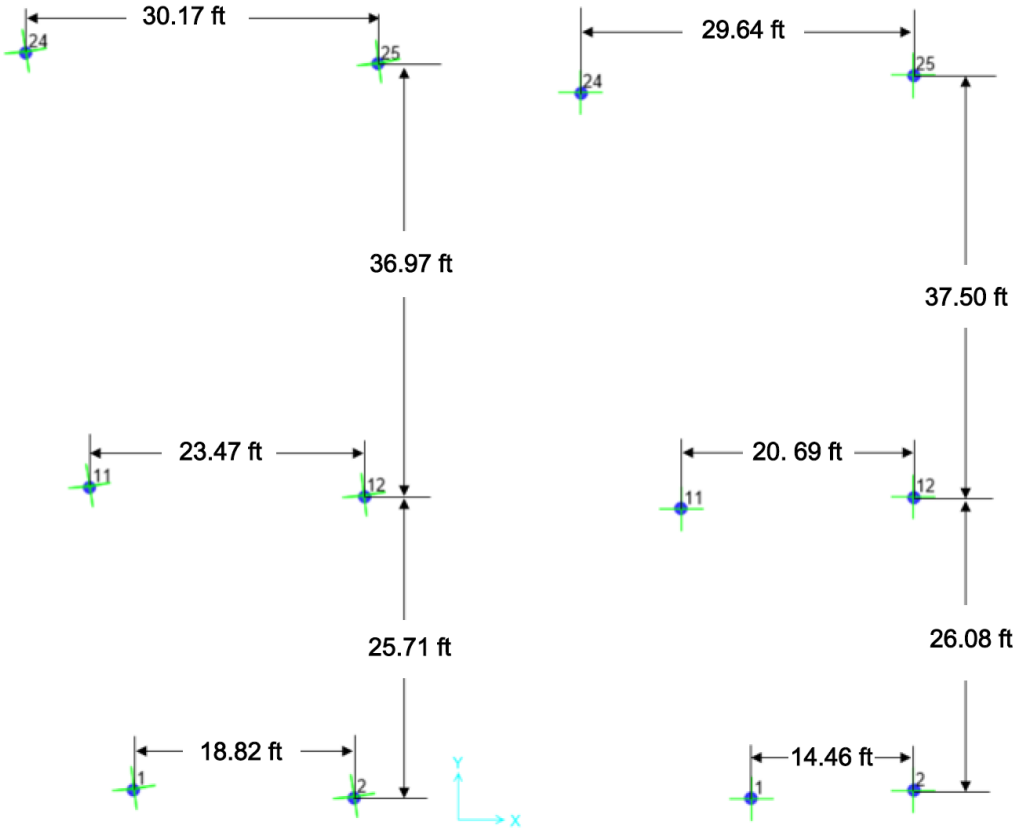

(a) (b)

Figure 4.10: Plan view base dimensions: (a) Original point cloud; (b) Structural plans
Source: Sofia Baptista and Jacob Solomon [25]

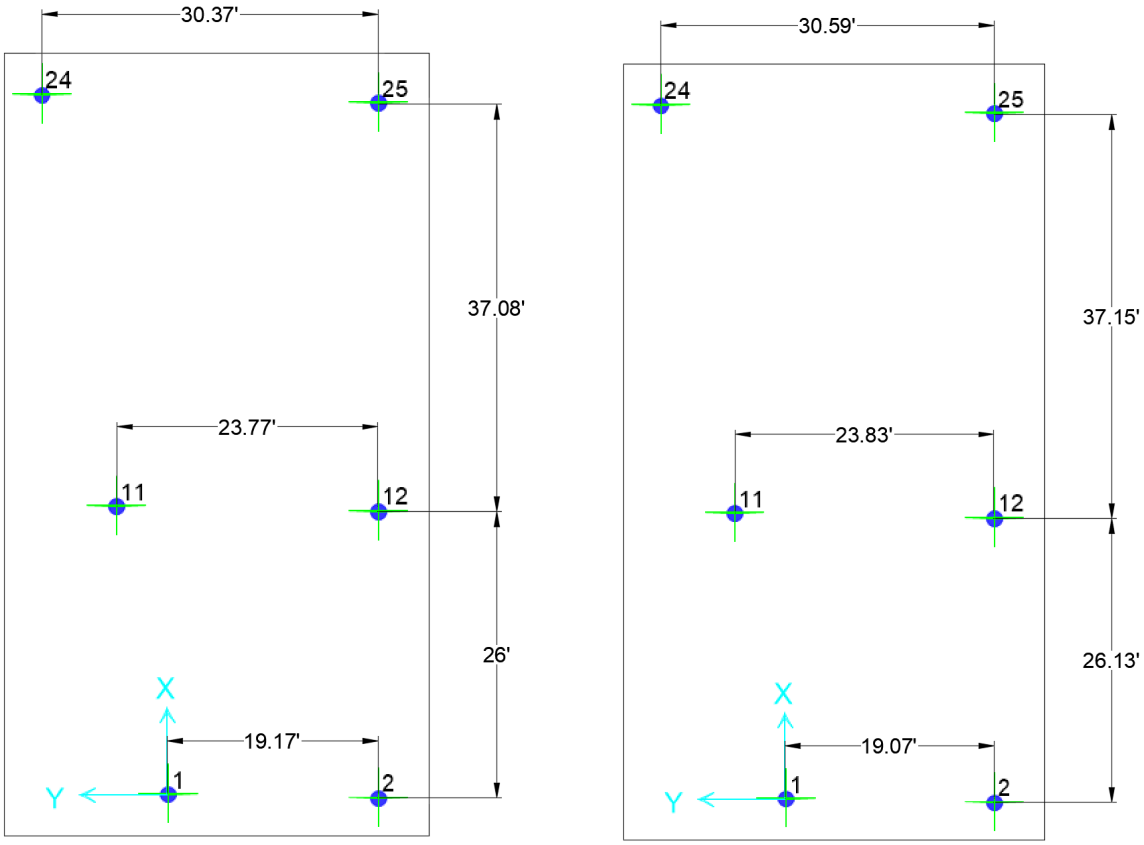

Figure 4.11: (a) New point cloud base dimensions; (b) On-site base dimensions

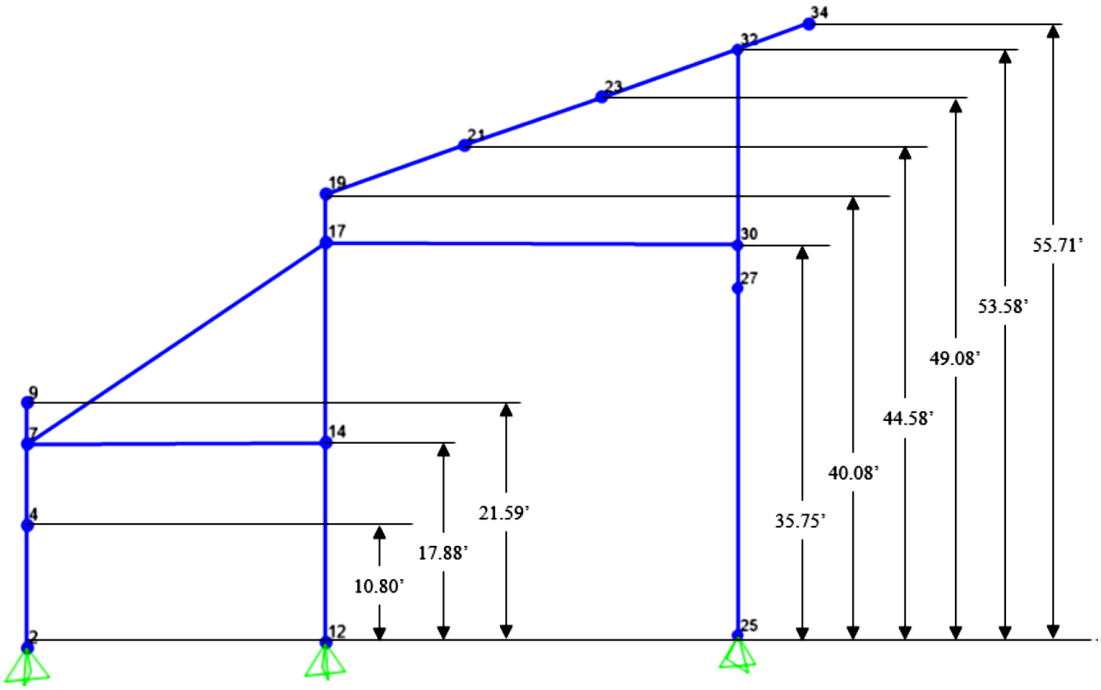

Figure 4.12: Original Point Cloud Elevation
Source: Sofia Baptista and Jacob Solomon [25]

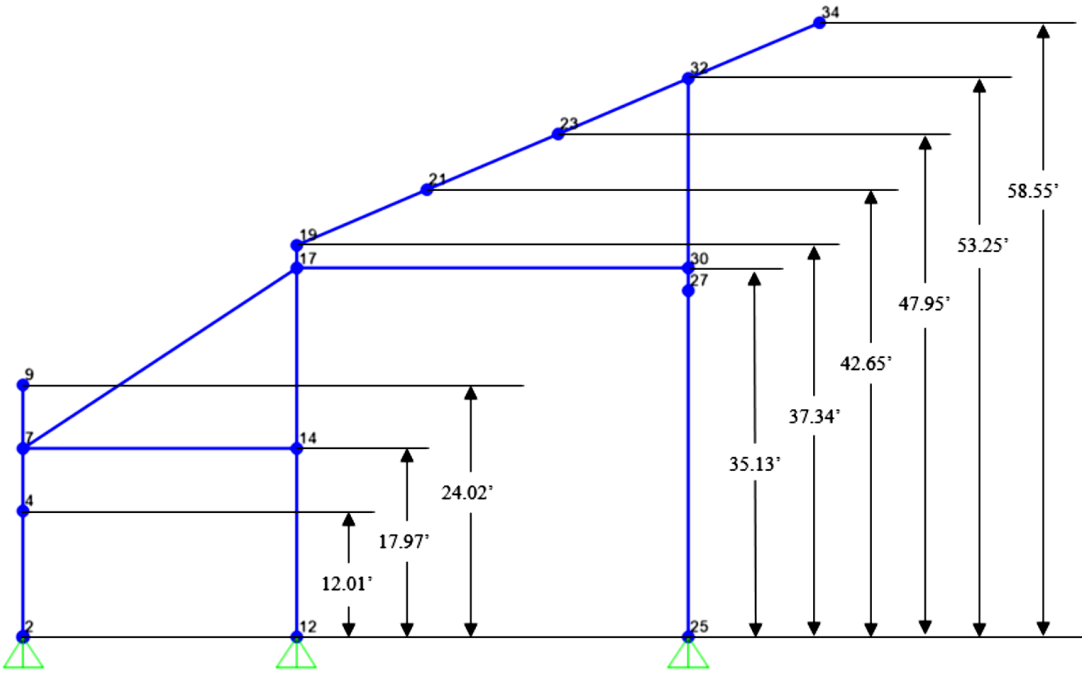

Figure 4.13: Structural plan elevation
Source: Sofia Baptista and Jacob Solomon [25]

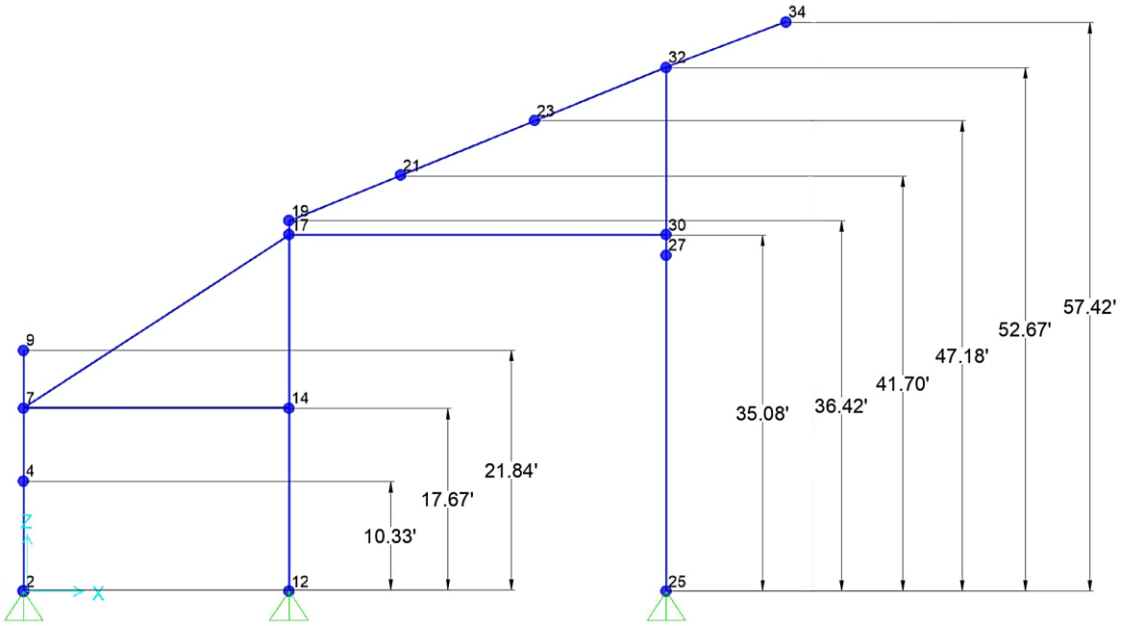

Figure 4.14: New point cloud elevation

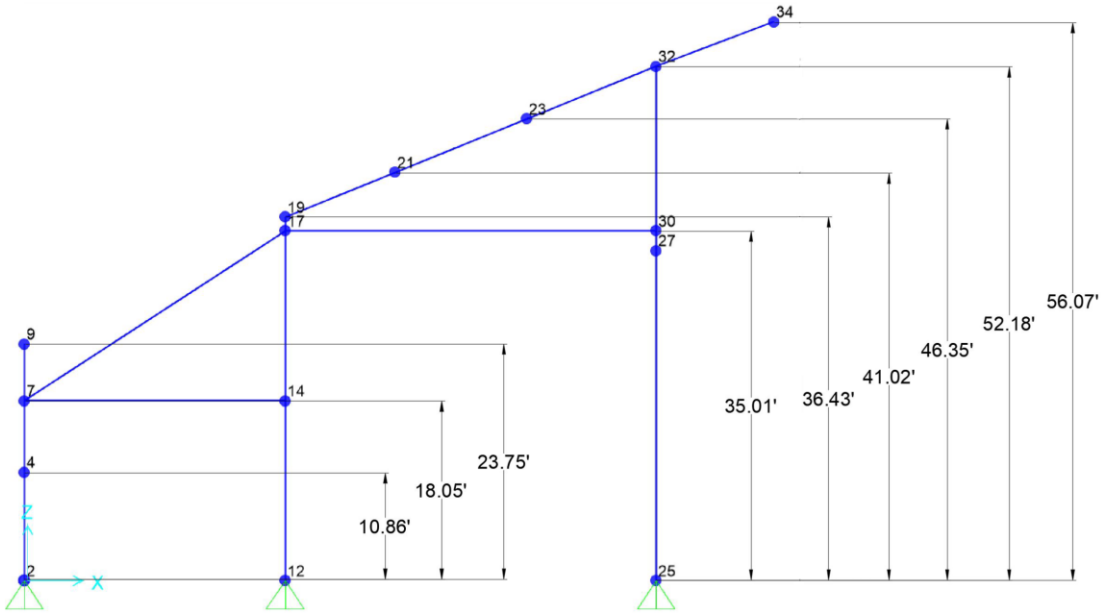

Figure 4.15: On-site measurement elevation

[25] notes that rendered the sections using the original point cloud was difficult enough to be unsuccessful and resorted to using the sections provided by the structural plans. This is important to note because it signifies that the only difference between the original point cloud and the structural plans is the dimensions. Table 4.5 displays the differences in member sizes found between the new point cloud and the structural plans. These differences are highlighted in yellow alongside their respective cross-sectional area percent differences. The member sizes are classified by their location via the joint labeling previously shown in Figure 4.6. As can be seen, the majority of the member sizes differed from those seen in the structural plans. Although these member sizes differed, it was realized that member size renderings for the new point cloud were within ± 2 section sizes of the member sizes given in structural plans and none exceeding a 30% difference. The one exception to this finding was the horizontal frame spanning Joints 3-4. This exception is due to the as-built section being a different member size than the one stated in the structural plans accounting for the outlier in the comparisons. The average without this outlier, for percent difference, was only about 13%.

Table 4.5: Member Size Comparison: Structural Plans vs. New Point Cloud

Frame Locations	Structural Plans	New PC	Cross-Sectional Area % Difference
Vertical at Base Joints 1-2	W18x65	W18x55	16.4%
Vertical at Base Joints 11-12	W10x49	W10x60	20.0%
Vertical at Base Joints 24-25	W12x65	W12x72	10.4%
L-Diagonals	L3x3x3/8	L3x3x3/8	0.0%
W-Diagonals at Joint 10	W8x28	W8x31	9.2%
W-Diagonals at Joint 15	W6x15	W6x20	29.1%
W-Diagonals between Joints 18 & 33, 19 & 34	W30x90	W30x90	0.0%
Horizontal at Joints 3-4	W18x35	W8x18	64.1%
Horizontals at Joints 8-9, 18-19	W18x65	W18x55	16.4%
Horizontals at Joints 20-23, 31-34	W16x40	W16x50	21.9%
Horizontal at Joints 13-14	W8x31	W8x40	25.0%
Horizontals between Joints 6 & 13, 7 & 14	W8x31	W8x31	0.0%
Horizontals between Joints 16 & 29, 17 & 30	W10x49	W10x45	7.9%
		Average =	17.0%
		True Average=	**13.0%**

4.4.2 Displacement and Reaction Comparison

For the displacements, Table 4.6 pits the results founded from the original point cloud to those of this study. As can be seen by the percentage differences, there was a varied gap of percent difference ranging from nearly 0% to just under 30%. Similarly, Table 4.7 shows the displacement percent difference between the point cloud from the original study and the structural plans of the stadium. The percent difference in this comparison ranged between nearly 0% to just over 26%. Table 4.8 displays the displacement percent difference between the new point cloud and the

structural plans. These results produced a visibly higher percent difference when compared to the values seen in Table 4.7 which is expected after the results seen in Table 4.6. The new point cloud differed in displacement values from a range starting just over 25% to just over 39%.

Table 4.6: Displacement comparison between point cloud models

Joint Displacements, U_3 (in)			
Joint Number	**Original PC**	**New PC**	**% Difference**
8	-0.007	-0.005	21.6
9	-0.007	-0.006	12.7
18	-0.017	-0.013	25.6
19	-0.018	-0.013	29.4
20	-0.164	-0.116	29.2
21	-0.153	-0.109	28.8
31	-0.027	-0.027	0.6
32	-0.028	-0.027	5.0

Table 4.7: Displacement comparison between original point cloud and structural plans

Joint Displacements, U_3 (in)			
Joint Number	**Structural Plans**	**Original PC**	**% Difference**
8	-0.009	-0.007	24.7
9	-0.010	-0.007	26.3
18	-0.018	-0.017	4.4
19	-0.018	-0.018	0.1
20	-0.188	-0.164	12.9
21	-0.169	-0.153	9.4
31	-0.036	-0.027	24.2
32	-0.037	-0.028	24.5

Table 4.8: Percent difference between new point cloud and structural plans

Joint Displacements, U_3 (in)			
Joint Number	**Structural Plans**	**New PC**	**% Difference**
8	-0.009	-0.005	39.1
9	-0.010	-0.006	38.9
18	-0.018	-0.013	29.7
19	-0.018	-0.013	29.4
20	-0.188	-0.116	38.2
21	-0.169	-0.109	35.6
31	-0.036	-0.027	25.5
32	-0.037	-0.027	28.1

Tables 4.9-4.11 exhibit how the three data sources displacements differed from the displacements found by the model created by the on-site dimensions. The model was created with the member sizes dictated by the structural plans with the exception of the outlier member size that was clearly different from what was designed in the structured plan. That outlying member was assumed to be an 8x31 W-section consistent with the frame members around it. Overall, it can be seen that the new point cloud in this study was the most accurate in displacement value to the model created using the actual dimensions. The original point cloud did have two occurrences of higher accuracy than the new point cloud but failed to be more accurate in the remaining cases. The structural plans failed to produce legitimately accurate answers which could be due to its dimensioning being farther off from the actual dimensions, on average, as well different members being put in place during construction.

Table 4.9: Joint Displacement Comparison - On-Site Model vs. Original Point Cloud

Joint Displacements, U_3 (in)			
Joint Number	**On-Site Measurements**	**Original PC**	**% Difference**
8	-0.006	-0.007	17.8
9	-0.006	-0.007	14.2
18	-0.014	-0.017	22.3
19	-0.014	-0.018	27.8
20	-0.116	-0.164	41.7
21	-0.106	-0.153	44.9
31	-0.028	-0.027	3.6
32	-0.028	-0.028	1.3

Table 4.10: Joint Displacement Comparison - On-Site Model vs. Structural Plans

Joint Displacements, U_3 (in)			
Joint Number	**On-Site Measurements**	**Structural Plans**	**% Difference**
8	-0.006	-0.009	51.4
9	-0.006	-0.010	63.1
18	-0.014	-0.018	29.5
19	-0.014	-0.018	27.8
20	-0.116	-0.188	62.4
21	-0.106	-0.169	60.1
31	-0.028	-0.036	28.5
32	-0.028	-0.037	33.8

Table 4.11: Joint Displacement Comparison - On-Site Model vs. New Point Cloud

Joint Displacements, U_3 (in)			
Joint Number	**On-Site Measurements**	**New PC**	**% Difference**
8	-0.006	-0.006	2.7
9	-0.006	-0.006	0.5
18	-0.014	-0.013	9.0
19	-0.014	-0.013	9.7
20	-0.116	-0.117	0.8
21	-0.106	-0.110	4.2
31	-0.028	-0.027	4.3
32	-0.028	-0.027	3.8

The final results needing comparison were that of the base joint reactions. Table 4.12 is a representation of the difference in values between both sets of point cloud models. Unlike the displacements, these differences were found to be much closer with the greatest percent difference not exceeding 11%. With regard to the difference between the original point cloud model and the structural plans, Table 4.13 shows the original authors were able to obtain fairly accurate results as their largest percent difference did not exceed 12%. Similarly, the new point cloud model generated fairly accurate results and is shown in Table 4.14. The largest percent difference was under 12% when compared to the structural plans.

Table 4.12: Reaction comparison between point cloud models

Base Joint Reactions, F3 (Kips)			
Joint Number	**Original PC**	**New PC**	**% Difference**
1	8.57	8.09	5.7
2	7.81	7.37	5.6
11	18.18	18.38	1.1
12	17.67	17.68	0.1
24	25.65	28.38	10.7
25	26.06	28.18	8.1

Table 4.13: Reaction comparison between structural plans and original point cloud

Base Joint Reactions, F3 (Kips)			
Joint Number	**Structural Plans**	**Original PC**	**% Difference**
1	8.46	8.57	1.3
2	7.84	7.81	0.4
11	16.98	18.18	7.1
12	15.86	17.67	11.4
24	27.13	25.65	5.4
25	27.67	26.06	5.8

Table 4.14: Reaction comparison between structural plans and new point cloud

Base Joint Reactions, F3 (Kips)			
Joint Number	**Structural Plans**	**New PC**	**% Difference**
1	8.46	8.09	4.5
2	7.84	7.37	6.0
11	16.98	18.38	8.2
12	15.86	17.68	11.5
24	27.13	28.38	4.6
25	27.67	28.18	1.8

The last set of table comparisons is the reactions found by the on-site dimension model against the three other data sources. Tables 4.15-4.17 detail the percent differences in each case. In all three cases, it can be concluded that all the data sources were capable of providing accurate results. Most accurate of all was the original point cloud results which was not the case for the dimension or displacement results. This gives the indication that although a point cloud may be less accurate in one aspect of a structure's behavior, it can be more precise in a different area. The structural plans had percent differences all fall below 10.5%, the new point cloud all fall below 6.2% and the original point cloud fall below 5.9% including four reactions that were nearly identical to the true reaction of the structure.

Table 4.15: Base Joint Reaction Comparison - On-Site Model vs Original Point Cloud

Base Joint Reactions, F3 (Kips)			
Joint Number	**On-Site Measurements**	**Original PC**	**% Difference**
1	8.573	8.574	0.0
2	7.861	7.812	0.6
11	18.252	18.181	0.4
12	17.721	17.666	0.3
24	27.255	25.652	5.9
25	26.912	26.063	3.2

Table 4.16: Base Joint Reaction Comparison - On-Site Model vs Structural Plans

Base Joint Reactions, F3 (Kips)			
Joint Number	**On-Site Measurements**	**Structural Plans**	**% Difference**
1	8.573	8.463	1.3
2	7.861	7.841	0.3
11	18.252	16.983	7.0
12	17.721	15.861	10.5
24	27.255	27.13	0.5
25	26.912	27.674	2.8

Table 4.17: Base Joint Reaction Comparison - On-Site Model vs New Point Cloud

Base Joint Reactions, F3 (Kips)			
Joint Number	**On-Site Measurements**	**New PC**	**% Difference**
1	8.573	8.085	5.7
2	7.861	7.374	6.2
11	18.252	18.381	0.7
12	17.721	17.678	0.2
24	27.255	28.384	4.1
25	26.912	28.177	4.7

Figures 4.16 and 4.17 show a box and whisker diagram representing the ranges and averages of the percent differences found for each data source compared to the on-site model. These averages are marked with an ‘X’ alongside red lines indicating the differences between the averages of each point cloud set. For the displacements, Figure 3.16 shows that the new point cloud was the data source with the smallest range and the smallest average percent difference at about 4.4%. The largest range was found for the original point cloud which had a higher percent difference average (22%) than the original point cloud but proved to have a smaller percent difference average than the structural plans (45%). Overall, the differences between these averages are shown via the red lines indicating the exact difference in average that exists between the data sources.

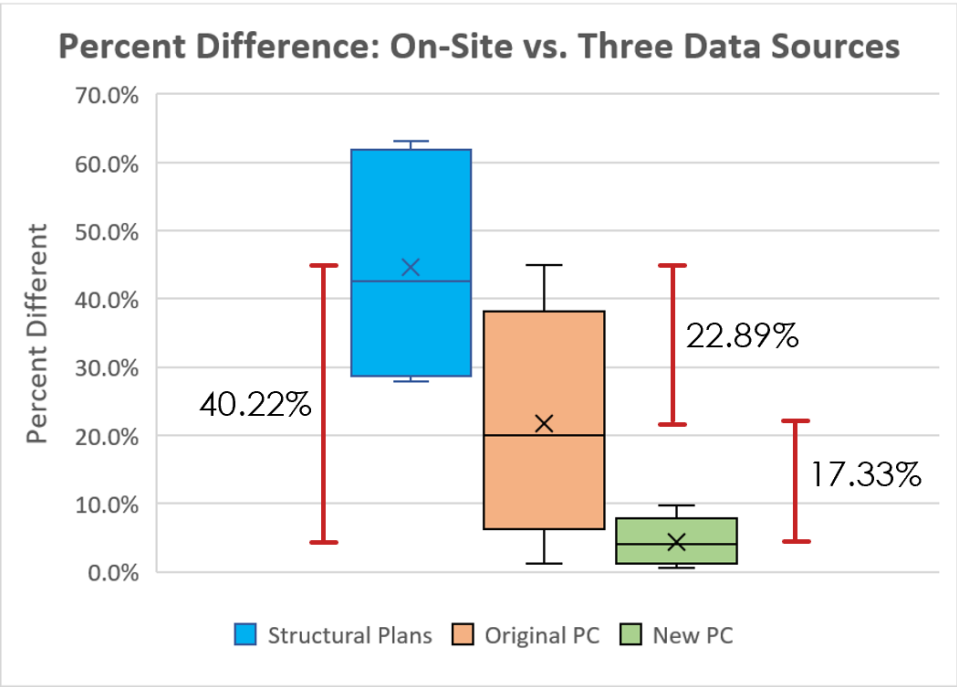

Figure 4.16: Ranges and averages of displacement percent difference given by the three data sources when compared to the on-site model

Unlike the displacement comparison, the base reaction box and whisker diagram shown in Figure 3.17 shows a much smaller difference in percent difference results. The differences between the average percent difference three data sources when compared to the on-site model never exceeded 2%. Additionally, the original point cloud proved to have the smallest percent difference average while the new point cloud and structural plans had nearly the same average percent difference. The structural plans however, had the largest range of the three data sources. All the averages for the data sources never exceeded 4% indicating a much more accurate collection of results than those found through the displacements.

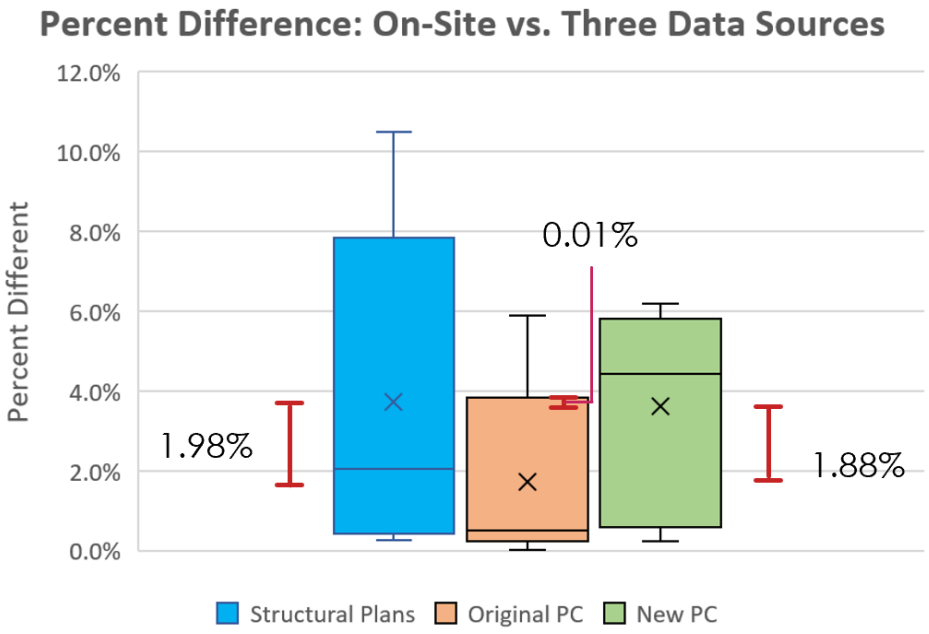

Figure 4.17: Ranges and averages of base reaction percent difference given by the three data sources when compared to the on-site model

CHAPTER 5 - PEDESTRIAN BRIDGE ANALYSIS

5.1 Structural Plans Analysis

5.1.1 Model Generation Using Structural Plans

Using Autodesk Inventor, a model of Parking Garage VI - H Pedestrian Bridge was created based on the structural plans. The structural materials were defined on SAP2000 following the steps presented in Section 4.1. ASTM A500 was used for the HSS sections and ASTM A572 for the wide flange beams. The section properties were defined via use of the materials list within the structural plans and are seen in Table 5.1. These sections include HSS10x10x3/8 for the top and bottom chords, HSS6x4x3/8 for the vertical and splice vertical members, HSS10x10x3/8 for the end vertical members of span 2, HSS10x4x3/8 for the end vertical members of span 1 and 3, HSS4x4x1/4 for the diagonal members, HSS3x3x1/4 for the brace diagonal members, and W12x22 for the floor beams and the splice floor beams.

Table 5.1: Member Sizes Given by Structural Plans

Key	Location	Member Section
A	Top Chord	HSS 10x10x3/8
B	Bottom Chord	HSS 10x10x3/8
C	Vertical/Splice Vertical	HSS 6x4x3/8
D	End Vertical - Span 2	HSS 10x10x3/8
E	End Vertical - Spans 1 & 3	HSS 10x4x3/8
F	Diagonal	HSS 4x4x1/4
G	Brace Diagonal	HSS 3x3x1/4
H	Floor Beam	W12x22

To represent the concrete deck, which has a minimum compressive strength of 4,000 psi and a maximum weight of 145 pcf, distributed loads were applied to the floor beams and splice floor beams. The distributed loads were calculated based on a 5-inch deck and a tributary width of 8 feet except as noted in Appendix F. For the dynamic modal analysis, only the dead load was taken into account. For the static analysis, an additional 100 psf was added to floor beams as stated in the structural plans. Figure 5.1 shows the undeformed shape of the bridge once imported into SAP2000.

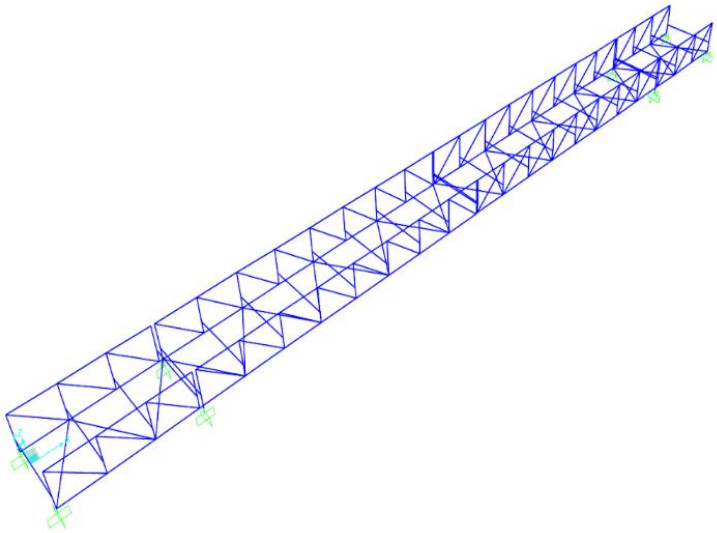

Figure 5.1: Image from SAP2000: Undeflected frame model

5.1.2 Structural Plans Static Analysis Results

The bridge underwent static analysis in SAP2000 based on the dimensions and sections listed in the structural plans. The structure was subjected to both dead and live load, provided by the structural plans, and produced the deformed shape seen in Figure 5.2. The largest deformation

occurred at the midpoints of the center span with a value of -3.66 inches in the Z-direction. The deformation of the center span of the structure and the location of its maximum displacement are labeled in Figure 5.3. Additionally, Figure 5.4 shows the location of the base joints and Table 5.2 shows the reactions founded at these points on the bridge structure. Note, only four reactions are shown because the bridge is symmetrical and the end span on the opposite end of the bridge produced the same reaction forces.

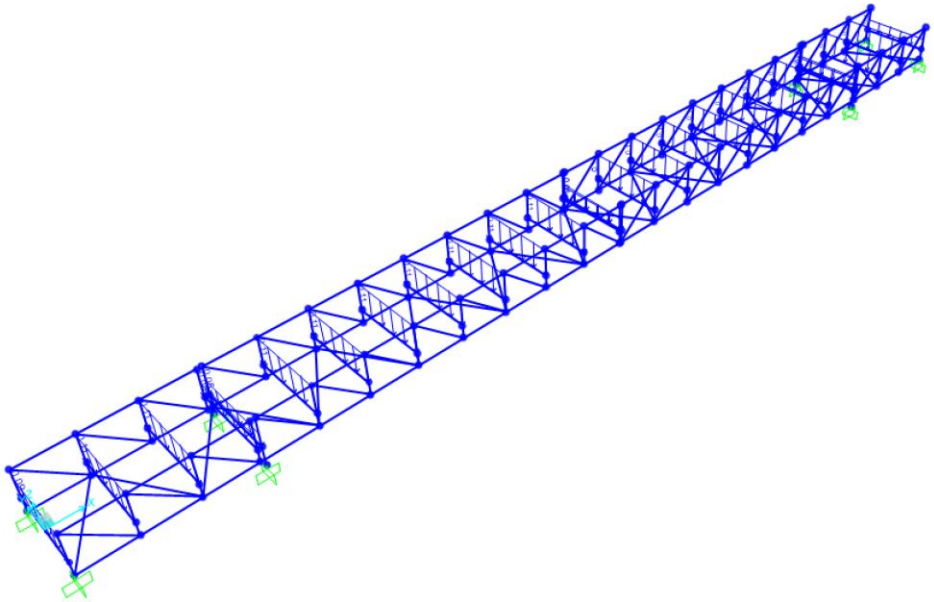

Figure 5.2: Dead and live load on structural plan model

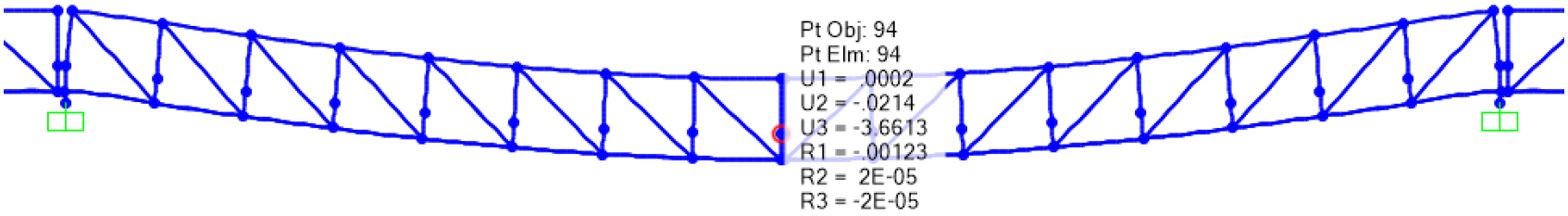

Figure 5.3: Deformed shape of structural plan model after loads are applied. Maximum deflection occurs at the node 94 circled in red having a value of U_3 = -3.6613 in

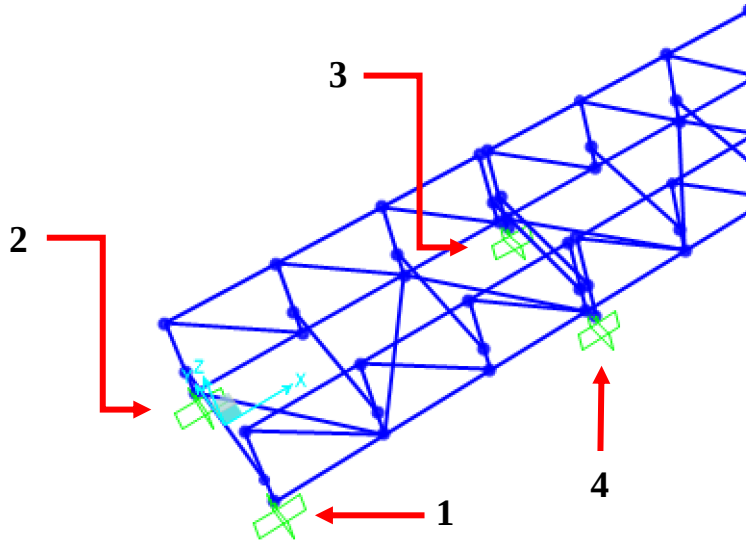

Figure 5.4: Base joint labeling for bridge models

Table 5.2: Base Joint Reactions for Structural Plans

Base Joint	Reactions, R_3 (kip)
1	11.44
2	11.43
3	79.41
4	79.47

5.1.3 Structural Plans Modal Shape Results

A dynamic modal analysis was performed for the structural plans in SAP2000 for Parking Garage VI - H Pedestrian Bridge. Nine modes were analyzed in total since following the eighth mode, the dynamic motion of the bridge became limited to the end spans. This is important to note because the movement of the first eight modes, as noted in the subsequent figures, is limited to the center span. Moreover, the upcoming figures are still images of the movement of the bridge in respect to each of its modes. The starting positions are an exaggeration of the movement created by SAP2000 in order to allow a user to visualize the behavior of movement given by the selected mode.

Figure 5.5 shows the first modal shape of the bridge rotating about the X-axis in a concave motion creating torsion. Mode 2, also shown in Figure 5.5, illustrates a bending movement of the bridge in the Z-direction. In mode 3, Figure 5.6, the bridge rotates about its X-axis in a convex motion in torsion. Figure 5.6, mode 4, shows the bridge moving laterally in the Y-direction in an out-of-phase motion with a slight rotation about its X-axis. In mode 5, Figure 5.7, the bridge bends in an out-of-phase motion in the Z-direction. In Figure 5.7, mode 6, the bridge moves laterally in the Y-direction with the ends moving in-phase while the center moves out-of-phase. In mode 7,

Figure 5.8, the bridge rotates about the X-axis out-of-phase with its mirrored sides on the X-Z Plane and Y-Z plane and with torsion. In Figure 5.8, mode 8, the bridge moves laterally in the Y-direction with two portions moving in-phase while the other two portions move out-of-phase with respect to the first two portions. Lastly, mode 9 shown in Figure 5.9 indicates that span 2 seizes to move in any direction while spans 1 and 3 begin to move in-phase laterally in the Y-direction.

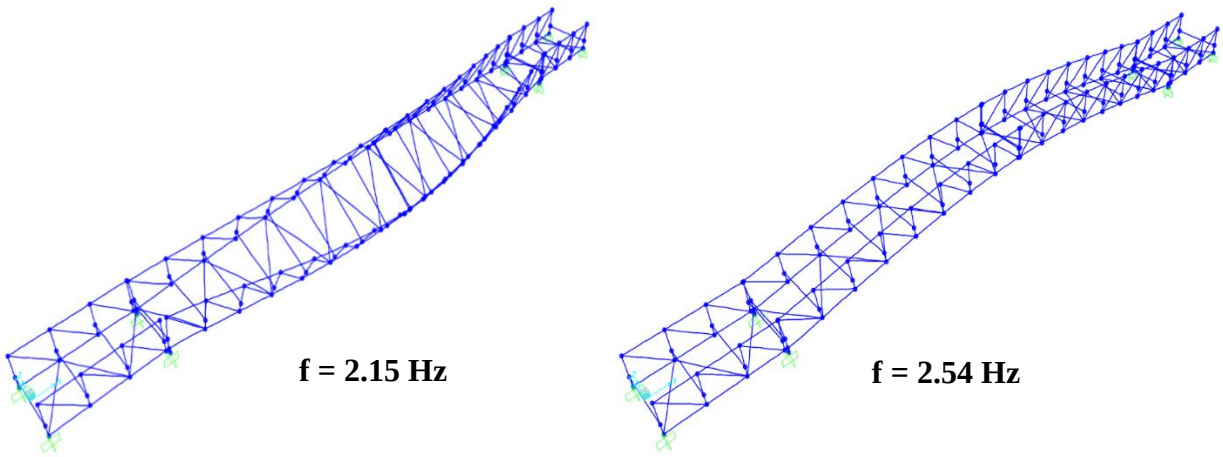

(a) (b)

Figure 5.5: Structural Plans - (a) Mode Shape 1; (b) Mode Shape 2

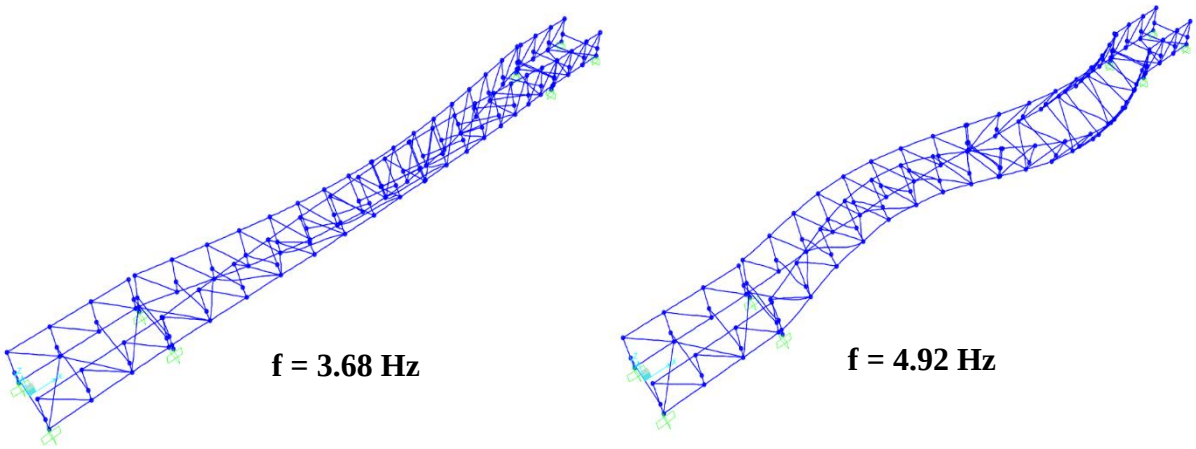

(a) (b)

Figure 5.6: Structural Plans - (a) Mode Shape 3; (b) Mode Shape 4

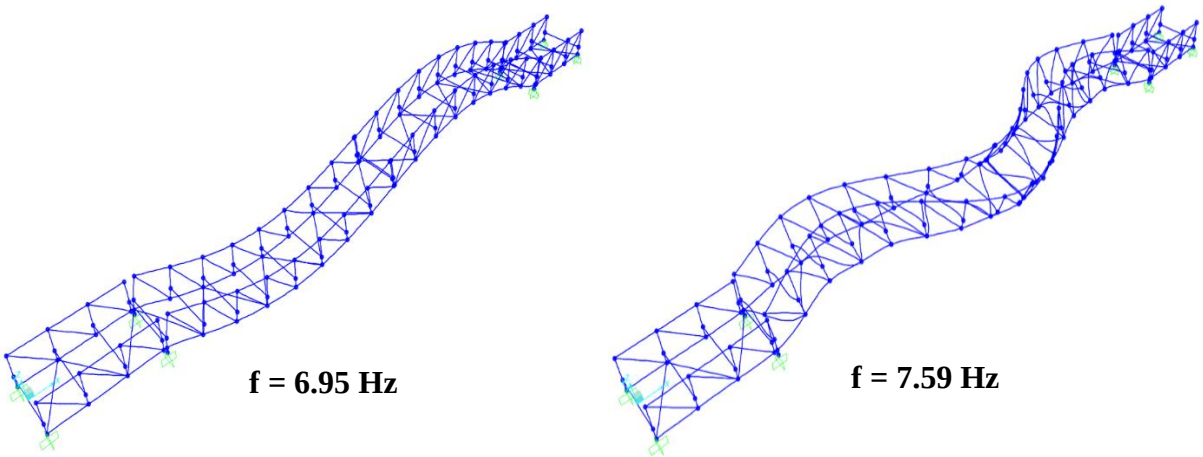

(a) (b)

Figure 5.7: Structural Plans - (a) Mode Shape 5; (b) Mode Shape 6

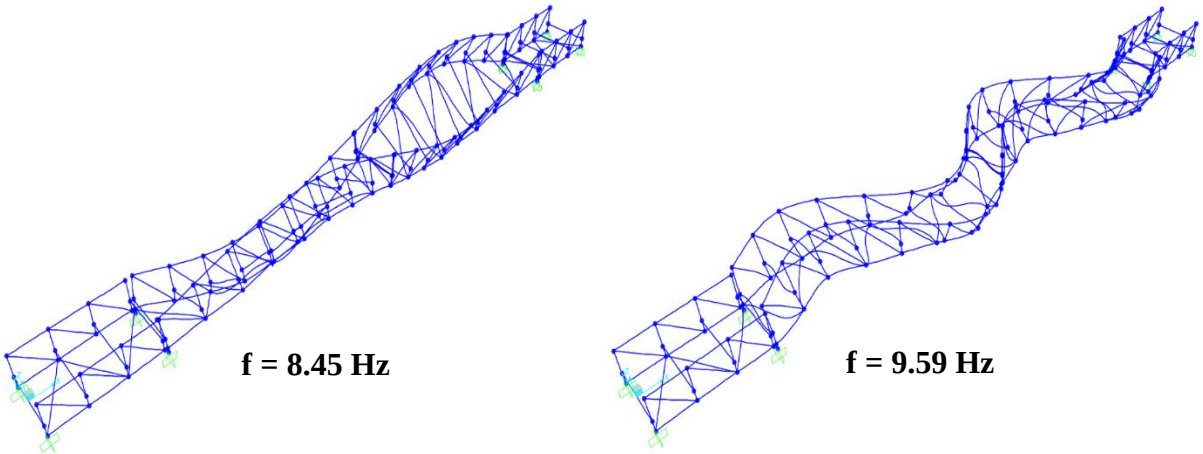

(a) (b)

Figure 5.8: Structural Plans - (a) Mode Shape 7; (b) Mode Shape 8

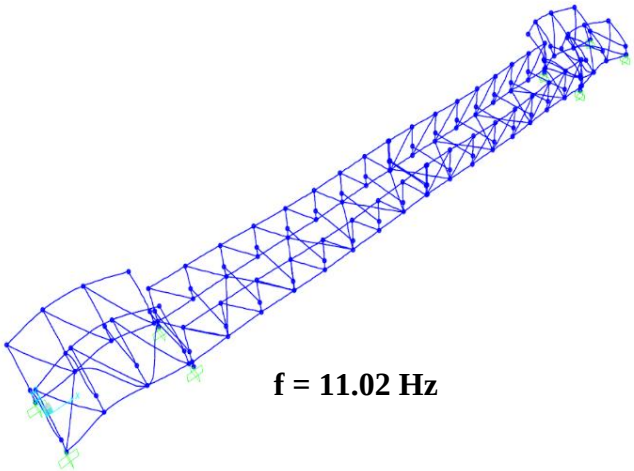

Figure 5.9: Structural Plans - Mode Shape 9

The modes shown in the previous figures have accompanying periods, frequencies and eigenvalues which are all displayed in Table 5.3. Table 5.4 illustrates the modal load participation factors found as a result of the structural plan model analysis. A comparison of all these results versus those produced through point cloud technology is further expanded upon in Section 5.3.

Table 5.3: Structural Plans - Modal Periods, Frequencies and Eigenvalues

Mode	Period (sec)	Frequency, f (Hz)	Eigenvalue, λ (rad^2/sec^2)
1	0.458	2.15	182.1
2	0.347	2.54	254.5
3	0.250	3.68	535.0
4	0.205	4.92	954.7
5	0.137	6.95	1907.2
6	0.134	7.59	2272.3
7	0.115	8.45	2816.9
8	0.105	9.59	3632.5
9	0.101	11.02	4793.8

Table 5.4: Structural Plans - Load Participation Factors

Direction	Static (%)	Dynamic (%)
U_X	10.37	1.70
U_Y	99.55	82.63
U_Z	99.15	56.46

5.2 Point Cloud Analysis

5.2.1 Model Generation Using Point Cloud

Following the registration process outlined in Section 3.5.2.2, Autodesk Recap was used to open the edited point cloud. Recap was chosen due to the program's ability of opening the file format Cyclone Register 360 uses. Recap also has the capability of turning scans on and off which directly affects the density of the point cloud. For the fine point cloud, all 11 scans were turned on which would take an on-site scanning time of 5 hours and 45 minutes. For the medium point cloud,

7 of the 11 scans were left on and the 4 remaining scans were turned off which would have taken an on-site scanning time of 3 hours. For the coarse point cloud, 4 of the 11 scans were left on and the 7 remaining scans were turned off which would have taken 1 hour and 36 minutes to scan on-site. This ability to turn scans off and on, provided by Recap, is the defining tool that allowed a user to establish three levels of point cloud density for comparison.

Once the appropriate density level was chosen, the file was saved as a rcp file in order to be compatible with Autodesk Inventor. Inventor was operated to render sections using the point cloud data inserted from Recap. The user of Inventor must use the point cloud visual as a base for estimating, to the best of their ability, an accurate section size for members of the pedestrian bridge. The same steps were followed from Section 4.1 once the point cloud visual was imported into Inventor.

5.2.2 Point Cloud Static Analysis Results

As done for the structural plans, the bridge underwent static analysis in SAP2000 based on the dimensions and sections rendered using the three point cloud densities. The structure was once again subjected to both dead and live load as provided by the structural plans. Each maximum deformation for each respective point cloud is seen in Figures 5.10-5.12. The largest deformation occurred at the midpoints of every point cloud model case but with varying values. For the fine point cloud, the maximum displacement was given as -3.53 inches as shown in Figure 5.10. For the medium point cloud, the maximum displacement was -3.03 inches as shown in Figure 5.11. Lastly, the coarse point cloud produced a maximum deformation of -3.47 inches as shown in Figure 5.12. Additionally, the base joint reactions for each set of point cloud data are shown in

Tables 5.5-5.8. The labeling of these base joints can be referred to in Figure 5.4 of section 5.1.2 as it is applicable to every model.

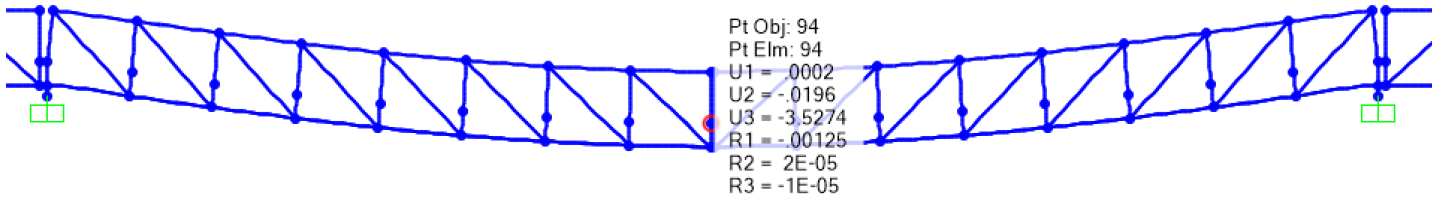

Figure 5.10: Deformed shape fine point cloud after loads are applied. Maximum deflection occurs at the node 94 circled in red having a value of U3 = -3.5274 in

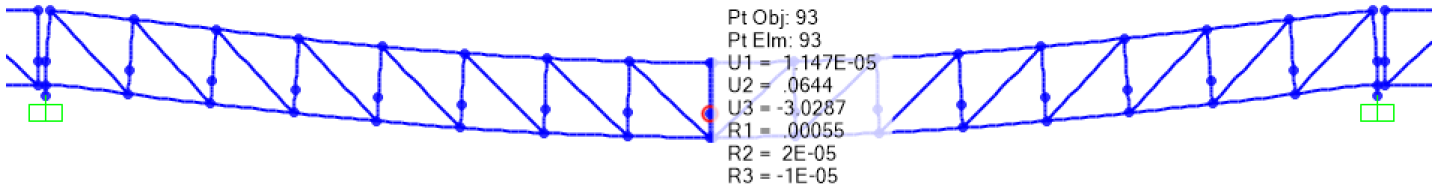

Figure 5.11: Deformed shape of medium point cloud after loads are applied. Maximum deflection occurs at the node 93 circled in red having a value of U3 = -3.0287 in

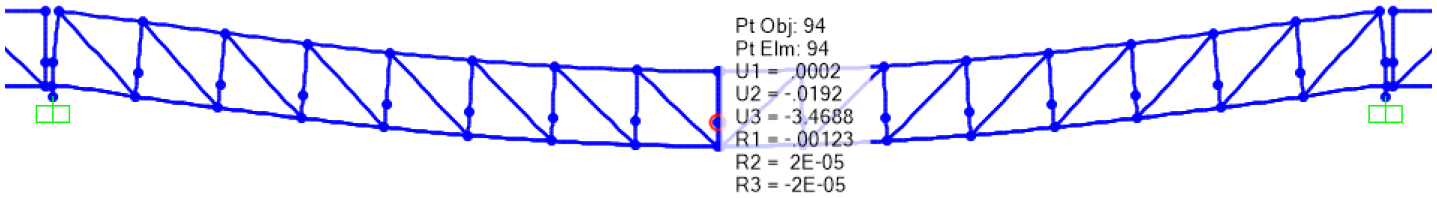

Figure 5.12: Deformed shape of coarse point cloud after loads are applied. Maximum deflection occurs at the node 94 circled in red having a value of U3 = -3.4688 in

Table 5.5: Base Joint Reactions for Fine Point Cloud

Base Joint	Reactions, R_3 (kip)
1	11.46
2	11.45
3	79.38
4	79.46

Table 5.6: Base Joint Reactions for Medium Point Cloud

Base Joint	Reactions, R_3 (kip)
1	11.47
2	11.72
3	79.47
4	79.09

Table 5.7: Base Joint Reactions for Coarse Point Cloud

Base Joint	Reactions, R_3 (kip)
1	11.44
2	11.43
3	79.41
4	79.47

5.2.3 Point Cloud Modal Shape Results

All nine modes for all three point clouds produced similar mode shapes to those given by the structural plans. The description of the mode shapes seen in Sections 5.2.2.1-5.2.2.3 can be referenced in Section 5.1.2 as their dynamic movement was the same as those seen for the structural plans for each respective mode. Although the still images of the bridge frame structure

may differ in their starting position from those seen in the structural plans, the movement itself remained identical. For all three point clouds, what differed consistently were the numeric values, albeit not drastically, which are shown via the frequencies given on the figures. Additionally, the time periods and eigenvalues of each mode for each point cloud density can be seen in the tables following each set of mode shapes. The results are further clarified in a comparative analysis given in Section 5.3.

5.2.3.1 Fine Point Cloud Modal Shapes

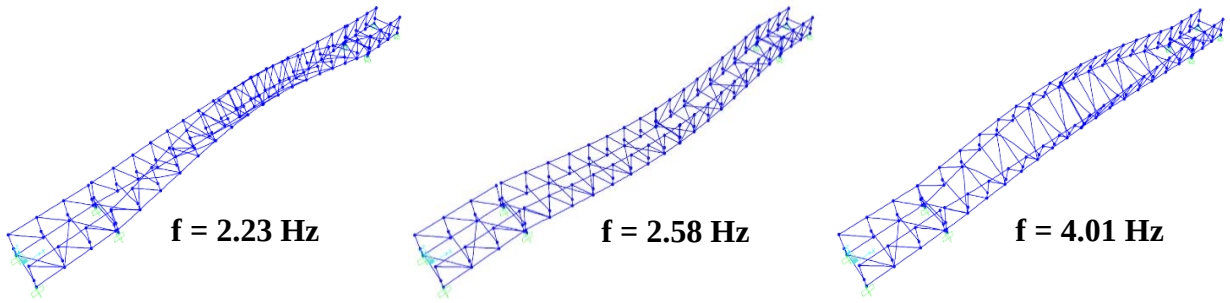

(a) (b) (c)

Figure 5.13: Fine Point Cloud - (a) Mode Shape 1; (b) Mode Shape 2; (c) Mode Shape 3

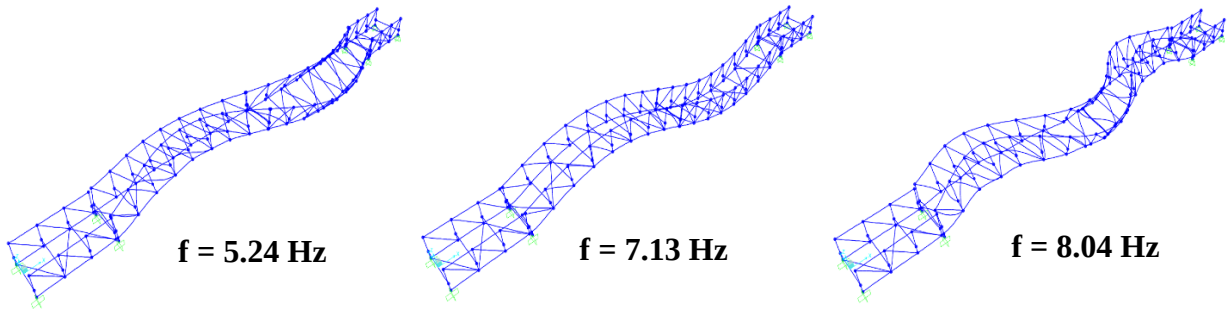

(a) (b) (c)

Figure 5.14: Fine Point Cloud - (a) Mode Shape 4; (b) Mode Shape 5; (c) Mode Shape 6

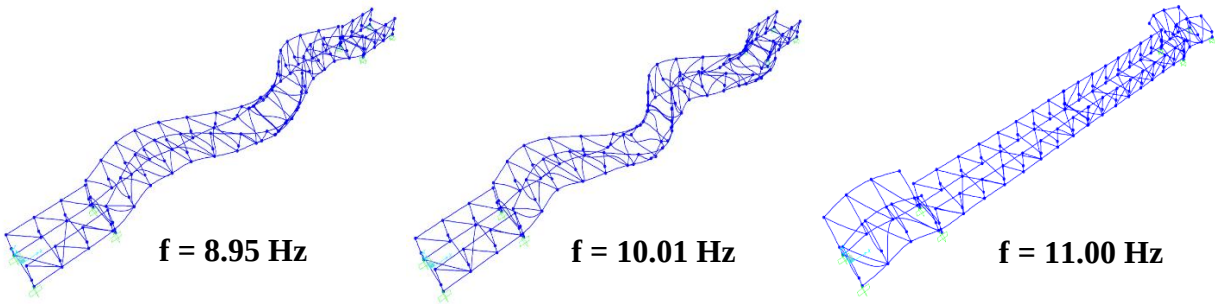

(a) (b) (c)

Figure 5.15: Fine Point Cloud - (a) Mode Shape 7; (b) Mode Shape 8; (c) Mode Shape 9

Table 5.8: Fine Point Cloud - Periods, Frequencies and Eigenvalues

Mode	**Period (sec)**	**Frequency, f (Hz)**	**Eigenvalue, λ (rad^2/sec^2)**
1	0.448	2.23	196.6
2	0.388	2.58	262.9
3	0.249	4.01	634.4
4	0.191	5.24	1083.2
5	0.140	7.13	2005.9
6	0.124	8.04	2554.9
7	0.112	8.95	3162.1
8	0.100	10.01	3958.8
9	0.091	11.00	4779.8

Table 5.9: Fine Point Cloud - Load Participation Factors

Direction	**Static (%)**	**Dynamic (%)**
U_X	11.31	1.93
U_Y	99.37	80.62
U_Z	99.20	56.27

5.2.3.2 Medium Point Cloud Modal Shapes

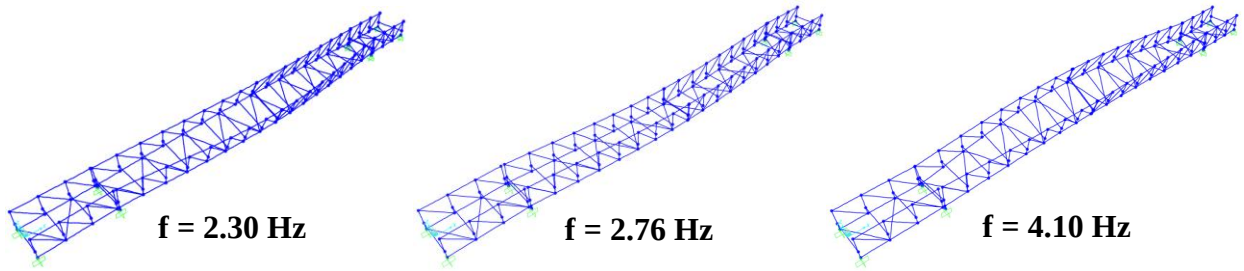

(a) (b) (c)

Figure 5.16: Medium Point Cloud - (a) Mode Shape 1; (b) Mode Shape 2; (c) Mode Shape 3

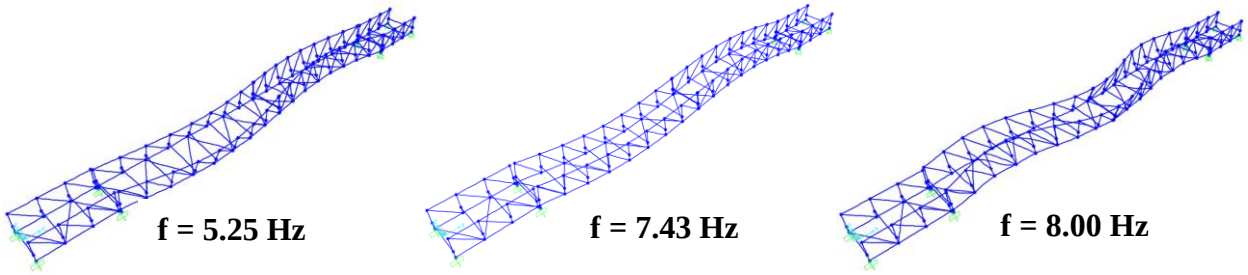

(a) (b) (c)

Figure 5.17: Medium Point Cloud - (a) Mode Shape 4; (b) Mode Shape 5; (c) Mode Shape 6

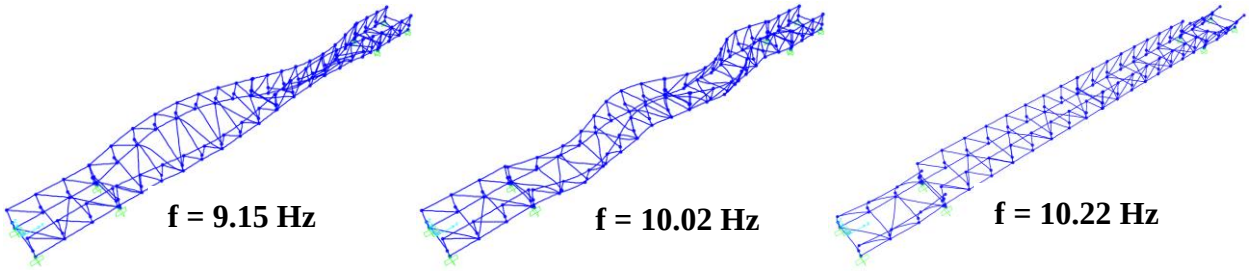

(a) (b) (c)

Figure 5.18: Medium Point Cloud - (a) Mode Shape 7 (b) Mode Shape 8; (c) Mode Shape 9

Table 5.10: Medium Point Cloud - Periods, Frequencies and Eigenvalues

Mode	Period (sec)	Frequency, f (Hz)	Eigenvalue, λ (rad^2/sec^2)
1	0.435	2.30	208.3
2	0.363	2.76	300.4
3	0.244	4.10	663.9
4	0.191	5.25	1087.0
5	0.135	7.43	2181.1
6	0.125	8.00	2529.0
7	0.109	9.15	3308.6
8	0.100	10.02	3964.3
9	0.098	10.22	4125.8

Table 5.11: Medium Point Cloud - Load Participation Factors

Direction	Static (%)	Dynamic (%)
U_X	11.16	1.97
U_Y	99.46	81.47
U_Z	99.60	63.42

5.2.3.3 Coarse Point Cloud Modal Shapes

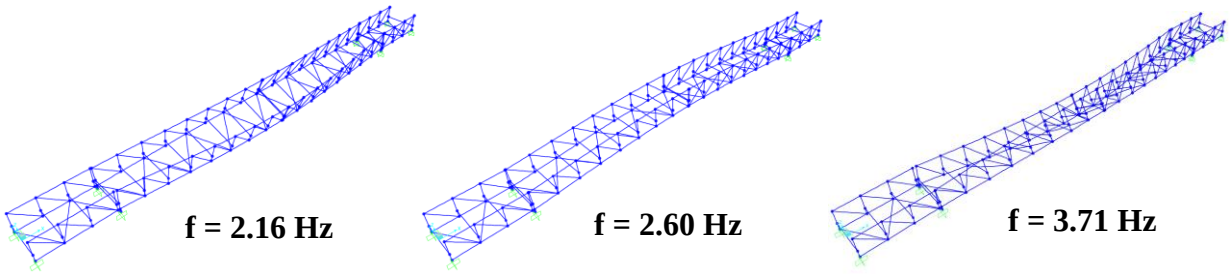

(a) (b) (c)

Figure 5.19: Coarse Point Cloud - (a) Mode Shape 1; (b) Mode Shape 2; (c) Mode Shape 3

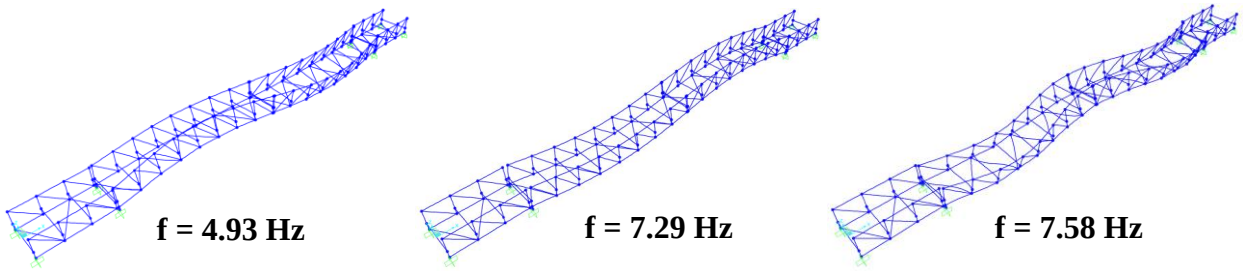

(a) (b) (c)

Figure 5.20: Coarse Point Cloud - (a) Mode Shape 4; (b) Mode Shape 5; (c) Mode Shape 6

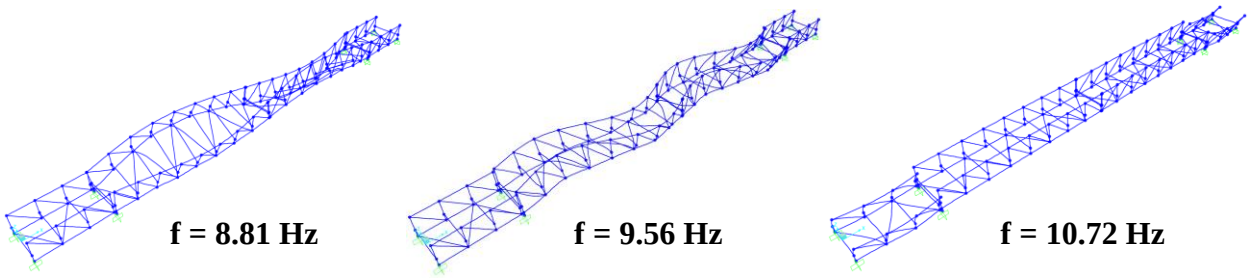

(a) (b) (c)

Figure 5.21: Coarse Point Cloud - (a) Mode Shape 7; (b) Mode Shape 8; (c) Mode Shape 9

Table 5.12: Coarse Point Cloud - Periods, Frequencies and Eigenvalues

Mode	**Period (sec)**	**Frequency, f (Hz)**	**Eigenvalue, λ (rad^2/sec^2)**
1	0.463	2.16	184.5
2	0.385	2.60	265.9
3	0.270	3.71	542.2
4	0.203	4.93	960.0
5	0.137	7.29	2095.4
6	0.132	7.58	2270.3
7	0.114	8.81	3060.9
8	0.105	9.56	3604.3
9	0.093	10.72	4539.9

Table 5.13: Coarse Point Cloud - Load Participation Factors

Direction	Static (%)	Dynamic (%)
U_X	12.25	2.21
U_Y	99.48	81.69
U_Z	99.24	56.55

5.3 Comparative Analysis Results

The results of the three point cloud models were compared to those of the structural plan model to observe any correlation between a point cloud's density and its accuracy of results. In terms of length, width, height and spacing, the three point clouds all proved extremely accurate when dimensioned alongside the structural plans. All the point cloud cases did not exceed ±1 inch from the structural plan measurements, in all three directions, providing an accuracy consistently near or above 99%. Having completed on-site measurements at the pedestrian bridge, the structural plans proved to have the same dimensions as the as-built structure with no difference exceeding ±1 inch. With this in mind, the structural plan model was taken as the representative of the results for the as-built structure which the point clouds aimed to match as closely as possible.

5.3.1 Static Analysis Comparison

For the structural analysis, percent difference became apparent between the three point cloud data sets when compared to the structural plans. The fine point cloud's maximum deflection differed by 3.7% making it quite close to the actual deformation value. The medium point cloud's maximum deflection differed by 17.3% which is expected when using a less dense point cloud.

The coarse point cloud however, differed by only 5.3% making it also close in value to the actual deflection value given by the structural plans. With that said, it can be seen that the fine point cloud proved the most accurate of the three point cloud densities.

In terms of base joint reactions, Tables 5.14-5.16 show the percent differences each point cloud set had when compared to the structural plans. The fine point cloud and the coarse point cloud produced extremely similar results with two base joints being near zero and the other two being in the high 17% range. The medium point cloud produced the most accurate results overall with only one base joint exceeding a 17% difference while another was under 16% and the final two were under 1%. This is the opposite of what was found for the deformation in which the medium point cloud produced the least accurate result.

Table 5.14: Base Joint Comparison: Structural Plans vs Fine Point Cloud

Base Joint	Structural Plans	Fine PC	% Difference
1	13.94	11.46	17.80
2	13.93	11.45	17.81
3	79.47	79.38	0.12
4	79.49	79.46	0.03

Table 5.15: Base Joint Comparison: Structural Plans vs Medium Point Cloud

Base Joint	Structural Plans	Medium PC	% Difference
1	13.94	11.47	17.74
2	13.93	11.72	15.82
3	79.47	79.47	0.01
4	79.49	79.09	0.50

Table 5.16: Base Joint Comparison: Structural Plans vs Coarse Point Cloud

Base Joint	Structural Plans	Coarse PC	% Difference
1	13.94	11.44	17.95
2	13.93	11.43	17.95
3	79.47	79.41	0.08
4	79.49	79.47	0.02

5.3.2 Dynamic Modal Analysis Comparison

For the dynamic modal analysis of the structural plans, the first mode yielded the longest period (T) and conversely, the lowest frequency (f). This is due to the direct relationship between periods and frequencies as derived in Equation 4. In order to obtain the eigenvalue, the natural frequency has to be found as shown in Equation 5. Once the natural frequency is calculated, Equation 6 is used to find the eigenvalue (λ) and shows the correlation between eigenvalues and natural frequencies. This link illustrates why the first mode also provided the lowest eigenvalue. As each mode progressed, the periods of the data sources would decrease dictating an increase in natural frequency and eigenvalue.

$$T = {}^{1}/_{\mathrm{f}} \tag{4}$$

$$\omega = 2\pi \times \mathrm{f} \tag{5}$$

$$\omega^2 = \lambda \tag{6}$$

In regards to the point cloud density cases, the results followed the same pattern produced by the structural plans. The first mode produced the longest period, the lowest frequency and the lowest eigenvalue. Consequently, the last mode produced the shortest period, highest frequency and highest eigenvalue. The 9th mode was shown in all the analysis models as it indicated that the frequency reached a high enough value to affect the shorter end spans rather than the central span.

5.3.2.1 Fine Point Cloud Comparison

When the point cloud results are compared to those of the structural plans, percent differences become evident which can be attributed to the different member sizes rendered for the two data sources as shown in Table 5.17. The member size changes are highlighted in yellow and the guide to the Key is shown in Appendix G. What can be seen is that for HSS members, obtaining the correct width and height for the members is easily done but obtaining the correct thickness is extremely difficult to match correctly. The largest cross-sectional area percent difference was 32.1% while three others were below 30%. Half the members rendered were an exact match for the members given in the structural plans. Overall, the average cross-sectional area difference was just under 12% considering all the members of the structure.

Table 5.18 shows the first sets of result comparisons between the structural plans and the fine point cloud case. Since the period and frequency are directly associated, both contain almost the same percent differences for each mode. This is supported by the fact that no period or frequency varies by any more than 0.73% for the same mode which can be attributed to rounding errors. The percent differences were calculated in respect to the original structural plan values. The overall percent differences for the periods and frequencies ranged between 0.15% - 8.89%

confirming that the fine point cloud member sizes were not identical to those given by the structural plans. The point cloud values were found to have shorter periods and higher frequencies compared to the structural plan values with the exception of the final mode. This result reinforced the decision to terminate the assessment at the ninth mode since the values no longer followed the pattern seen in modes 1-8.

The percent differences were magnified in the eigenvalue results since they represent the squared value of natural frequencies. The percent difference doubled from the values seen between the period and frequency for each respective mode. The percentages ranged from 0.58% - 19.6% giving the results a more noticeable difference. Similar to the comparison mentioned before, the point cloud values had higher eigenvalues than the structural plans in all modes except the ninth.

Table 5.17: Member Size Comparison - Fine Point Cloud vs. Structural Plans

Key	**Location**	**Structural Plans**	**Fine PC**	**Cross-Sectional Area % Difference**
A	Top Chord	HSS 10x10x3/8	HSS 10x10x3/8	0.0%
B	Bottom Chord	HSS 10x10x3/8	HSS 10x10x3/8	0.0%
C	Vertical/Splice Vertical	HSS 6x4x3/8	HSS 6x4x5/16	16.1%
D	End Vertical - Span 2	HSS 10x10x3/8	HSS 10x10x1/2	26.5%
E	End Vertical - Spans 1 & 3	HSS 10x4x3/8	HSS 10x4x3/8	0.0%
F	Diagonal	HSS 4x4x1/4	HSS 4x4x5/16	19.4%
G	Brace Diagonal	HSS 3x3x1/4	HSS 3x3x3/8	32.1%
H	Floor Beam	W12x22	W12x22	0.0%
			Average =	**11.8%**

Table 5.18: Result Comparison - Fine Point Cloud vs. Structural Plans

Mode	Period, T (sec)		% Difference	Frequency, f (Hz)		% Difference	Eigenvalue, λ (rad^2/sec^2)		% Difference
	Structural Plans	Fine PC		Structural Plans	Fine PC		Structural Plans	Fine PC	
1	0.466	0.448	3.74	2.15	2.23	3.89	182.1	196.6	7.92
2	0.394	0.388	1.61	2.54	2.58	1.63	254.5	262.9	3.29
3	0.272	0.249	8.16	3.68	4.01	8.89	535.0	634.4	18.57
4	0.203	0.191	6.12	4.92	5.24	6.52	954.7	1083.2	13.46
5	0.144	0.140	2.49	6.95	7.13	2.56	1907.2	2005.9	5.18
6	0.132	0.124	5.69	7.59	8.04	6.04	2272.3	2554.9	12.44
7	0.118	0.112	5.62	8.45	8.95	5.95	2816.9	3162.1	12.26
8	0.104	0.100	4.21	9.59	10.01	4.40	3632.5	3958.8	8.98
9	0.091	0.091	0.15	11.02	11.00	0.15	4793.8	4779.8	0.29

The dynamic modal load participation factors of the individual data sources are compared in Table 5.19. Since the values themselves are already percentages, the percent difference is taken as the difference between the two values. As shown, the participation factor results proved to be in close proximity in all three directions with the largest difference barely exceeding 2%. A further explanation of these values is touched upon in the conclusion of this report.

Table 5.19: Load Participation Comparison - Fine Point Cloud vs. Structural Plans

Direction	Static (%)		% Difference	Dynamic (%)		% Difference
	Structural Plans	Fine PC		Structural Plans	Fine PC	
U_X	10.37	11.31	0.94	1.70	1.93	0.23
U_Y	99.55	99.37	0.19	82.63	80.62	2.01
U_Z	99.15	99.20	0.05	56.46	56.27	0.19

5.3.2.2 Medium Point Cloud Comparison

As expected, the medium point cloud produced a less accurate cross-sectional area average than that found for the fine point cloud. The member size comparison chart is shown in Table 5.20. The member size differences are highlighted in yellow and the guide to the Key is shown in Appendix G. Once again, the height and widths of the HSS members matched well but the thickness were difficult to match. The largest cross-sectional area percent difference was once again 32.1% while two others were below 30%. Two of the members rendered were a match of the members given in the structural plans. Overall, the average cross-sectional area difference was about 17% which was just over 5% worse than that found in the fine point cloud.

As was the case for the highest density point cloud, the medium density cloud had little variance between the periods and frequencies of the same mode. The values differed by no more than 1.2% which is slightly worse than the 0.73% seen in the fine point cloud also due to rounding errors. The overall percent differences, for the periods and frequencies, differed in range from the values observed for the fine point cloud. Table 5.21 displays the percent differences of the period and frequencies, found via the medium point cloud, ranging between 4.28% - 11.4%. This range confirms two findings: 1) The point cloud rendering of member sizes differed from those in the structural plans as well as fine point cloud; 2) The medium point cloud had larger percent differences when compared to those of the fine point cloud.

As expected, the medium point cloud produced results less accurate than the fine point cloud in all the modes except for the 6^{th}. Although less accurate, the medium point cloud never strayed more than 7.2% worse than the fine point cloud indicating the proximity the values had between the point clouds. The percent difference for the eigenvalues essentially doubled from the values seen between the period and frequency for each respective mode. The percent differences ranged from 9.13% - 24.08% giving yet another indication of the decrease in accuracy produced by the medium point cloud. The difference in percentages for eigenvalues between the two point clouds, whether more or less accurate, did not exceed 15% for any mode.

Table 5.20: Member Size Comparison - Medium Point Cloud vs. Structural Plans

Key	Location	Structural Plans	Medium PC	Cross-Sectional Area % Difference
A	Top Chord	HSS 10x10x3/8	HSS 10x10x1/2	26.5%
B	Bottom Chord	HSS 10x10x3/8	HSS 10x10x1/2	26.5%
C	Vertical/Splice Vertical	HSS 6x4x3/8	HSS 6x4x3/8	0.0%
D	End Vertical - Span 2	HSS 10x10x3/8	HSS 10x10x3/8	0.0%
E	End Vertical - Spans 1 & 3	HSS 10x4x3/8	HSS 10x4x5/16	16.7%
F	Diagonal	HSS 4x4x1/4	HSS 4x4x5/16	19.4%
G	Brace Diagonal	HSS 3x3x1/4	HSS 3x3x3/8	32.1%
H	Floor Beam	W12x22	W12x19	15.1%
			Average =	**17.0%**

Table 5.21: Results Comparison - Medium Point Cloud vs. Structural Plans

Mode	Period, T (sec)		% Difference	Frequency, f (Hz)		% Difference	Eigenvalue, λ (rad^2/sec^2)		% Difference
	Structural Plans	Medium PC		Structural Plans	Medium PC		Structural Plans	Medium PC	
1	0.466	0.435	6.49	2.15	2.30	6.94	182.1	208.32	14.37
2	0.394	0.363	7.95	2.54	2.76	8.64	254.5	300.36	18.02
3	0.272	0.244	10.2	3.68	4.10	11.4	535.0	663.89	24.08
4	0.203	0.191	6.28	4.92	5.25	6.70	954.7	1086.98	13.86
5	0.144	0.135	6.49	6.95	7.43	6.94	1907.2	2181.13	14.36
6	0.132	0.125	5.21	7.59	8.00	5.50	2272.3	2529.04	11.30
7	0.118	0.109	7.73	8.45	9.15	8.38	2816.9	3308.64	17.46
8	0.104	0.100	4.28	9.59	10.02	4.47	3632.5	3964.26	9.13
9	0.091	0.098	7.79	11.02	10.22	7.23	4793.8	4125.82	13.93

Table 5.22 presents the dynamic modal load participation factors comparison between the medium point cloud model and the structural plans. Similar to the fine point cloud, the medium point cloud produced very small differences in the load participation factors. The largest difference was noted at 6.96% which was more than three times the largest provided by the fine point cloud. The fine point cloud also produced the most accurate percent difference of 0.05% compared to the medium point cloud's 0.10%. These numbers indicate that although the point clouds may differ in accuracy for certain aspects of the structure, they provide quite similar results when compared.

Table 5.22: Load Participation Comparison - Medium Point Cloud vs. Structural Plans

Direction	**Static (%)**		**% Difference**	**Dynamic (%)**		**% Difference**
	Structural Plans	**Medium PC**		**Structural Plans**	**Medium PC**	
U_X	10.37	11.16	0.78	1.70	1.97	0.27
U_Y	99.55	99.46	0.10	82.63	81.47	1.16
U_Z	99.15	99.60	0.45	56.46	63.42	6.96

5.3.2.3 Coarse Point Cloud Comparison

Surprisingly, the coarse point cloud produced the most accurate member size matches when compared to the two previous point clouds. The differences in member sizes are seen in Table 5.23. As can be seen, all but two member sizes matched those found in the structural plans. The two members that differed were by a percentage of 16.7% and 21.6% respectively. Having so many matching members lowered the average cross-sectional area difference to just under 5% making the coarse point cloud the most accurate of the three point clouds in terms of member sizes.

The variances between the percent differences for periods and frequencies once more resulted in little discrepancy. The values fluctuated by no more than 0.22% which was the smallest difference of all three point clouds. Table 5.24 displays the percent differences of the period and frequencies, found via the coarse point cloud, ranging between 0.04% - 4.82%. This range was the smallest in range and value making it the most accurate of the three point clouds. Although it was the most accurate overall, it was slightly less accurate in 3 of the 9 modes when compared to both the fine and medium clouds. Even with three less accurate modes, the coarse point cloud was neither more or less accurate than the other two data sources by any more than 11%. The percent difference for the eigenvalues ranged from 0.09% - 9.86% further establishing the accuracy found through this point cloud data set. The difference in percentages between all three point clouds, in respect to eigenvalues, never differed by more than 23% at any point during its worst case. Overall, the coarse point cloud proved slightly more accurate in all three facets of results.

Table 5.23: Member Size Comparison - Coarse Point Cloud vs. Structural Plans

Key	**Location**	**Structural Plans**	**Coarse PC**	**Cross-Sectional Area % Difference**
A	Top Chord	HSS 10x10x3/8	HSS 10x10x3/8	0.0%
B	Bottom Chord	HSS 10x10x3/8	HSS 10x10x3/8	0.0%
C	Vertical/Splice Vertical	HSS 6x4x3/8	HSS 6x4x3/8	0.0%
D	End Vertical - Span 2	HSS 10x10x3/8	HSS 10x10x3/8	0.0%
E	End Vertical - Spans 1 & 3	HSS 10x4x3/8	HSS 10x4x5/16	16.7%
F	Diagonal	HSS 4x4x1/4	HSS 4x4x3/8	21.6%
G	Brace Diagonal	HSS 3x3x1/4	HSS 3x3x1/4	0.0%
H	Floor Beam	W12x22	W12x22	0.0%
			Average =	**4.8%**

Table 5.24: Results Comparison - Coarse Point Cloud vs. Structural Plans

Mode	Period, T (sec)		% Difference	Frequency, f (Hz)		% Difference	Eigenvalue, λ (rad^2/sec^2)		% Difference
	Structural Plans	Coarse PC		Structural Plans	Coarse PC		Structural Plans	Coarse PC	
1	0.466	0.463	0.65	2.15	2.16	0.65	182.1	184.52	1.31
2	0.394	0.385	2.16	2.54	2.60	2.21	254.5	265.87	4.47
3	0.272	0.270	0.66	3.68	3.71	0.66	535.0	542.17	1.33
4	0.203	0.203	0.27	4.92	4.93	0.29	954.7	959.97	0.55
5	0.144	0.137	4.60	6.95	7.29	4.82	1907.2	2095.36	9.86
6	0.132	0.132	0.04	7.59	7.58	0.05	2272.3	2270.30	0.09
7	0.118	0.114	4.07	8.45	8.81	4.26	2816.9	3060.85	8.66
8	0.104	0.105	0.39	9.59	9.56	0.36	3632.5	3604.34	0.77
9	0.091	0.093	2.76	11.02	10.72	2.68	4793.8	4539.86	5.30

Table 5.25 presents the dynamic modal load participation factors comparison between the coarse point cloud model and the structural plans. Similar to the previous point clouds, the coarse cloud produced very small differences in the load participation factors. The largest difference was observed to be 1.88% which was the smallest worst-case difference for all three point clouds; however, the coarse point cloud proved to garner a mixture of more and less accurate results in when compared to the medium and fine point clouds. This outcome solidifies that the point clouds can prove to be more accurate in one aspect of a structure and less accurate in another but still maintain a certain level of accuracy tolerance throughout the system.

Table 5.25: Load Participation Comparison - Coarse Point Cloud vs. Structural Plans

Direction	Static (%)		% Difference	Dynamic (%)		% Difference
	Structural Plans	Coarse PC		Structural Plans	Coarse PC	
U_X	10.37	12.25	1.88	1.70	2.21	0.51
U_Y	99.55	99.48	0.08	82.63	81.69	0.94
U_Z	99.15	99.24	0.09	56.46	56.55	0.08

5.3.3 Point Cloud Frequency Comparison

Tables 5.26 – 5.28 display the percent differences between each point cloud when compared against each other for each respective mode. As can be seen in these tables, the percent difference of the numerical values found all fall under 10% for the same mode. Only one of these percent differences was above 9% while all others fell below 8%. This consistent percent difference symbolizes the propinquity of the results produced by all three point clouds. These

differences can be almost completely attributed to member size differences but still show relative accuracy between each point cloud set.

Table 5.26: Point Cloud Frequency Comparison - Fine vs Medium

Frequency, f (Hz)			
Mode	**Fine PC**	**Medium PC**	**% Difference**
1	2.23	2.30	2.94
2	2.58	2.76	6.89
3	4.01	4.10	2.30
4	5.24	5.25	0.18
5	7.13	7.43	4.28
6	8.04	8.00	0.51
7	8.95	9.15	2.29
8	10.01	10.02	0.07
9	11.00	10.22	7.09

Table 5.27: Point Cloud Frequency Comparison - Fine vs Coarse

Frequency, f (Hz)			
Mode	**Fine PC**	**Coarse PC**	**% Difference**
1	2.23	2.16	3.12
2	2.58	2.60	0.57
3	4.01	3.71	7.55
4	5.24	4.93	5.85
5	7.13	7.29	2.21
6	8.04	7.58	5.74
7	8.95	8.81	1.60
8	10.01	9.56	4.56
9	11.00	10.72	2.54

Table 5.28: Point Cloud Frequency Comparison - Medium vs Coarse

Frequency, f (Hz)			
Mode	**Medium PC**	**Coarse PC**	**% Difference**
1	2.30	2.16	5.89
2	2.76	2.60	5.92
3	4.10	3.71	9.63
4	5.25	4.93	6.01
5	7.43	7.29	1.98
6	8.00	7.58	5.25
7	9.15	8.81	3.80
8	10.02	9.56	4.62
9	10.22	10.72	4.90

Figure 5.22 displays a box and whisker diagram representing the ranges and averages of the percent differences found for the frequencies of each point cloud when compared to the structural plans. These averages are marked with an ‘X’ alongside red lines indicating the differences between the averages of each point cloud set. The smallest range and most accurate average were found in the coarse point cloud results with the average falling just below 2%. The largest range was given by the fine point cloud which had a higher percent difference average (4.5%) than the coarse point cloud but proved to have a smaller percent difference average than the medium point cloud (7.4%). Overall, the differences between these averages are shown via the red lines indicating the exact difference in average that exists between the data sources. With the largest difference being under 6%, the results indicate that although an accuracy difference exists between the point cloud sets, it is not drastic.

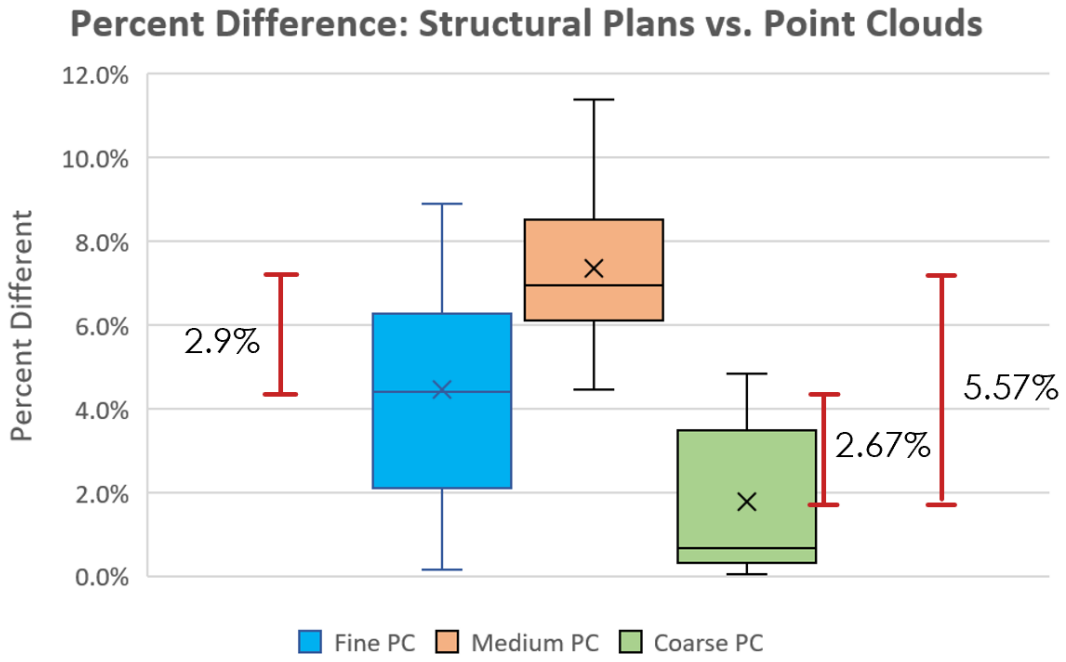

Figure 5.22: Ranges and averages of frequency percent differences when comparing the three point clouds to the structural plans

5.3.4 Modal Assurance Criterion

The Modal Assurance Criterion (MAC) functions as a method to measure the consistency between estimates of a modal vector [26]. This type of analysis allows for an improved confidence factor in the assessment of a modal vector from different excitation locations [26]. MAC essentially serves as a determination of similarity between two mode shapes. These mode shape sources have to come from one experimental set of data and either another experimental set of data or from a FEA model [26]. The MAC is obtained through the calculation shown in Equation 6. The equation denotes ψ_1 and ψ_2 as the two vector sets for comparison. The subscript n represents the number of degrees of freedom while the subscripts j and k represent the number of modes in each set [26].

$$MAC\ (\psi_1, \psi_2) = \frac{\left|\{\psi_1\}_{n\times j}^{H}\{\psi_2\}_{n\times k}\right|^2}{\{\psi_1\}_{n\times j}^{H}\{\psi_1\}_{n\times j}\{\psi_2\}_{n\times k}^{H}\{\psi_2\}_{n\times k}} \quad (6)$$

In order to complete a proper MAC analysis, the length of the modal vectors for each source should be the same but the amount of modes being compared does not [26]. The correlation is quantified through a scalar value between zero and one [26]. These values signify that if the MAC outputs a value of 1, the two mode shapes are identical [27]. If the MAC outputs a number near zero, the two mode shapes have no consistent correspondence [28]. Anything in between zero and one represents the similarity percentage between the two mode shapes; for example, a value of 0.63 denotes that one mode shape matches the other at about 63%.

For this study, the structural plans and three point cloud models underwent the MAC analysis against actual experimental data extracted from the pedestrian footbridge as provided by [29]. The experimental mode shape data was collected through the use of sensors in ten different locations (five on each side) on the footbridge and obtained solely the vertical displacements in the Z-direction. In order to achieve deflections, the bridge was excited by the golf-cart being driven across back and forth. This excitation created displacements at the ten scan locations leading to five mode shapes which were developed in Matlab as seen in Figure 5.22. It is important to note that having only 5 sensors on each side limits the MAC analysis. As Figure 5.23 denotes, the less sensors a user has, the more susceptible to producing misleading results as will be seen in the subsequent tables.

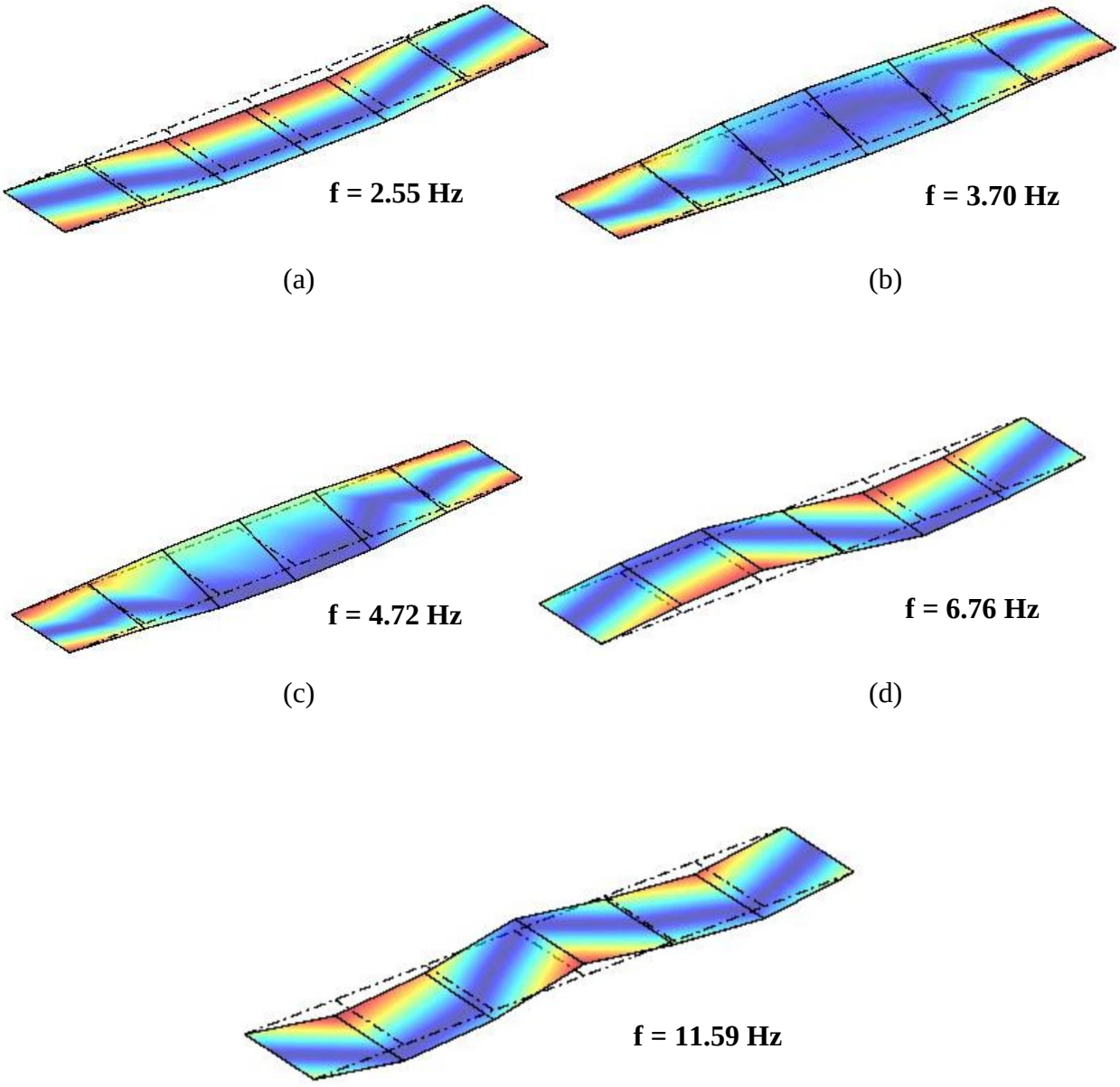

Figure 5.23: Experimental data run in Matlab – (a) Mode Shape 1; (b) Mode Shape 2; (c) Mode Shape 3; (d) Mode Shape 4; (e) Mode Shape 5

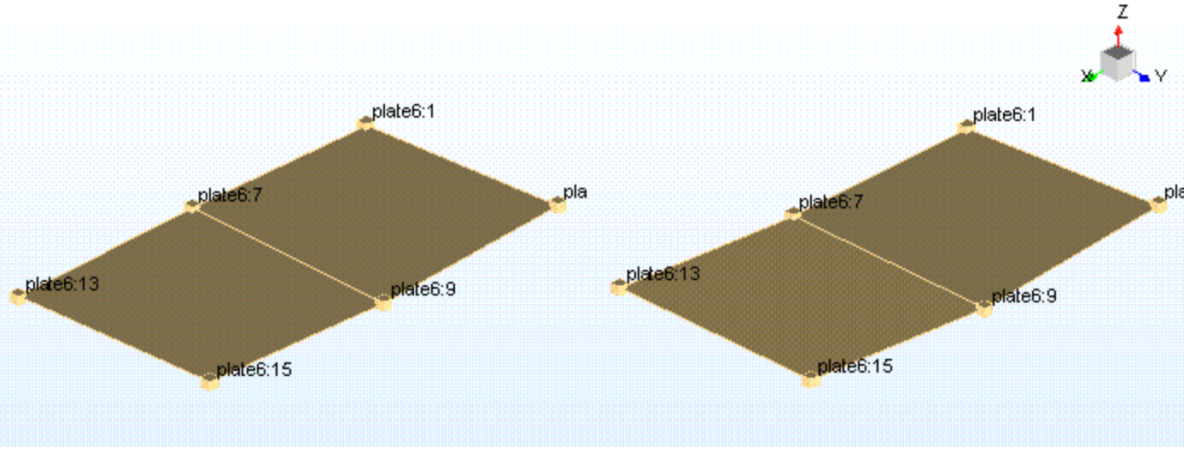

(a)

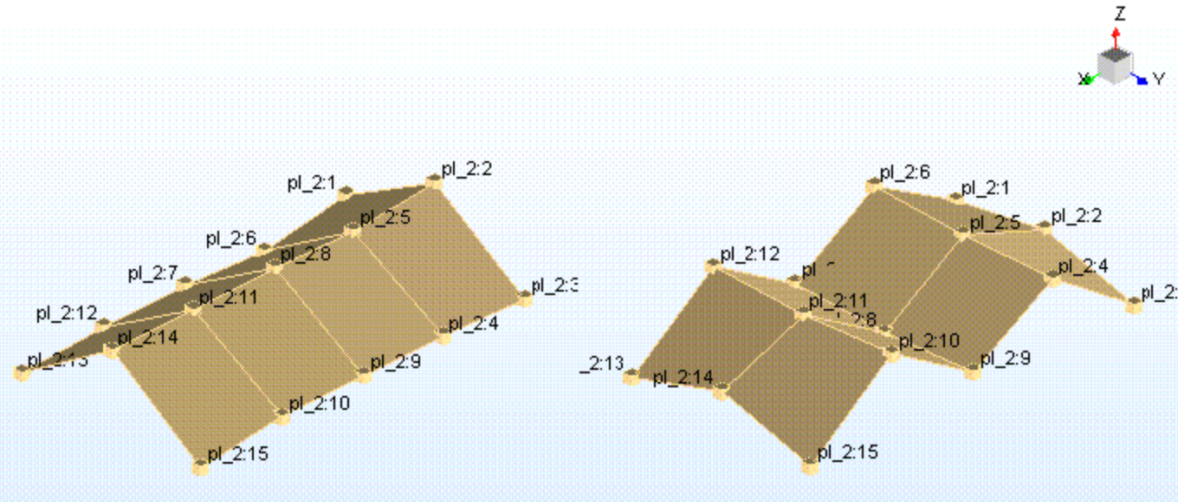

(b)

Figure 5.24: (a) Mode shapes move similarly since only 6 sensors are being used; (b) Additional sensors on the same structure show more truthful mode shapes and their apparent differences
Source: Siemens PLM Community [27]
https://community.plm.automation.siemens.com/t5/Testing-Knowledge-Base/Modal-Assurance-Criterion-MAC/ta-p/368008

For each individual FEA point cloud model and the FEA structural plan model, ten displacements for each mode were collected in order to compare their values to those found in the experimental case. In order to match the five modes collected via the data of the sensors, the

dynamic modal analysis that was completed for 9 modes had to be increased to 18 modes. The final product was a 18x5 MAC matrix for each FEA model mode versus the individual experimental modes. The results are shown in a 3D bar graph known as a MAC matrix.

A MAC matrix is simply a series of 3D bar graphs that visually represent the quantified correspondence between two modes [24]. The x-axis of these 3D graphs represents the mode number of the non-experimental sources such as the point clouds or the structural plans. The y-axis represents the mode number for the experimental data. The z-axis is the correspondence between two mode shapes being compared quantified between zero and one.

5.3.4.1 Structural Plans MAC

Figure 5.25 displays the correspondence between the mode shapes given by the structural plans and experimental data. As can be seen in Table 5.29, the nine MAC values of significance that are visible in Figure 5.25 are also bolded within the table. Five mode correlations exceed 90%, three exceed 80% and one exceeds 70%. The highest value found was 97.4% and it is representative of the second mode obtained from the experimental data being nearly identical to the third mode found from the structural plans.

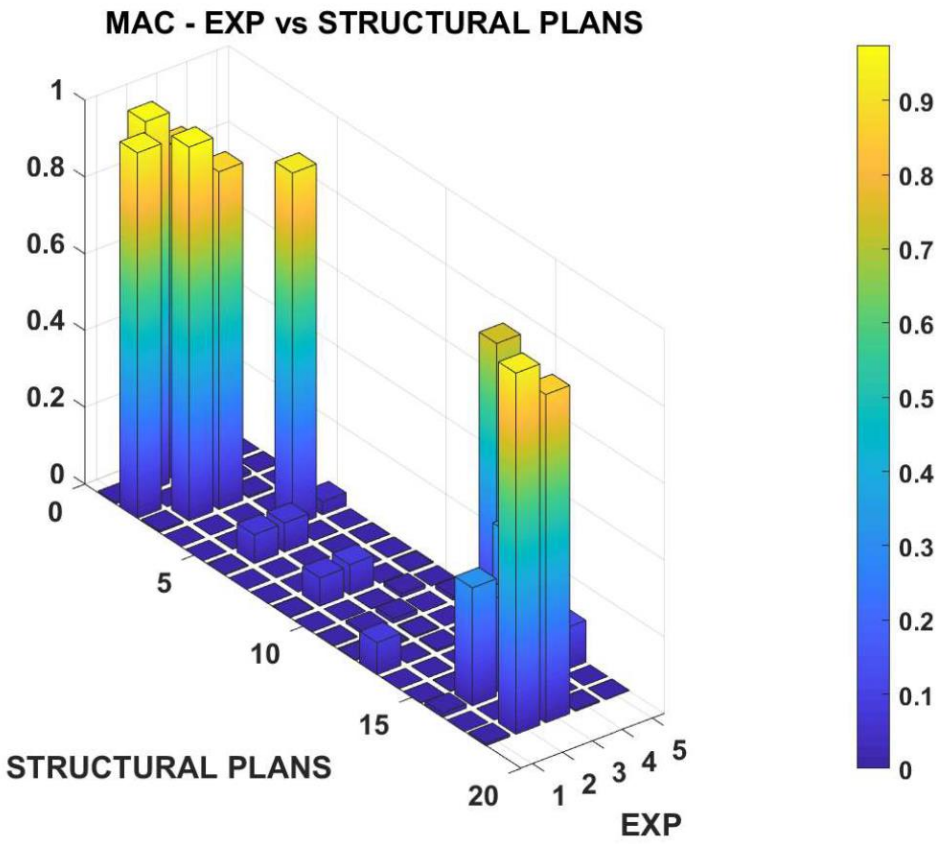

Figure 5.25: MAC - Experimental mode shapes vs. Structural plan mode shapes

Table 5.29: MAC values for Experimental mode shapes vs. Structural plan mode shapes

Structural Plans Mode Number	Experimental Mode Number				
	1	2	3	4	5
1	0.004	**0.966**	**0.871**	0.004	0.000
2	**0.952**	0.000	0.095	0.009	0.001
3	0.005	**0.974**	**0.880**	0.004	0.000
4	0.000	0.000	0.000	0.001	0.001
5	0.000	0.001	0.000	**0.921**	0.034
6	0.002	0.075	0.076	0.000	0.000
7	0.000	0.000	0.000	0.001	0.001
8	0.000	0.000	0.000	0.000	0.001
9	0.002	0.074	0.078	0.000	0.002
10	0.000	0.001	0.001	0.010	0.000
11	0.002	0.008	0.012	0.000	0.010
12	0.002	0.003	0.003	0.000	0.005
13	0.083	0.001	0.005	0.001	**0.743**
14	0.000	0.000	0.000	0.005	0.000
15	0.000	0.001	0.000	0.351	0.013
16	0.011	0.307	0.245	0.000	0.109
17	0.000	0.001	0.000	0.000	0.000
18	0.006	**0.941**	**0.855**	0.004	0.001

Table 5.30 gives a comprehensive look at the structural plan MAC results compared to the experimental results. The table provides the percent differences for frequencies as well as the respective MAC value for said mode comparison. Choosing the highest MAC value for each experimental mode, the corresponding structural plan mode was chosen for frequency comparison. The table shows that overall, the structural plans maintain close proximity in frequency with the frequency found by the experimental data. The lone exception is the comparison between structural plan mode 3 and experimental mode 3 which produced a frequency percent difference of 22%.

Figure 5.26 gives a side by side comparison of the most accurate mode shape comparison between the structural plans and experimental data.

Table 5.30: Frequency Comparison via MAC value - Experimental vs Structural Plans

Structural Plans		***Experimental***			
Mode	**Frequency, f (Hz)**	**Mode**	**Frequency, f (Hz)**	**% Difference**	**MAC Value**
2	2.54	1	2.55	0.4	0.952
3	3.68	2	3.7	0.5	0.974
3	3.68	3	4.72	22.0	0.880
5	6.95	4	6.76	2.8	0.921
13	12.65	5	11.59	9.1	0.743

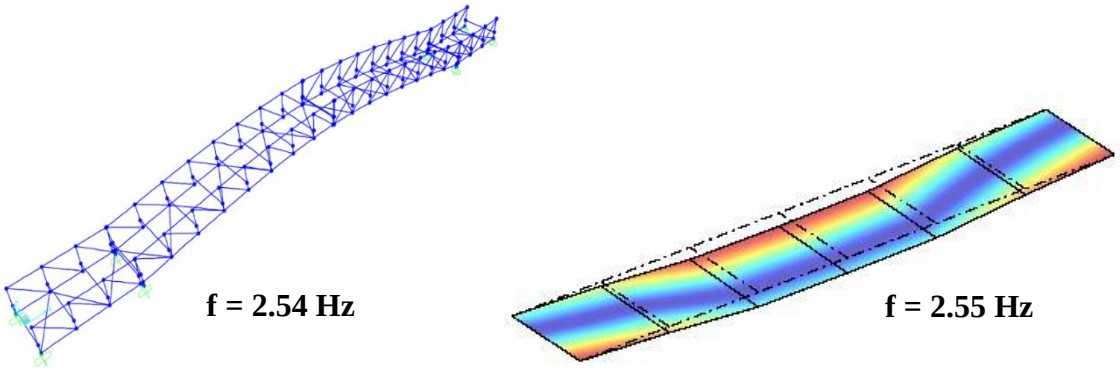

Figure 5.26: Mode shape 2 of the structural plans and mode shape 1 of the experimental data showing identical movement bending in the Z-direction at nearly identical frequencies

5.3.4.2 Fine Point Cloud MAC

Figure 5.27 and Table 5.31 display the MAC results for the fine point cloud versus the experimental data. Just as was shown for the structural plans, the values of significance seen in

Figure 5.27 are bolded in Table 5.31. The fine point cloud MAC results output ten values of significance. Of the ten values, five were above 90%, three above 80% and the last two above 70%. When compared to the values the structural plan MAC produced, the fine point cloud showed extremely similar results in terms of MAC values of significance. This similarity in results signifies the accuracy point cloud data can achieve to in-field results even when compared to structural plans.

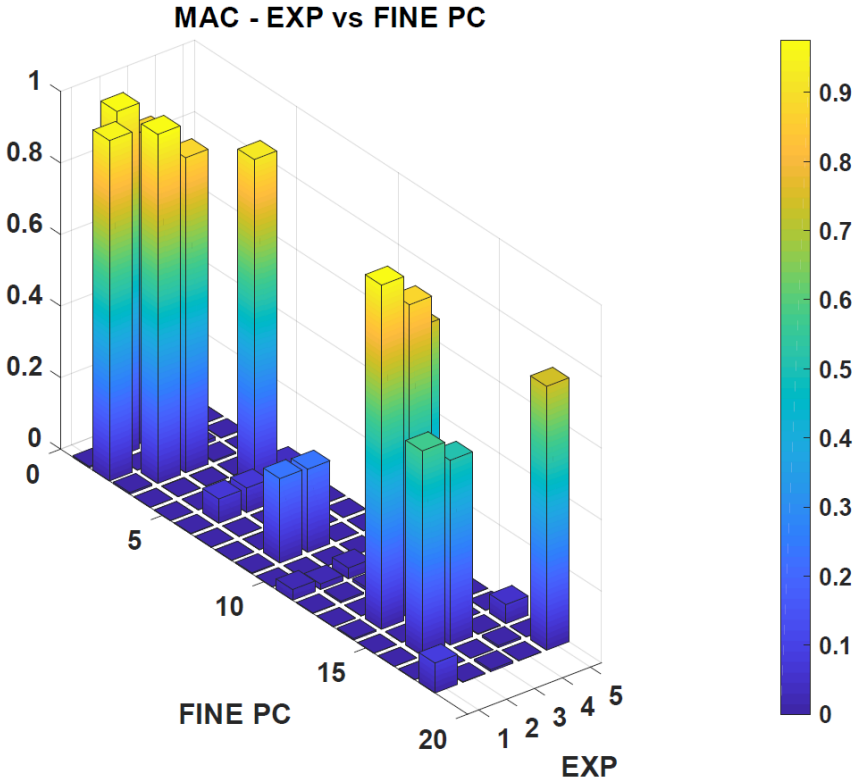

Figure 5.27: MAC - Experimental mode shapes vs. Fine point cloud mode shapes

Table 5.31: MAC values for Experimental mode shapes vs. Fine point cloud mode shapes

Fine Point Cloud Mode Number \ Experimental Mode Number	1	2	3	4	5
1	0.004	**0.966**	**0.870**	0.004	0.000
2	**0.952**	0.000	0.096	0.009	0.001
3	0.005	**0.976**	**0.881**	0.004	0.000
4	0.000	0.000	0.000	0.001	0.001
5	0.000	0.001	0.000	**0.920**	0.034
6	0.001	0.068	0.068	0.000	0.000
7	0.000	0.000	0.000	0.001	0.001
8	0.000	0.000	0.000	0.000	0.001
9	0.003	0.236	0.232	0.001	0.000
10	0.000	0.000	0.000	0.001	0.001
11	0.030	0.015	0.030	0.000	0.108
12	0.001	0.004	0.008	0.000	0.010
13	0.000	0.001	0.000	**0.746**	0.030
14	0.004	**0.962**	**0.877**	0.004	0.001
15	0.000	0.001	0.000	0.000	0.000
16	0.000	0.573	0.516	0.002	0.053
17	0.000	0.000	0.000	0.006	0.000
18	0.084	0.001	0.005	0.001	**0.737**

As was the case in section 5.3.4.1, Table 5.32 gives a comprehensive look at the fine point cloud MAC results compared to the experimental results. The fine point cloud proved to stay within a 15% difference of the frequencies provided by the experimental data. Although the structural plans managed to get smaller percent differences overall, the fine point cloud managed to get a smaller range making the results have less of an outlier affect. Neither the smallest percent difference was attributed to the highest MAC value nor the largest percent difference attribute to the worst MAC value. Figure 5.28 gives a side by side comparison of Mode 3 from the fine point cloud and mode 2 of the experimental data.

Table 5.32: Frequency Comparison via MAC value - Experimental vs Fine Point Cloud

Fine Point Cloud		***Experimental***			
Mode	**Frequency, f (Hz)**	**Mode**	**Frequency, f (Hz)**	**% Difference**	**MAC Value**
2	2.58	1	2.55	1.2	0.952
3	4.01	2	3.7	8.4	0.976
3	4.01	3	4.72	15.0	0.881
5	7.13	4	6.76	5.5	0.92
18	13.18	5	11.59	13.7	0.737

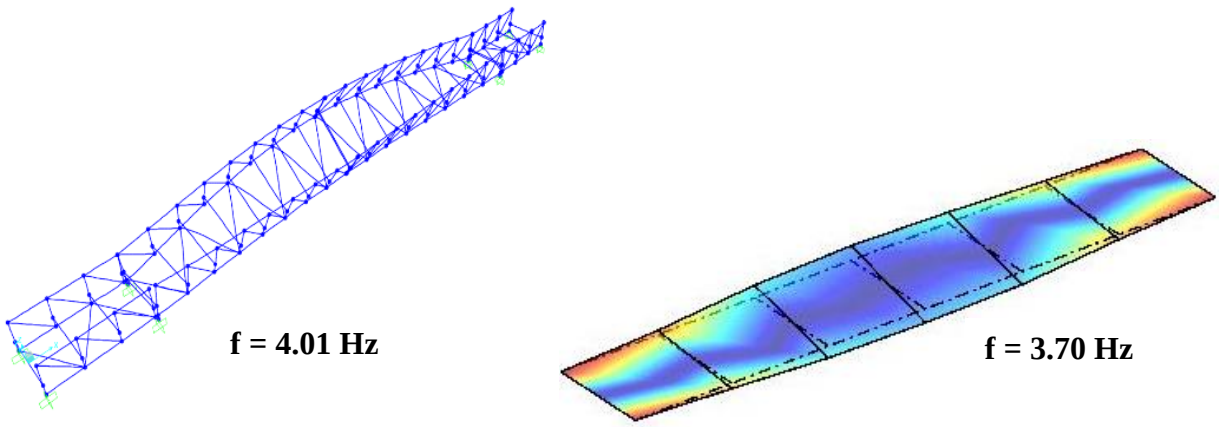

Figure 5.28: Mode shape 3 of the fine point cloud and mode shape 2 of the experimental data showing similar movement of torsion about the x-axis with frequencies in close proximity

5.3.4.3 Medium Point Cloud MAC

Figure 5.29 and Table 5.33 show the MAC results for medium point cloud versus the experimental data. What can be seen immediately is the increase in significant MAC values when compared to the fine point cloud results. The bolded values shown in Table 5.33 indicate that there are ten values of significance which is one more than the structural plans were able to produce.

These ten values contain seven values above 90%, one above 80% and two above 70%. These results make it the most similar to the experimental data by far due to the high unity it was able to achieve in many of its values. Its highest value of 98.7% makes it the highest correspondence value seen yet. Also, this value breaks the pattern seen with the previous two MAC results as it occurred when the second mode of the experimental data was compared to the sixteenth mode of the medium point cloud.

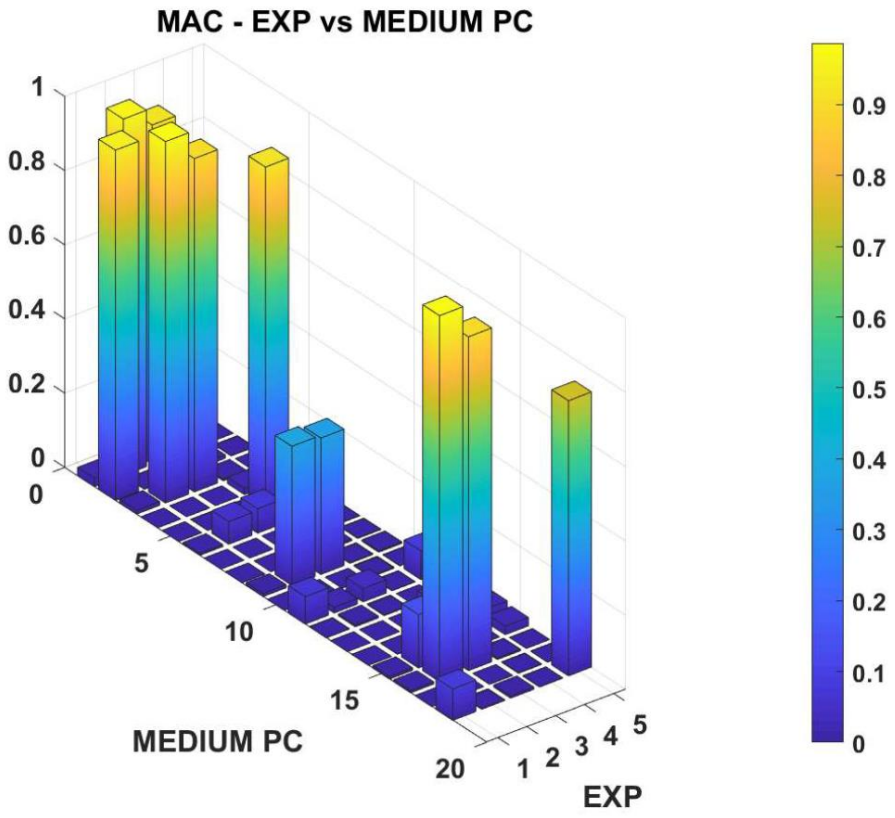

Figure 5.29: MAC - Experimental mode shapes vs. Medium point cloud mode shapes

Table 5.33: MAC values for Experimental mode shapes vs. Medium point cloud mode shapes

Medium Point Cloud Mode Number \ Experimental Mode Number	1	2	3	4	5
1	0.022	**0.961**	**0.915**	0.005	0.000
2	**0.944**	0.001	0.071	0.009	0.001
3	0.010	**0.974**	**0.899**	0.004	0.000
4	0.000	0.000	0.000	0.017	0.002
5	0.000	0.001	0.000	**0.920**	0.034
6	0.005	0.061	0.066	0.001	0.003
7	0.000	0.000	0.000	0.001	0.001
8	0.000	0.000	0.000	0.004	0.001
9	0.008	0.375	0.368	0.002	0.004
10	0.000	0.000	0.000	0.003	0.001
11	0.074	0.015	0.036	0.001	0.077
12	0.001	0.005	0.002	0.000	0.004
13	0.000	0.000	0.000	0.044	0.004
14	0.000	0.001	0.000	**0.719**	0.030
15	0.007	0.144	0.149	0.001	0.023
16	0.006	**0.987**	**0.900**	0.004	0.000
17	0.000	0.000	0.000	0.001	0.001
18	0.084	0.002	0.006	0.001	**0.742**

Table 5.34 shows the frequency percent difference between the medium point cloud and the experimental data. Unlike the previous percent differences, the medium point cloud proved to have two enormous percent errors. Unexpectedly, the mode comparison with the highest MAC value produced the greatest percent error of over 200%. The smallest percent error the medium point cloud was able to achieve was 8.2% for the respective mode comparison. The medium point cloud proved to have the most and highest significant MAC values overall but also attained the largest percent error yet. The large percent error is an indication that the data is limited by the number of sensors used.

Although the MAC value was the highest for the comparison between the medium point cloud's 16th mode and the experimental data's 2nd mode, the huge percent error in frequency shows that the movement is different. In order to adjust for this limitation, a combination of significant MAC value and frequency proximity was completed in Table 5.35 in order to show the more accurate frequency and MAC comparison. This adjusted table shows that using Mode 3 of the medium point cloud produces a much better percent error of just under 11% while still producing a MAC value above 97%. Figure 5.30 gives a side by side comparison of mode shape comparison between Mode 3 of both the medium point cloud and the experimental data.

Table 5.34: Frequency Comparison via MAC value - Experimental vs Medium Point Cloud

Medium Point Cloud		***Experimental***			
Mode	**Frequency, f (Hz)**	**Mode**	**Frequency, f (Hz)**	**% Difference**	**MAC Value**
2	2.76	1	2.55	8.2	0.944
16	12.20	2	3.7	229.7	0.987
1	2.30	3	4.72	51.3	0.915
5	7.43	4	6.76	9.9	0.92
18	13.53	5	11.59	16.7	0.742

Table 5.35: Frequency Comparison via MAC value - Experimental vs Medium Point Cloud (Adjusted)

Medium Point Cloud		***Experimental***			
Mode	**Frequency, f (Hz)**	**Mode**	**Frequency, f (Hz)**	**% Difference**	**MAC Value**
2	2.76	1	2.55	8.2	0.944
3	4.10	2	3.7	10.8	0.974
3	4.10	3	4.72	13.1	0.899
5	7.43	4	6.76	9.9	0.920
18	13.53	5	11.59	16.7	0.742

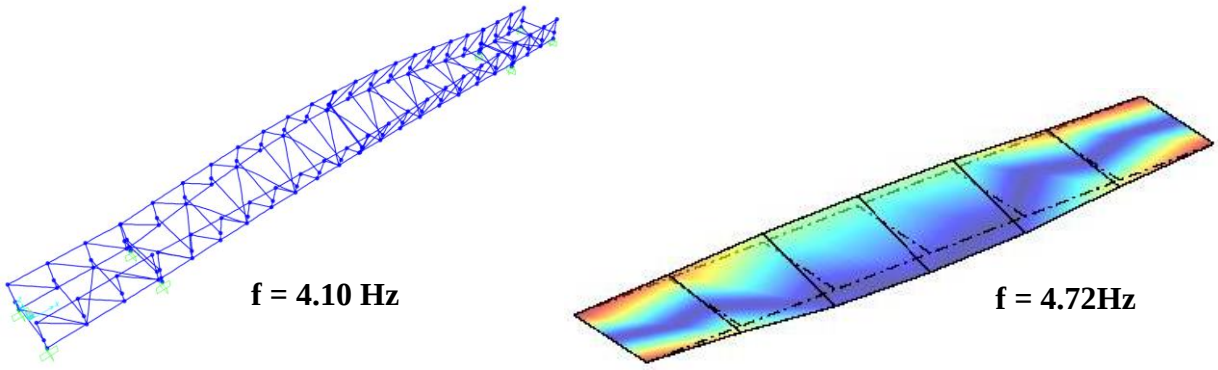

Figure 5.30: Mode shape 3 of the fine point cloud experimental data showing similar movement of torsion about the x-axis with frequencies within approximately 13% of each other

5.3.4.4 Coarse Point Cloud MAC

Lastly, Figure 5.31 and Table 5.36 illustrate the MAC outcomes found between the coarse point cloud and the experimental data. Figure 5.31 looks quite similar to the figures seen for structural plans and medium point cloud. Table 5.36 shows that nine values of significance were bolded with five values above 90%, three values above 80% and one value above 70%. These percentages match those found by the structural plans and that includes its highest correspondence

value of 97.4%. This value occurred when the experimental data's second mode was being compared to the coarse point cloud's third mode. This comparison stayed in line with the trend seen in the structural plans and fine point cloud making the medium point cloud the only one to have its highest MAC value occur at a different mode comparison.

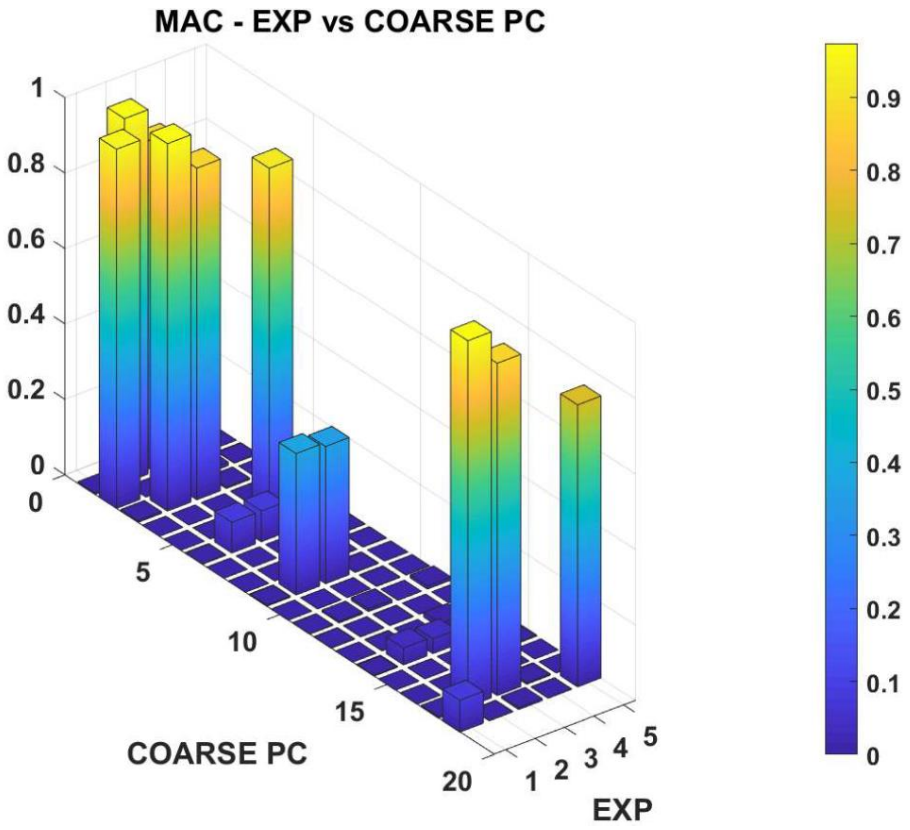

Figure 5.31: MAC - Experimental mode shapes vs. Coarse point cloud mode shapes

Table 5.36: MAC values for Experimental mode shapes vs. Coarse point cloud mode shapes

Coarse Point Cloud Mode Number \ Experimental Mode Number	1	2	3	4	5
1	0.004	**0.966**	**0.871**	0.004	0.000
2	**0.952**	0.000	0.095	0.009	0.001
3	0.005	**0.974**	**0.879**	0.004	0.000
4	0.000	0.000	0.000	0.001	0.001
5	0.000	0.001	0.000	**0.923**	0.034
6	0.002	0.081	0.081	0.001	0.000
7	0.000	0.000	0.000	0.001	0.001
8	0.000	0.000	0.000	0.000	0.001
9	0.003	0.375	0.364	0.001	0.000
10	0.000	0.000	0.000	0.001	0.001
11	0.001	0.004	0.007	0.000	0.008
12	0.001	0.001	0.001	0.000	0.000
13	0.000	0.001	0.000	0.013	0.001
14	0.002	0.044	0.039	0.000	0.034
15	0.000	0.000	0.000	0.044	0.002
16	0.000	0.001	0.000	0.001	0.000
17	0.004	**0.970**	**0.881**	0.004	0.000
18	0.084	0.001	0.005	0.001	**0.747**

Table 5.37 shows the frequency comparison between the coarse point cloud and the experimental data. The coarse point cloud was able to produce one of the worst percent differences at 179.2% but also the smallest percent differences at 0.2%. Unlike the previous tables, the smallest percent difference did correlate to the highest MAC value. These last values showed that the fine point cloud, although having the least amount of significant MAC values, produced the closest frequency range to that of the experimental data. Due to a significant percent difference being calculated, it is clear that Mode 17 of the coarse point cloud is not the best option to compare with Mode 3 of the experimental data. Table 5.38 shows the adjusted values with Mode 17 being replaced with Mode 3 for the coarse point cloud reducing the percent difference from 179.2% to

21.4%. Overall, the fine point cloud produced the smallest worse case percent error and the best overall accuracy when compared to the other sources and their adjusted tables. Figure 5.32 gives a side by side comparison of mode shape comparison between Mode 5 of the coarse point cloud and Mode 4 of the experimental data.

Table 5.37: Frequency Comparison via MAC value – Experimental vs Coarse Point Cloud

Coarse Point Cloud		***Experimental***			
Mode	**Frequency, f (Hz)**	**Mode**	**Frequency, f (Hz)**	**% Difference**	**MAC Value**
2	2.60	1	2.55	2.0	0.952
3	3.71	2	3.70	0.3	0.974
17	13.18	3	4.72	179.2	0.880
5	7.29	4	6.76	7.8	0.921
18	13.70	5	11.59	18.2	0.743

Table 5.38: Frequency Comparison via Mac Value - Experimental vs Coarse Point Cloud (Adjusted)

Coarse Point Cloud		***Experimental***			
Mode	**Frequency, f (Hz)**	**Mode**	**Frequency, f (Hz)**	**% Difference**	**MAC Value**
2	2.60	1	2.55	2.0	0.952
3	3.71	2	3.70	0.3	0.974
3	3.71	3	4.72	21.4	0.879
5	7.29	4	6.76	7.8	0.921
18	13.70	5	11.59	18.2	0.743

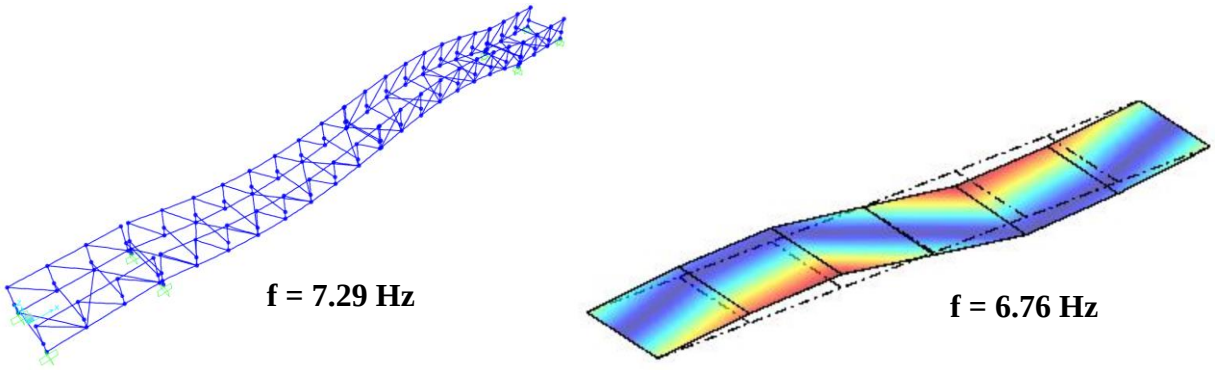

Figure 5.32: Mode shape 5 of the fine point cloud and mode shape 4 of the experimental data showing similar movement of out-of-phase bending in the Z-direction with a frequency difference of less than 8%

CHAPTER 6 - CONCLUSION

6.1 Spectrum Stadium Interpretation

The comparison between the results provided by the original stadium study and the study described in Chapter 4 of this thesis provided several conclusions to be touched upon. The first inference is that point cloud technology is heavily relied on human judgment. This judgment is an essential factor in the accuracy of results. As presented in Section 4.4, both the original and new point cloud model differed in dimension from each other as well as from the structural plan model. This is highlighted by both point cloud models having a worst-case dimension percent difference just over 30% when compared to the structural plans. A numerical difference so significant can play a huge role in the results obtained when completing an analysis.

That being said, caution is advised when assuming structural plans match the existing structure. After completing on-site measurements, it was found that both the original and new point cloud had more accurate dimensional values for the as-built structure than the structural plans had. This finding shows how advantageous point cloud technology can be when discussing existing structures. The new point cloud proved to be extremely accurate in terms of dimensioning as the average accuracy was found to be above 98% with its worst single dimension difference still being about 92% accurate. These findings show that structural plans cannot always be taken at face value for accurately representing an existing structure as changes during the construction process may have occurred. Delving in further, the displacement and reaction percent differences were much more apparent for the data sources. The original point cloud, when compared to the control model, was able to obtain an accuracy of 72% or better for the displacements with the exception of two

outliers that were below 60%. On the other hand, the new point cloud managed to obtain an accuracy of 90% and above for the displacements emphasizing how accurate point cloud technology can be while also highlighting how different users can obtain different results. The structural plans produced the worse percent difference of all the sources. This is directly due to the higher percent error seen in its dimensioning as well as the drastically incorrect frame that did not nearly match the size of the one seen in the as-built structure.

The result comparisons between the joint reactions proved much different than those given by the displacement. All three data sources provided accurate results when compared to the on-site model reaction values. Unlike for the displacements, the original point cloud study proved to be the most accurate of the three data sources. Such results suggest that rendering models for analysis through the use of point cloud could provide inaccurate results in one structural aspect but extremely accurate results in another depending on how important member size choices are for that specific analysis.

Focusing on the comparison between the two point clouds, it becomes clear that different users can create similar models but produce different results. This dilemma is emphasized by the two point clouds having dimensional accuracy above 90% when compared with each other. Unfortunately, this similarity does not always translate to member section rendering. [25] mentions in their report that the struggle to render on Revit proved so difficult they had to lean on the section sizes given by the structural plans. This type of difficulty directly changed the results the authors produced and further suggests that the judgment of users during the member section size decision process is purely subjective.

In the future, the goal would be to find a way to improve inaccuracies in all facets of the structural analysis. A denser point cloud would make the rendering process much simpler as it would provide clearer visuals for member size decisions. Also, the use of multiple opinions on member size decisions could prove to limit human error via a general consensus but also may add time to the rendering process. Having users improve their knowledge and skill in point cloud compatible programs would also allow for an easier modeling process. Lastly, the evolution of the point cloud technology itself could have endless potential. Overall, this study proved that structural plans cannot always be depended on when analyzing existing structures. An alternative to structural plans is necessary and point cloud technology has shown its ability to achieve accuracies above 98%. Such results suggest that with proper care, methodology and understanding, it is completely viable to use point clouds for structural analysis.

6.2 Pedestrian Bridge Interpretation

6.2.1 Bridge Static Analysis Conclusion

The comparisons between the three sets of point clouds and the structural plans produced a clear conclusion. The use of point cloud technology can be deduced as a feasible alternative to structural plans as was the case for the Spectrum Stadium analysis. For the three point cloud density models, none were below 82% accurate for displacements or reactions when compared to the structural plan model. With that said, the fine point cloud was found to have the most accurate maximum deformation while the medium point cloud was found to have the most accurate reactions overall.

As with any technology, point cloud still proved to have its mixture of pros and cons. In terms of advantages, point cloud technology can serve as an excellent substitute or even improve on structural plans. The time saved by allowing a scanner to collect the structural data rather than measuring the structure entirely by hand is considerably more efficient considering structural plans are not always reliable dimensionally. Additionally, the ability to input the data points into a program that has model rendering capabilities, such as Autodesk Inventor, gives a user the base for recreating the structure when compared to rendering from a blank canvas as is the case for structural plans. This method of using point clouds to recreate an as-built structure has proven to achieve highly accurate results.

Contra to the benefits, a few disadvantages exist when it comes to using this data collection method. The experience of the user can directly impact results. A first-time user will struggle to gather results efficiently and accurately compared to someone who has rendered point clouds before. The accuracy overall depends on a multitude of factors such as density of the point cloud, visual blockages of structural members, weather, program of choice and human judgment. The largest factor of issue being human judgment as mentioned throughout this thesis. One user may find a member to be a size above another user or provide dimensions that differ by several inches. Section size decisions and dimensioning have the most direct effect on the calculated results produced via FEA software.

Moreover, technical difficulties during scanning is a factor that does not exist for structural plans. For the scanning of the bridge, the first attempt had to be cancelled halfway through due to technical difficulties that occurred after 5 hours spent on-site. The second attempt was completed successfully but only after another 5 hours and 45 minutes at the site. This can cause impactful

delays on project scheduling. That being said, the time it takes to thoroughly scan a structure is much more efficient than traditional measuring techniques which makes this aspect of point cloud technology a potential advantage. Additionally, structural plans for existing structures are not always correct making point cloud technology advantageous as it would better reflect the as-built structure.

Although the denser point clouds proved more accurate in both deformations and reactions when compared to the least dense, all three point clouds produced extremely similar results. The proximity between the values given by all three point cloud results remained consistently close through all the results. The largest difference was the displacement value given by the medium point cloud when compared to the fine point cloud which still differed by less than 14%. Overall, the fine point cloud proved the most accurate considering both displacement and reaction results which is not surprising as denser point clouds allows for easier and more accurate rendering. With the ability to garner accuracies above 96%, point cloud technology once again proves its ability as a reliable tool for analyzing existing structures.

6.2.2. Bridge Dynamic Modal Analysis Conclusion

For all the point cloud density models, accuracies above 88% were found for frequencies and periods when compared to the structural plans. Conversely, the results produced for the eigenvalues had an accuracy of just over 76%, at its worst case, which is consistent with the correlation natural frequency has with eigenvalues as previously stated in Equation 5 in Section 5.3.2. For the dynamic modal load participation factors for the nine modes of all three point cloud densities, the Y-direction had the strongest impact contributing a minimum of 80%. The Z-

direction also had an impact but to a lesser extent at over 56% for the fine and coarse point clouds and over 63% for the medium point cloud. The X-direction displayed almost no impact for all the point clouds with a participation factor consistently under 2.5%. These results were found to have 93% or above accuracy for all three point clouds indicating strong accurateness.

The rendering process is more cumbersome when compared to the structural plans. The time to render through the use of structural plans took approximately 12 hours but the time it took to render the point clouds was lengthier. For the fine point cloud, about 16 hours was needed to render the structure as it was the first time the user had used this technology to create a model. For the medium point cloud, 14 hours of work was needed as the density was quite similar to the fine point cloud and a user's skill with the program had improved. Lastly, the coarse point cloud took about 16 hours to render, an increase from the medium point cloud due to the difficulty in choosing appropriate member sizes stemming from the lack of density in the point cloud. It must be noted that this was the case for one user as a more experienced user may find their total work time significantly decreased due to their expertise with a program. This footnote is supported by the time improvement seen between the fine and medium point cloud as the user improved their understanding of the technology.

In terms of point cloud density, this study proved that altering the density of the point cloud did change the overall accuracy of the results but not drastically as no point cloud frequency differed by more than 10% from each other at any matching mode. The results that did change are directly due to the different member sizes as dictate by human judgment. In this case, the coarse point cloud was unexpectedly the most accurate overall but not significantly. This is most likely

an outlier and not true to the findings as the coarse point cloud should produce less accurate results just as the medium point cloud did.

The reason the coarse point cloud proved the most accurate is most likely due to an underlying bias that existed with the user during the rendering process. Having known the correct member sizes and having extremely difficulty choosing an accurate member size due to the lack of density given by the point cloud, a user may have defaulted to member size thicknesses that were given in the structural plans. This was done unknowingly as a user was carrying out educated guesses via the use of the shapes produced by the point cloud but was clearly influenced by the known member sizes. In the future, eliminating such bias when conducting the study would more accurately reflect the accuracy of a low-density point cloud.

The fine point cloud proved the easiest to render and use on the FEA program but also provided the least accurate results overall when compared to structural plans. Once again, least accurate by no means implies glaringly inaccurate but, rather slightly less accurate than the medium and coarse point clouds. This is supported by the fact that the fine point cloud was still able to output the same general range of percent difference in its results. However, the MAC analysis completed showed that the fine point cloud produced higher values than even the structural plans when compared to the experimental data. Such a finding indicates that point cloud technology has the capability to produce results that closer match the true dynamic behavior of a structure than what is given by structural plans.

In general, what can be concluded from all the results is that the middle ground would be sufficient for assessing structural integrity. When time is of the essence for structural integrity analysis, extra scans that could add hours to an on-site visit could prove detrimental to an

engineer's goal. The medium point cloud in this case was able to provide results that were completely acceptable in accuracy while being able to minimize the number of scans applied. Using 7 of the 11 scans (about 63% of the total scans) still allowed a user to obtain a point cloud density that was well visualized and did not add much difficulty to the rendering process as opposed to the coarse point cloud. If the medium point cloud scan was completed, it would only take about 3 hours compared to the 5 hours and 45 minutes it took to complete the fine point cloud scan. This combination of similar rendering ease to the fine point cloud, time saved on-site and acceptable accuracy results makes a medium point cloud density the best option for scanning existing structures.

To summarize, although the point cloud technology has its advantages and disadvantages, the technology has proven to be able to achieve high accuracy in this study. Although maximizing point cloud density does help ease the rendering process for users, the results are not affected as drastically as one may think. In order to save time but still provide ease of use, the maximum number of scans that can be completed is not necessary for obtaining accurate results. In general, if engineers can complete 60%-70% of the maximum number of scans possible, it should be sufficient to yield accurate results while also saving time on-site. This study demonstrates that point cloud technology serves as a powerful tool for engineers to use on existing structures.

6.3 Future Potential

Having done both static and dynamic modal analysis using point cloud does not mean the technology is limited to this form of analysis. Point cloud has use in other engineering facets such as spotting structural discontinuities, signaling seepage and monitoring deformation over time.

This is vital for structures that are susceptible to settlement movement as it directly effects their behavior. Laser scanning can become a vital resource after extreme events such as earthquakes or hurricanes considering time efficiency when compared to traditional. This type of efficiency can make the difference when determining the integrity of a structure prior to catastrophic failure.

These scanners have a broad range of potential uses when considering the issues engineers come across in the field. Structures such as underground tunnels can create difficulty during inspection due to a lack of light. LiDAR scanners can mitigate this issue since they are capable of scanning without the presence of light. Scanners can become of use to amusement parks since they can scan rides from a distance in order to check for deflections and/or deformations without any intrusion to daily operations. Scanners are also not limited to stationary tripods. Several models of scanners can be car-mounted allowing for larger areas to be scanned at one time. Should access be difficult for cars, aerial drone scanners can be utilized. The aerial drone scanners have the ability to scan even larger areas which becomes essential during high-impact events. Technology such as this would provide a strong basis for improving city infrastructure as multiple structures could be scanned at once.

The possibilities point cloud presents far exceed just the few mentioned within this conclusion. Seeing the capability these scanners already have, improvement of their ability will further reinforce their presence within the engineering field. With the abundance of future potential uses point cloud technology can provided engineers, it will not be long before this method of data collection becomes commonplace within the community. If the technology continues to grow and improve, as well as its users, it has the capacity to become the standard modeling source within engineering much like Autodesk accomplished over hand drafting.

APPENDIX A: PEDESTRIAN BRIDGE SCANNING TIME LOG

Date : 11/11/2018 **Overall Start Time:** 9:00 AM **Overall End Time:** 2:45 PM

Scan Location	Reference Point Set Up Time	Scanner Set Up Time	Scanning Time	Capturing Targets	Comments	Total Time (mins)
1	9:07 AM to 9:20 AM	9:20 AM to 9:33 AM	9:33 AM to 9:43 AM	9:43 AM to 9:54 AM		47
2		9:56 AM to 10:01 AM	10:01 AM to 10:09 AM	10:09 AM to 10:20 AM		24
3		10:21 AM to 10:31 AM	10:31 AM to 10:36 AM	10:36 AM to 10:57 AM	Trouble Finding Targets	36
4		11:00 AM to 11:05 AM	11:05 AM to 11:10 AM	11:10 AM to 11:18 AM		18
5		11:38 AM to 11:46 AM	11:46 AM to 11:53 AM	11:53 AM to 12:01 PM		23
6		12:01 PM to 12:09 PM	12:09 PM to 12:15 PM	12:15 PM to 12:24 PM		24
7		12:26 PM to 12:34 PM	12:34 PM to 12:41 PM	12:41 PM to 12:49 PM		23
8		12:50 PM to 12:55 PM	12:55 PM to 1:01 PM	1:02 PM to 1:09 PM		19
9		1:10 PM to 1:15 PM	1:15 PM to 1:22 PM	1:22 PM to 1:29 PM		19
10		1:30 PM to 1:41 PM	1:41 PM to 1:57 PM	1:57 PM to 2:07 PM		37
	2:07 PM to 2:17 PM	2:07 PM to 2:17 PM			Changed the Laser Position	10
11		2:20 PM to 2:26 PM	2:26 PM to 2:40 PM	2:40 PM to 2:45 PM		25
					Total:	**305**

APPENDIX B: SCAN LOCATION DIAGRAM WITH ACCOMPANYING PHOTOS

Scan Location Diagram

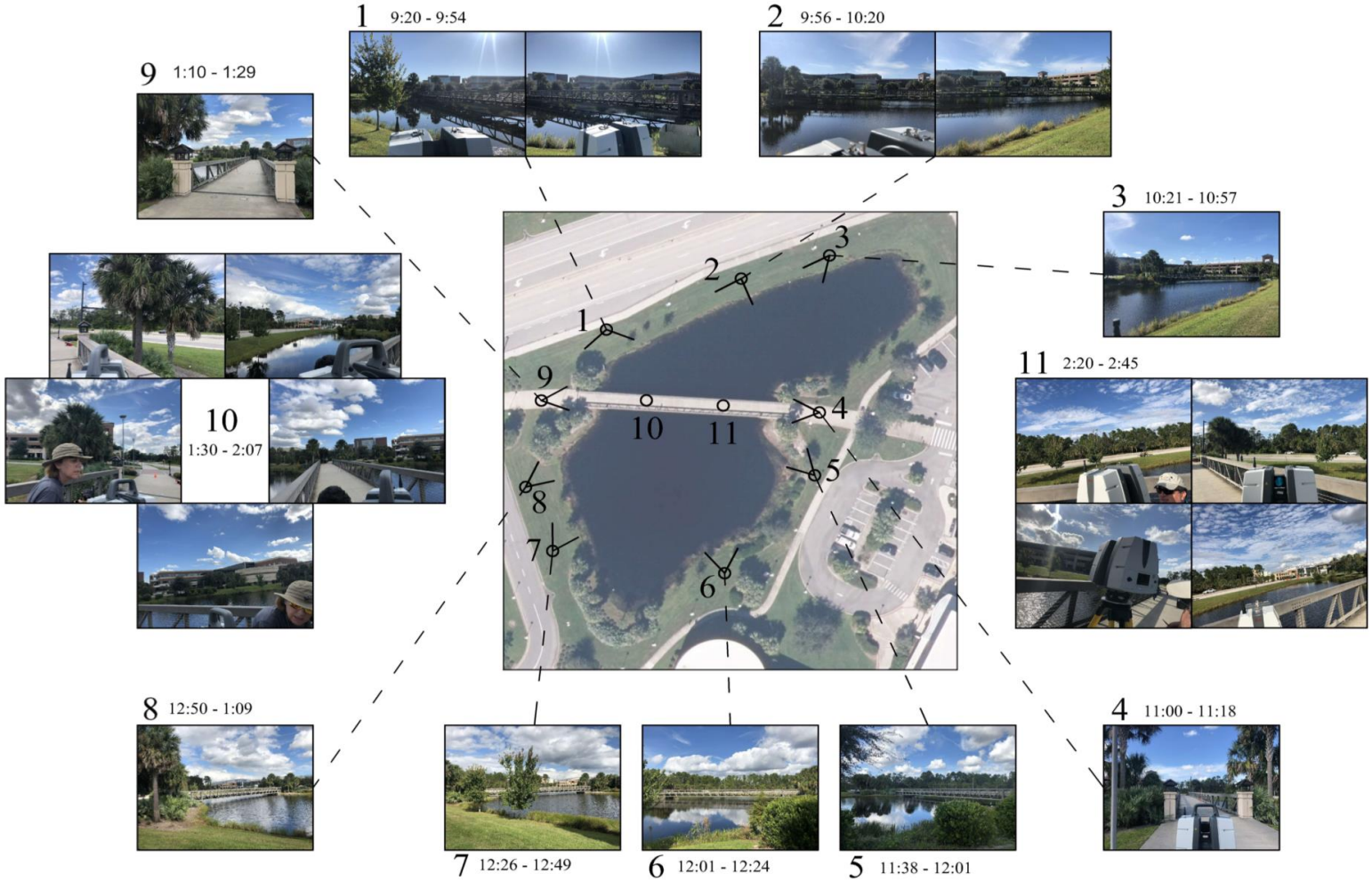

APPENDIX C: ON-SITE PROCEDURE VIA PHOTO DOCUMENTATION

(a) (b) (c)

Figure C.1: (a) Target placement on bridge; (b) Target height setup; (c) Tripod setup

(a) (b)

Figure C.2: (a) Tripod leveling; (b) Digital assistance scanner leveling

(a) (b)

Figure C.3: (a) Programming white balance and resolution; (b) Programming field of view and scan only

(a) (b)

Figure C.4: (a) Peephole used to visually mark and rotate scanner for desired angle; (b) Capturing of black and white target through scanner screen

APPENDIX D: LEICA CYCLONE REGISTER 360 REGISTRATION REPORT

Cyclone REGISTER 360
Registration Report

Nov 13, 2018

Certified by:

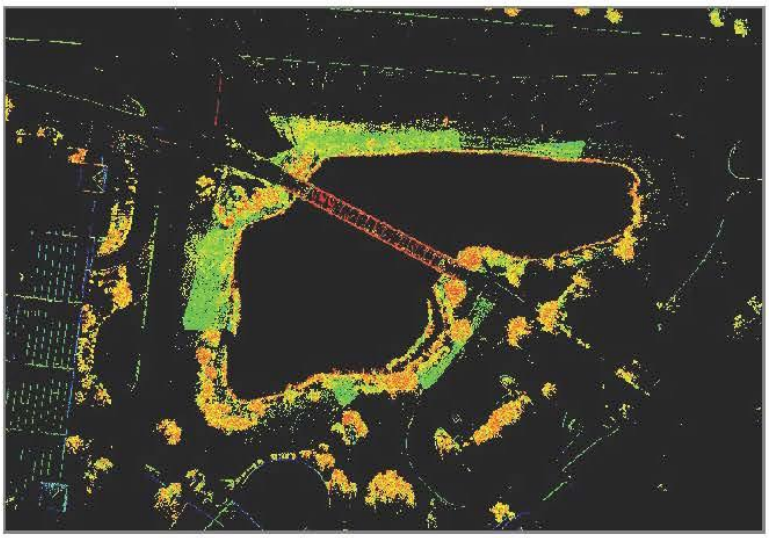

SiteMap 1

Overall Quality

Error Results for Bundle 1

Setup Count:	11
Link Count:	22
Strength:	33 %
Overlap:	21 %

Bundle Error 0 ft 7/16 in ✓	
Overlap 21 %	Strength 33 %
Cloud-to-Cloud 0 ft 1/2 in ✓	Target Error 0 ft 3/8 in ✓

Max error of 0 ft 9/16 in. Max error of 0 ft 13/16 in. Error greater than 0 ft 13/16 in.

Link-Quality Matrix (1 of 1) -

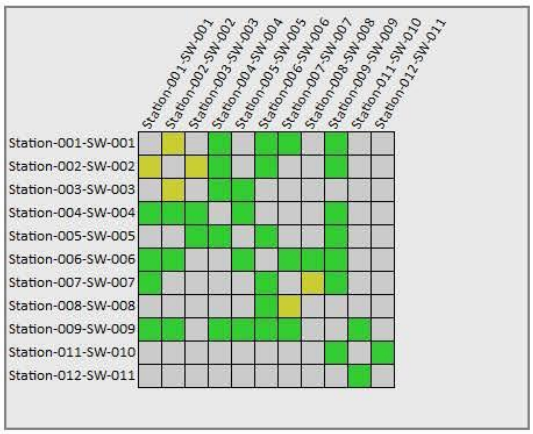

Link Error Results

1 Overview

Link Name	Setup 1	Setup 2	Overlap	Abs. Mean Error
Link 1	Station-001-SW-001	Station-002-SW-002	31 %	0 ft 5/8 in
Link 3	Station-001-SW-001	Station-004-SW-004	8 %	0 ft 3/8 in
Link 5	Station-001-SW-001	Station-006-SW-006	6 %	0 ft 3/8 in
Link 6	Station-001-SW-001	Station-007-SW-007	6 %	0 ft 5/16 in
Link 8	Station-001-SW-001	Station-009-SW-009	25 %	0 ft 1/2 in
Link 9	Station-002-SW-002	Station-003-SW-003	30 %	0 ft 11/16 in
Link 10	Station-002-SW-002	Station-004-SW-004	11 %	0 ft 1/2 in
Link 12	Station-002-SW-002	Station-006-SW-006	11 %	0 ft 1/2 in
Link 15	Station-002-SW-002	Station-009-SW-009	17 %	0 ft 1/2 in
Link 16	Station-003-SW-003	Station-004-SW-004	15 %	0 ft 5/16 in
Link 17	Station-003-SW-003	Station-005-SW-005	8 %	0 ft 3/8 in
Link 22	Station-004-SW-004	Station-005-SW-005	19 %	0 ft 1/8 in
Link 26	Station-004-SW-004	Station-009-SW-009	20 %	0 ft 1/8 in
Link 27	Station-005-SW-005	Station-006-SW-006	28 %	0 ft 3/16 in
Link 30	Station-005-SW-005	Station-009-SW-009	3 %	0 ft 1/8 in
Link 31	Station-006-SW-006	Station-007-SW-007	21 %	0 ft 5/16 in
Link 32	Station-006-SW-006	Station-008-SW-008	15 %	0 ft 1/2 in
Link 33	Station-006-SW-006	Station-009-SW-009	7 %	0 ft 1/4 in
Link 34	Station-007-SW-007	Station-008-SW-008	48 %	0 ft 5/8 in
Link 35	Station-007-SW-007	Station-009-SW-009	14 %	0 ft 3/16 in
Link 37	Station-011-SW-010	Station-012-SW-011	49 %	0 ft 5/16 in
Link 38	Station-009-SW-009	Station-011-SW-010	77 %	0 ft 3/8 in

2 Details

Link Name	Setup 1	Setup 2	Overlap	Abs. Mean Error
Link 1	Station-001-SW-001	Station-002-SW-002	31 %	0 ft 5/8 in
		Cloud to Cloud		0 ft 11/16 in
		Target	Mean Target Error:	0 ft 9/16 in

Target (Setup 1)	Target (Setup 2)	Error
t1	t1	0 ft 15/16 in
t2	t2	0 ft 9/16 in

		t3	t3	0 ft 1/8 in
Link Name	**Setup 1**	**Setup 2**	**Overlap**	**Abs. Mean Error**
Link 3	Station-001-SW-001	Station-004-SW-004	8 %	0 ft 3/8 in
		Cloud to Cloud		**0 ft 7/16 in**
		Target	Mean Target Error:	**0 ft 1/4 in**
		Target (Setup 1)	**Target (Setup 2)**	**Error**
		t1	t1	0 ft 5/16 in
		t2	t2	0 ft 1/4 in
		t3	t3	0 ft 1/4 in
Link Name	**Setup 1**	**Setup 2**	**Overlap**	**Abs. Mean Error**
Link 5	Station-001-SW-001	Station-006-SW-006	6 %	0 ft 3/8 in
		Cloud to Cloud		**0 ft 9/16 in**
		Target	Mean Target Error:	**0 ft 3/16 in**
		Target (Setup 1)	**Target (Setup 2)**	**Error**
		t1	t1	0 ft 3/16 in
		t2	t2	0 ft 3/16 in
		t3	t3	0 ft 3/16 in
Link Name	**Setup 1**	**Setup 2**	**Overlap**	**Abs. Mean Error**
Link 6	Station-001-SW-001	Station-007-SW-007	6 %	0 ft 5/16 in
		Cloud to Cloud		**0 ft 5/8 in**
		Target	Mean Target Error:	**0 ft 5/16 in**
		Target (Setup 1)	**Target (Setup 2)**	**Error**
		t1	t1	0 ft 1/4 in
		t2	t2	0 ft 1/4 in
		t3	t3	0 ft 3/8 in
Link Name	**Setup 1**	**Setup 2**	**Overlap**	**Abs. Mean Error**
Link 8	Station-001-SW-001	Station-009-SW-009	25 %	0 ft 1/2 in
		Cloud to Cloud		**0 ft 11/16 in**
		Target	Mean Target Error:	**0 ft 1/4 in**
		Target (Setup 1)	**Target (Setup 2)**	**Error**

		t1	t1	0 ft 1/4 in
		t2	t2	0 ft 1/4 in
		t3	t3	0 ft 1/4 in

Link Name	Setup 1	Setup 2	Overlap	Abs. Mean Error
Link 9	Station-002-SW-002	Station-003-SW-003	30 %	0 ft 11/16 in
		Cloud to Cloud		0 ft 11/16 in
		Target	Mean Target Error:	0 ft 11/16 in

Target (Setup 1)	Target (Setup 2)	Error
t1	t1	0 ft 15/16 in
t2	t2	0 ft 13/16 in
t3	Target 7	0 ft 7/16 in

Link Name	Setup 1	Setup 2	Overlap	Abs. Mean Error
Link 10	Station-002-SW-002	Station-004-SW-004	11 %	0 ft 1/2 in
		Cloud to Cloud		0 ft 1/2 in
		Target	Mean Target Error:	0 ft 1/2 in

Target (Setup 1)	Target (Setup 2)	Error
t1	t1	0 ft 3/4 in
t2	t2	0 ft 9/16 in
t3	t3	0 ft 5/16 in

Link Name	Setup 1	Setup 2	Overlap	Abs. Mean Error
Link 12	Station-002-SW-002	Station-006-SW-006	11 %	0 ft 1/2 in
		Cloud to Cloud		0 ft 1/2 in
		Target	Mean Target Error:	0 ft 1/2 in

Target (Setup 1)	Target (Setup 2)	Error
t1	t1	0 ft 13/16 in
t2	t2	0 ft 1/2 in
t3	t3	0 ft 3/16 in

Link Name	Setup 1	Setup 2	Overlap	Abs. Mean Error
Link 15	Station-002-SW-002	Station-009-SW-009	17 %	0 ft 1/2 in

		Cloud to Cloud		0 ft 11/16 in
		Target	Mean Target Error:	0 ft 1/2 in
		Target (Setup 1)	Target (Setup 2)	Error
		t1	t1	0 ft 11/16 in
		t2	t2	0 ft 1/2 in
		t3	t3	0 ft 3/8 in
Link Name	Setup 1	Setup 2	Overlap	Abs. Mean Error
Link 16	Station-003-SW-003	Station-004-SW-004	15 %	0 ft 5/16 in
		Cloud to Cloud		0 ft 5/8 in
		Target	Mean Target Error:	0 ft 5/16 in
		Target (Setup 1)	Target (Setup 2)	Error
		t1	t1	0 ft 3/8 in
		t2	t2	0 ft 3/8 in
		Target 7	t3	0 ft 1/4 in
Link Name	Setup 1	Setup 2	Overlap	Abs. Mean Error
Link 17	Station-003-SW-003	Station-005-SW-005	8 %	0 ft 3/8 in
		Cloud to Cloud		0 ft 11/16 in
		Target	Mean Target Error:	0 ft 3/8 in
		Target (Setup 1)	Target (Setup 2)	Error
		t1	t1	0 ft 3/8 in
		t2	t2	0 ft 7/16 in
		Target 7	t3	0 ft 3/8 in
Link Name	Setup 1	Setup 2	Overlap	Abs. Mean Error
Link 22	Station-004-SW-004	Station-005-SW-005	19 %	0 ft 1/8 in
		Cloud to Cloud		0 ft 3/4 in
		Target	Mean Target Error:	0 ft 1/8 in
		Target (Setup 1)	Target (Setup 2)	Error
		t1	t1	0 ft 1/8 in
		t2	t2	0 ft 1/16 in
		t3	t3	0 ft 1/8 in
Link Name	Setup 1	Setup 2	Overlap	Abs. Mean Error
Link 26	Station-004-SW-004	Station-009-SW-009	20 %	0 ft 1/8 in

		Cloud to Cloud		0 ft 1/16 in
		Target	Mean Target Error:	0 ft 3/16 in

Target (Setup 1)	Target (Setup 2)	Error
t1	t1	0 ft 1/8 in
t2	t2	0 ft 1/8 in
t3	t3	0 ft 1/4 in

Link Name	Setup 1	Setup 2	Overlap	Abs. Mean Error
Link 27	Station-005-SW-005	Station-006-SW-006	28 %	0 ft 3/16 in

		Cloud to Cloud		0 ft 7/16 in
		Target	Mean Target Error:	0 ft 3/16 in

Target (Setup 1)	Target (Setup 2)	Error
t1	t1	0 ft 1/4 in
t2	t2	0 ft 3/16 in
t3	t3	0 ft 1/16 in

Link Name	Setup 1	Setup 2	Overlap	Abs. Mean Error
Link 30	Station-005-SW-005	Station-009-SW-009	3 %	0 ft 1/8 in

		Cloud to Cloud		0 ft 3/8 in
		Target	Mean Target Error:	0 ft 1/8 in

Target (Setup 1)	Target (Setup 2)	Error
t1	t1	0 ft 1/8 in
t2	t2	0 ft 1/8 in
t3	t3	0 ft 1/8 in

Link Name	Setup 1	Setup 2	Overlap	Abs. Mean Error
Link 31	Station-006-SW-006	Station-007-SW-007	21 %	0 ft 5/16 in

		Cloud to Cloud		0 ft 3/4 in
		Target	Mean Target Error:	0 ft 5/16 in

Target (Setup 1)	Target (Setup 2)	Error
t1	t1	0 ft 5/16 in
t2	t2	0 ft 1/4 in
t3	t3	0 ft 5/16 in

Link Name	Setup 1	Setup 2	Overlap	Abs. Mean Error

Link Name	Setup 1	Setup 2	Overlap	Abs. Mean Error
Link 32	Station-006-SW-006	Station-008-SW-008	15 %	0 ft 1/2 in
		Cloud to Cloud		0 ft 5/16 in
		Target	Mean Target Error:	0 ft 3/4 in

Target (Setup 1)	Target (Setup 2)	Error
t1	t1	0 ft 11/16 in
t2	t2	0 ft 5/8 in
t3	t3	0 ft 7/8 in

Link Name	Setup 1	Setup 2	Overlap	Abs. Mean Error
Link 33	Station-006-SW-006	Station-009-SW-009	7 %	0 ft 1/4 in
		Cloud to Cloud		0 ft 9/16 in
		Target	Mean Target Error:	0 ft 1/4 in

Target (Setup 1)	Target (Setup 2)	Error
t1	t1	0 ft 1/4 in
t2	t2	0 ft 1/4 in
t3	t3	0 ft 1/4 in

Link Name	Setup 1	Setup 2	Overlap	Abs. Mean Error
Link 34	Station-007-SW-007	Station-008-SW-008	48 %	0 ft 5/8 in
		Cloud to Cloud		0 ft 3/8 in
		Target	Mean Target Error:	0 ft 7/8 in

Target (Setup 1)	Target (Setup 2)	Error
t1	t1	0 ft 5/8 in
t2	t2	0 ft 3/4 in
t3	t3	0 ft 1 1/8 in

Link Name	Setup 1	Setup 2	Overlap	Abs. Mean Error
Link 35	Station-007-SW-007	Station-009-SW-009	14 %	0 ft 3/16 in
		Cloud to Cloud		0 ft 5/8 in
		Target	Mean Target Error:	0 ft 3/16 in

Target (Setup 1)	Target (Setup 2)	Error
t1	t1	0 ft 1/4 in
t2	t2	0 ft 1/4 in
t3	t3	0 ft 1/16 in

Link Name	Setup 1	Setup 2	Overlap	Abs. Mean Error
Link 37	Station-011-SW-010	Station-012-SW-011	49 %	0 ft 5/16 in
		Cloud to Cloud		0 ft 5/16 in
		Target	Mean Target Error:	--

Link Name	Setup 1	Setup 2	Overlap	Abs. Mean Error
Link 38	Station-009-SW-009	Station-011-SW-010	77 %	0 ft 3/8 in
		Cloud to Cloud		0 ft 3/8 in
		Target	Mean Target Error:	--

Graphics

Bridge1

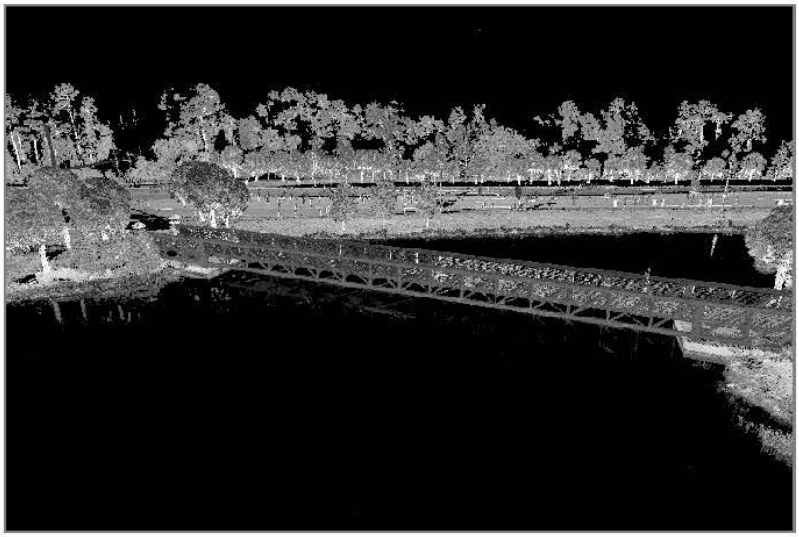

Bridge2

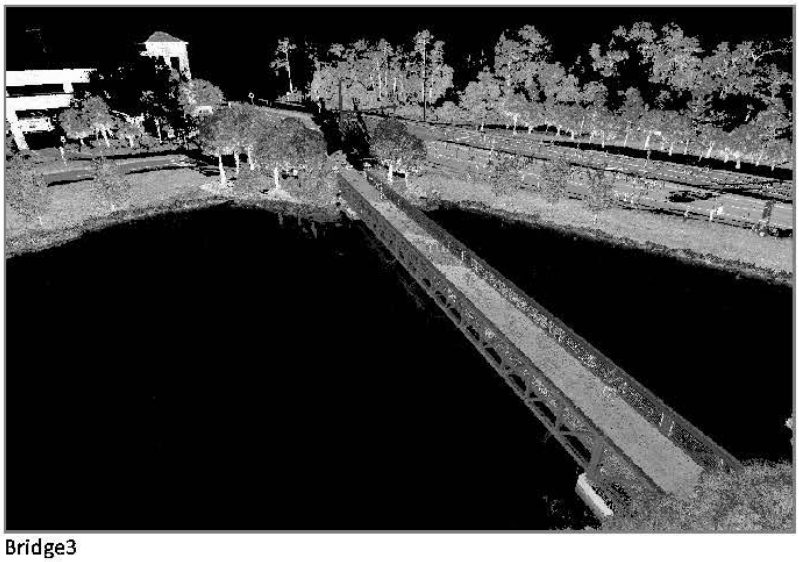

Bridge3

APPENDIX E: AUTODESK INVENTOR POINT CLOUD RENDERING PROCESS WITH ACCOMPANYING IMAGES

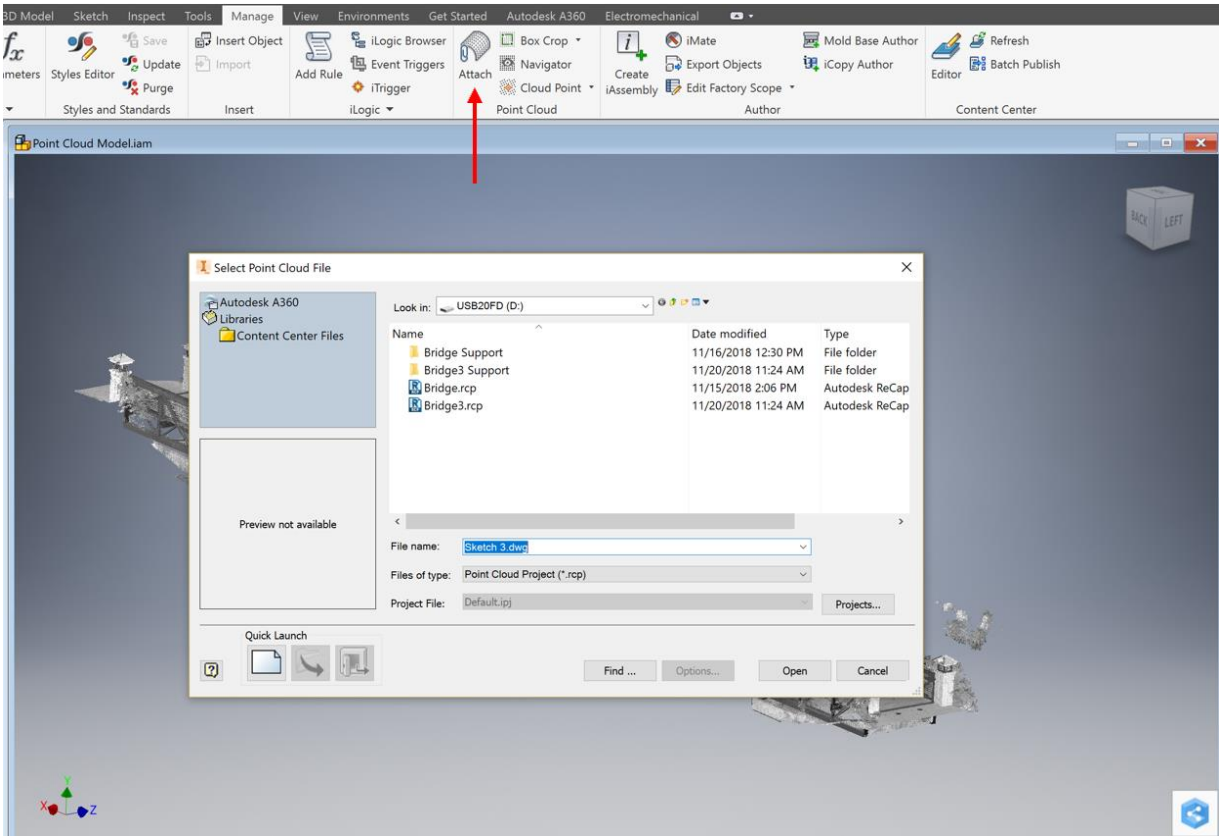

Figure E.1: Step 1 - Import point cloud recap data via the “Attach” option indicated by the red arrow. Choose appropriate file within pop up folder.

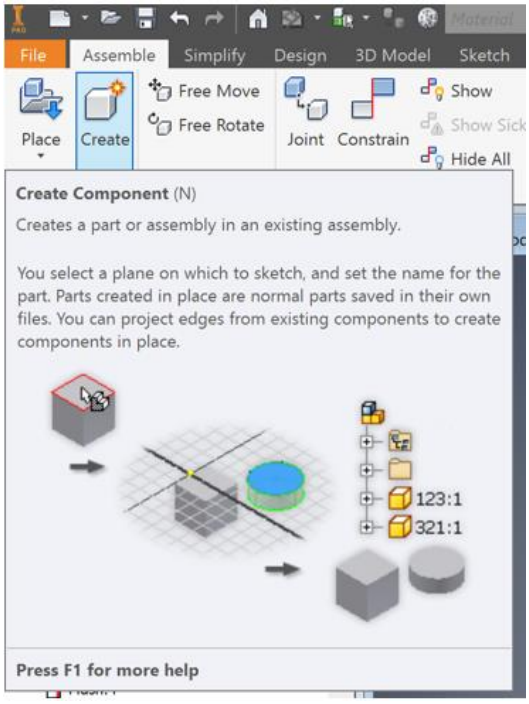

Figure E.2: Step 2 - Create a part using the “Create” option within the “Assemble” tab.

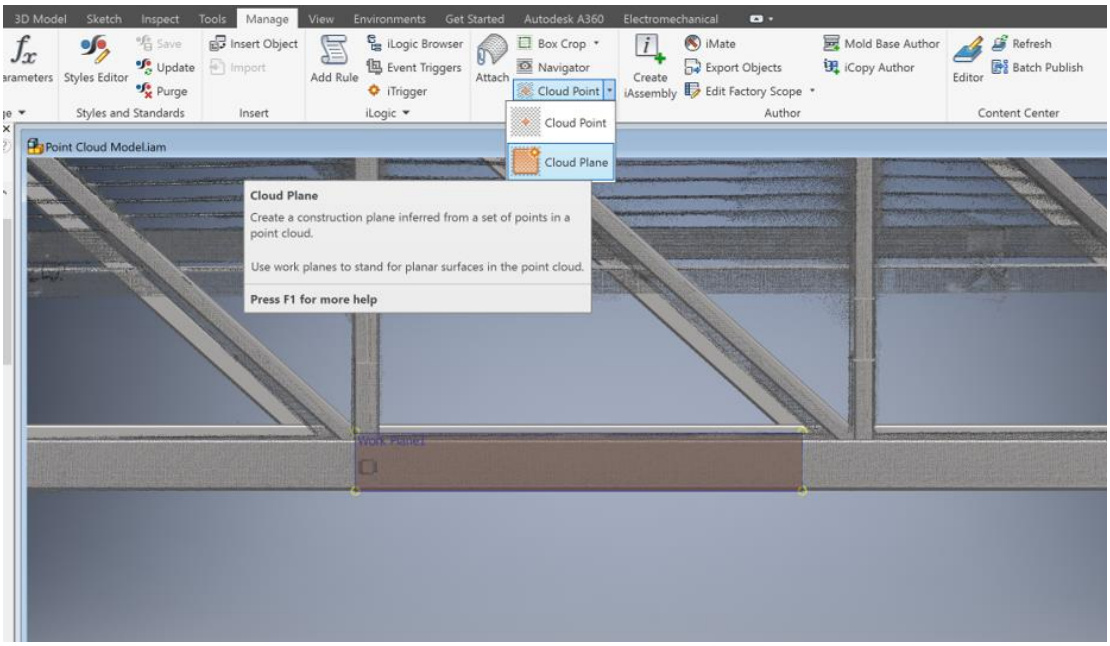

Figure E.3**:** Step 3 - Create a work plane in order to begin a 2D sketch on a flat surface.

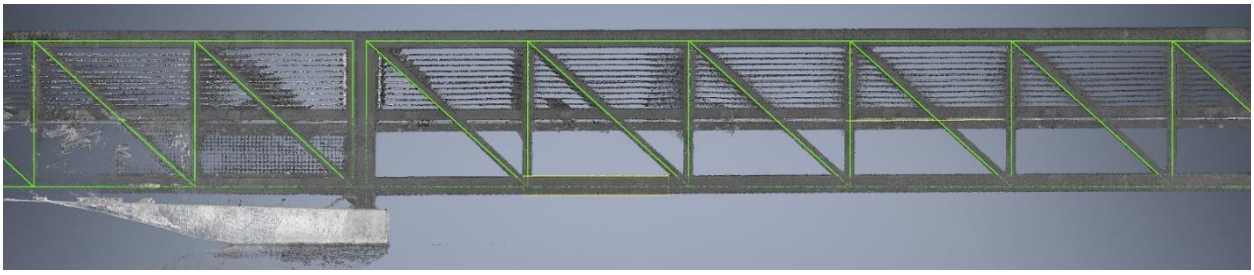

Figure E.4: Step 4 - Create a center-to-center sketch, to the best of the user's ability, lining up the sketch lines with the sections visible using the point cloud as reference.

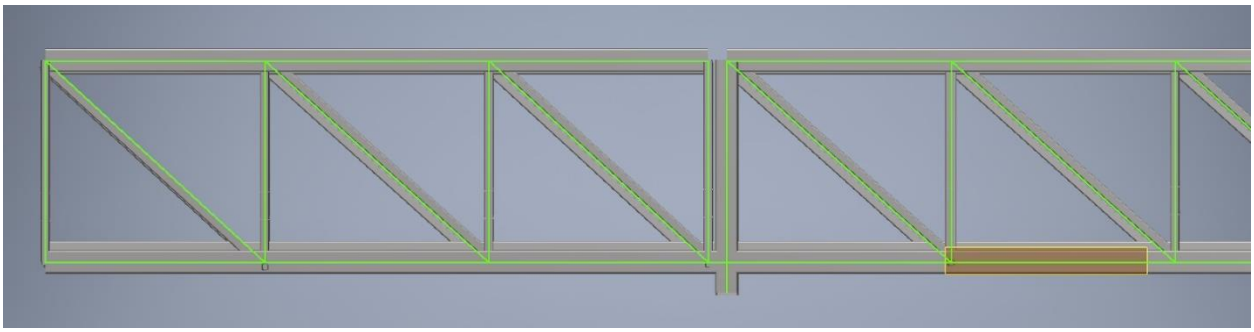

Figure E.5: Step 5 - Insert frames and offset accordingly to match, as best as possible, the sections seen in the point cloud.

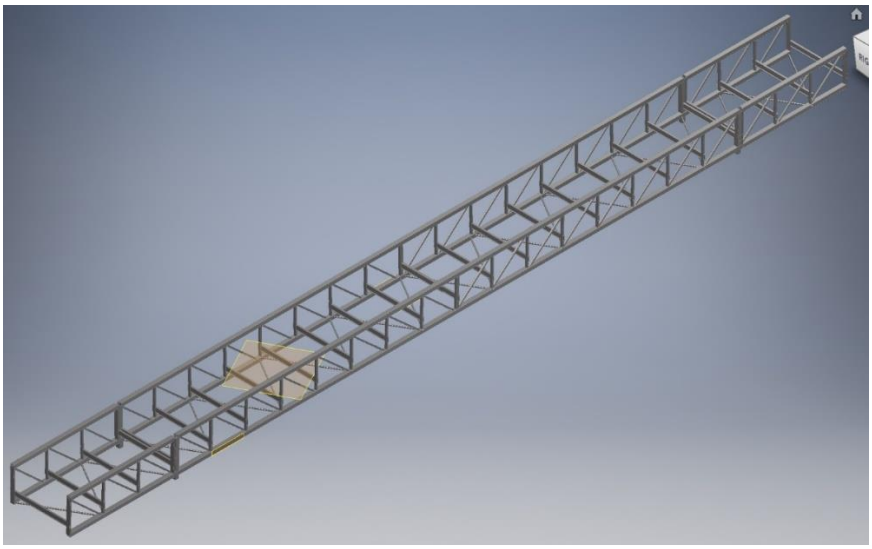

Figure E.6: Step 6 - Repeat Steps 1-5 for all applicable sides to obtain rendered model of entire structure.

APPENDIX F: PORTION OF SPECTRUM STADIUM STRUCTURAL PLAN

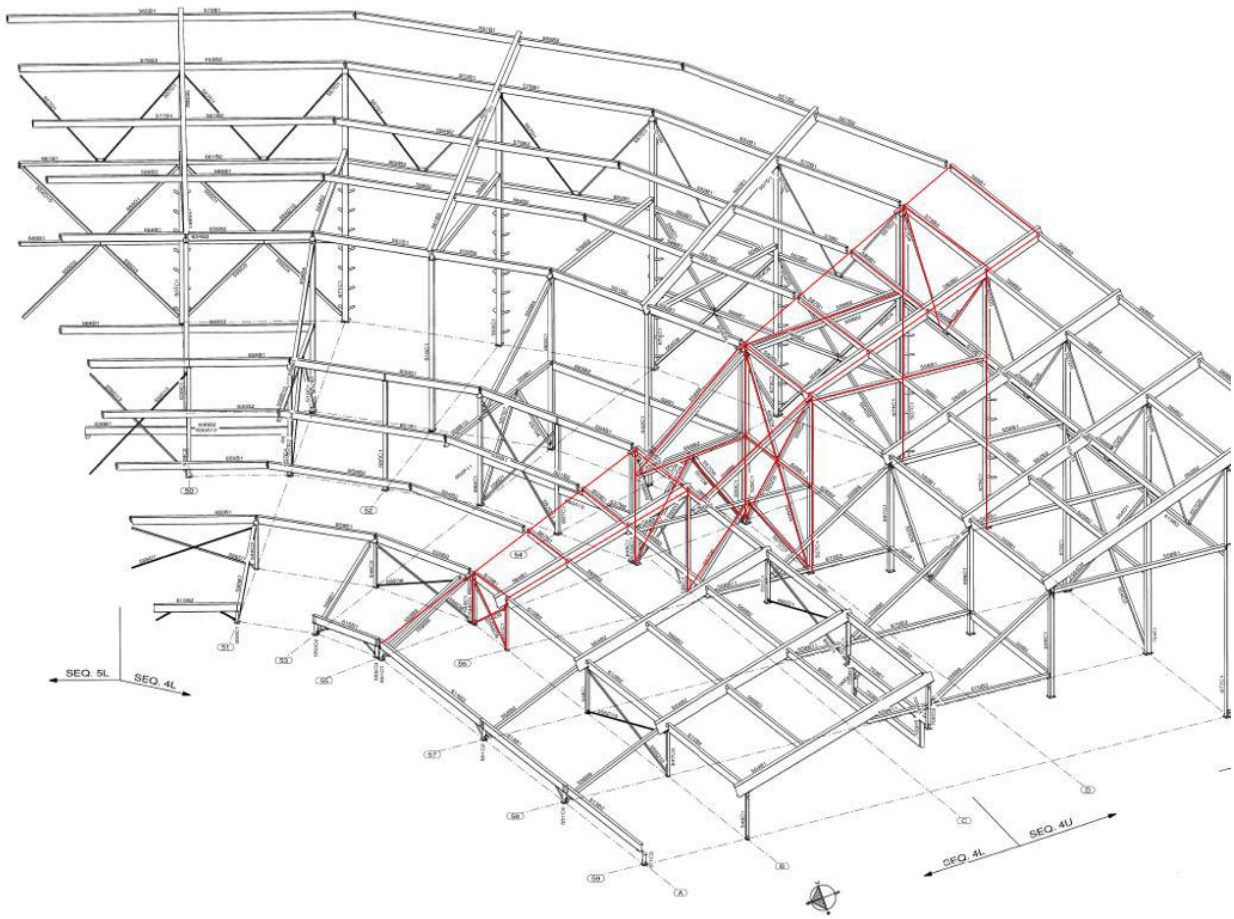

Figure F.1: Structural plan of Spectrum Stadium highlighting the section of interest

APPENDIX G: PORTION OF PEDESTRIAN BRIDGE STRUCTURAL PLAN

ALL DIMENSIONS SHOWN ALONG HORIZONTAL, UNLESS NOTED OTHERWISE.

RAILS AND DECK NOT SHOWN FOR CLARITY, SEE SECTION & DETAILS

■ — DENOTES LIGHTBOX LOCATION

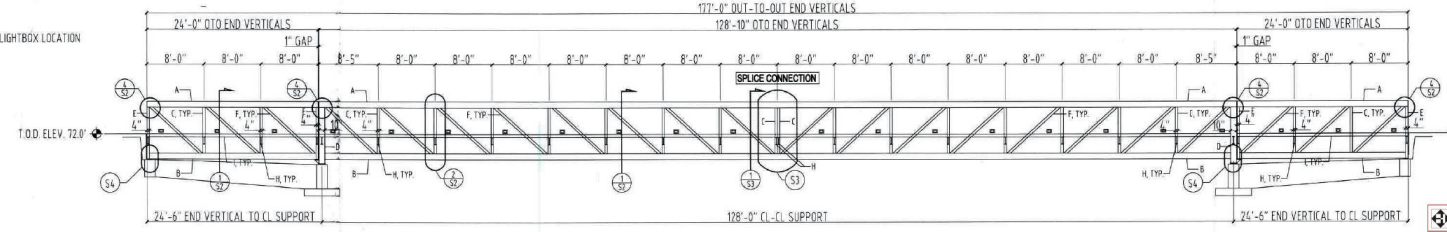

1/S1 VERTICAL TRUSS ELEVATION
NO SCALE

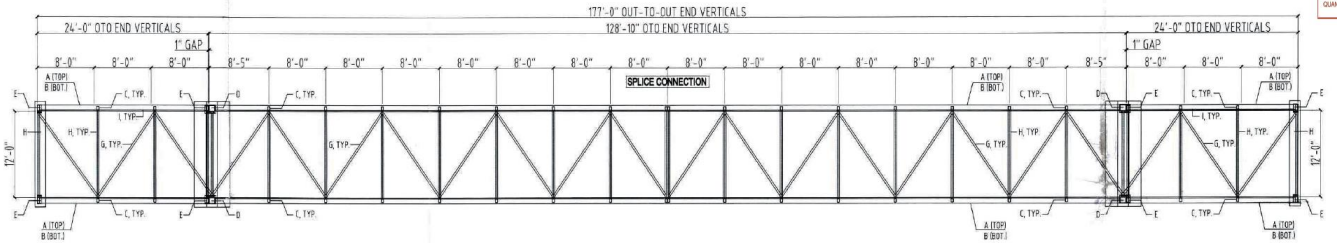

2/S1 HORIZONTAL TRUSS PLAN
NO SCALE

HASKELL SUBMITTAL REVIEW

Project Name:	UCF Parking Deck VI
Project Number:	41509
Submittal ID:	02850-01
Received On:	11/30/2010
Reviewed On:	12/3/2010
Reviewed By:	Kevin Lariviere
Action:	Approved as Noted

APPROVAL IS FOR GENERAL ARRANGEMENT ONLY AND DOES NOT RELIEVE SUPPLIER OR SUBCONTRACTOR FROM HIS RESPONSIBILITY FOR QUANTITIES, DIMENSIONS AND COMPLIANCE WITH THE DRAWINGS AND SPECIFICATIONS.

STRUCTURAL ONLY
CHANDER P. NANGIA LICENSE No. 21938 STATE OF FLORIDA PROFESSIONAL ENGINEER
NOV 17 2010

CHANDER P. NANGIA, PE
7423 HOLLOW RIDGE DR.
HOUSTON, TX 77095
FLORIDA PE # 21938

GENERAL NOTES

GOVERNING DESIGN CODES / REFERENCES:
Structural steel shall be designed in accordance with the "Manual of Steel Construction" s published by the American Institute of Steel Construction. Welded HSS Connections shall be designed in accordance with the American National Standards Institute / American Welding Society (ANSI/AWS) D1.1, and/or AISC "Specification for the Design of Steel Hollow Structural Sections."

DESIGN LOADS:
100 psf Uniform Live Load - 10,000 Lb. Vehicle Load - 30 psf Wind Load

FABRICATION:
Welding shall conform to the appropriate provisions of the ASNI / AWS D1.1 Structural Welding Code and/or ANSI / AWS D1.5 Bridge Welding Code. Welding electrodes to be a minimum E80 UNO. Unless shown otherwise, welds shall be a minimum recommended by AWS. EXCEL Bridge Mfg. Company is certified for Complex Steel Bridge construction with AISC and for High Strength Fabrication under the City of Los Angeles License #1582. Inpection and testing shall be by EXCEL's Quality Control Progarm.

MATERIALS:
Structural steel shall be ASTM A500 cold-formed welded square and rectangular hollow structural sections, and/or ASTM A572 plate and structural steel shapes. Splice bolts shall be ASTM A325 Anchor rods to be ASTM 1554 Grade 36 min.
Steel cable safety rails.
Concrete shall be structural concrete with a minimum compressive strength of concrete (fc) of 4,000 psi. Concrete to be regular concrete with maximum weight of 145 pcf.
Admixtures containing chloride salts shall not be used. Concrete deck surface shall receive a transverse broom finish. Steel Reinforcing shall be plain or deformed bars with a minimum yield strength (Fy) of 60,000 psi conforming to ASTM A615, Grade 60. Steel form deck shall be fabricated from galvanized steel sheet conforming to ASTM A1008 having a min. yeild strength of 33 ksi galvanized per ASTM 653. It shall be the responsibility of the contractor to produce documentation certifying the concrete materials, reinforcing steel, and construction methods used are in accordance with the above stated specifications and the construction drawings.

FINISHING:
Structural steel shall blast cleaned per SSPC-SP6, primed with Tnemic series 69 epoxy and top coated with Tnemic urethane enamel series 74, or approved equal. Color to be selected by owner.

SHIPPING:
EXCEL is responsible for delivery of the fabricated bridge to the jobsite only. Unloading, erection, and jobsite safety are the responsibilty of others. Trucks must be unloaded as close as possible to paved streets or roads. Purchaser is responsible for coordination and supplying unloading cranes, support dunnage, or other necessary items. Standard unloading time is 2 hrs. per truck. Purchaser will be responsible for all standby time and time over two hours, required by unloading.

MATERIALS LIST

KEY	DESCRIPTION	LOCATION
A	HSS 10 x 10 x 3/8	TOP CHORD
B	HSS 10 x 10 x 3/8	BOTTOM CHORD
C	HSS 6 x 4 x 3/8	VERTICAL / SPLICE VERTICAL
D	HSS 10 x 10 x 3/8	END VERTICAL - SPAN 2
E	HSS 10 x 4 x 3/8	END VERTICAL - SPAN 1 - 3
F	HSS 4 x 4 x 1/4	DIAGONAL
G	HSS 3 x 3 x 1/4	BRACE DIAGONAL
H	W 12 x 22	FLOOR BEAM / SPLICE FB
I	L 5 x 3 x 5/16	SIDE DAM
J	FL 1/4 x 6	TOE PLATE
K	PL 3/4" x 12" x 14"	BEARING PLATE
L	SHT 1/8" x 12" x 14"	UHMW POLY PAD
M	PL 1/2" x 12" x 14"	SETTING PLATE
N	L 3/4" x 3/4" x 1/8"	CABLE RAIL GUIDE ANGLE
O	FL 3/4 x 8 x 33"	CHORD SPLICE PLATE

PLAN SHEET INDEX

PROVIDE SAMPLE:
CABLE AND TERMINATION / TENSIONING DEVICE.

RECEIVED
THE HASKELL COMPANY
NOV 22 2010
JACKSONVILLE, FLORIDA
HOME OFFICE

EXCEL
BRIDGE MANUFACTURING CO.
12001 SHOEMAKER AVE.
SANTA FE SPRINGS, CA. 90670
(562) 944-0701
FAX (562) 944-4025
OUTSIDE CA. (800) 548-0054

Parking Garage VI - H Pedestrian Bridge
University of Central Florida - Orlando, FL

BRIDGE ELEVATION AND PLAN
GENERAL NOTES - MATERIALS LIST
PLAN SHEET INDEX

Bridge Size: 177'-0" Long x 12'-0" Wide
Design: TLV
Date: March 2010
Job Number: TLV1005 EXCEL10B007
Drawing Number: S1 of S8

Rev.	Date	Revision Description	By
3	7-28-10	Revised per Engineer Comments	TLV
4	9-10-10	Revised per Engineer Comments	TLV
5	9-13-10	Revised per Engineer Comments	TLV
6	10-29-10	Revised per Engineer Comments	TLV
7	11-12-10	Combined Bridge and Foundation Drawings	TLV

REFERENCES

[1] Autodesk Help, “About Point Clouds and LiDAR Data,” *Autodesk Support & Learning*, 01-May-2018. [Online]. Available: https://knowledge.autodesk.com/support/autocad-map-3d/learn-explore/caas/CloudHelp/cloudhelp/2019/ENU/MAP3D-Use/files/GUID-7C7DD8A7-B561-45B0-A803-852E0A667F3C-htm.html. [Accessed: 07-Feb-2019].

[2] Autodesk Help, “About Working With Point Clouds,” *Autodesk Support & Learning*, 14-Feb-2019. [Online]. Available: https://knowledge.autodesk.com/support/autocad/learn-explore/caas/CloudHelp/cloudhelp/2019/ENU/AutoCAD-Core/files/GUID-C0C610D0-9784-4E87-A857-F17F1F7FEEBE-htm.html. [Accessed: 07-Mar-2019].

[3] E. O'Day, “3D Laser Scanning: Different Type of Scanners,” *Ideate Inc & Imaginit Technologies*, 11-Jul-2013. [Online]. Available: https://www.ideateinc.com/blog/2013/07/3d-laser-scanning-different-type-of. [Accessed: 07-Feb-2019].

[4] “Point Cloud | Reverse Engineering | 3D Scanning,” *Reverse Engineering 3D*. [Online]. Available: http://www.reverse-engineering-3d.co.uk/laser-scanning/point-cloud-data/?doing_wp_cron=1549737456.8960700035095214843750. [Accessed: 09-Feb-2019].

[5] “Leica ScanStation P40 / P30 - High-Definition 3D Laser Scanning Solution,” *Leica Geosystems*. [Online]. Available: https://leica-geosystems.com/en-US/products/laser-scanners/scanners/leica-scanstation-p40--p30. [Accessed: 18-Nov-2018].

[6] 3DSCAN, “How does it work a 3D Laser Scanner?,” *3DScanit*, 14-Apr-2015. [Online]. Available: http://www.3dscan.it/en/blog/how-does-it-work-a-3d-laser-scanner/. [Accessed: 18-Nov-2018].

[7] “How does Laser Scanning work?,” *SurvTech Solutions*. [Online]. Available: http://floridalaserscanning.com/3d-laser-scanning/how-does-laser-scanning-work/. [Accessed: 07-Mar-2019].

[8] Absolute Geometries, “Laser Line Scanning Process,” *Laser Line Scanning | Laser Scanning*, 2009. [Online]. Available: http://www.absolutegeometries.com/laser_line_scanning_process.html. [Accessed: 18-Nov-2018].

[9] D. Gatziolis and H.-E. Andersen, *A guide to LIDAR data acquisition and processing for the forests of the Pacific Northwest*. United States Department of Agriculture, Forest Service, Pacific Northwest Research Station, 2008.

[10] S. Rubenzer, “Understanding Dynamic Analysis,” in *SEAWI presentation*, 27-Apr-2012. [Online]. Available: http://seawi.org/images/downloads/Annual_Conferences/understanding_dynamic_analysis_v8.pdf. [Accessed: 09-Feb-2019].

[11] S. Rajasekaran, *Structural dynamics of earthquake engineering: theory and application using Mathematica and MATLAB*. Boca Raton: CRC, 2009.

[12] A. K. Chopra, *Dynamics of structures theory and applications to earthquake engineering*, 4th ed. Hoboken, NJ: Pearson, 2017.

[13] B. Jafari, A. Khaloo, and D. Lattanzi, “Deformation Tracking in 3D Point Clouds Via Statistical Sampling of Direct Cloud-to-Cloud Distances,” *Journal of Nondestructive Evaluation*, vol. 36, no. 4, 2017.

[14] Q. Li and X. Cheng, “Comparison of Different Feature Sets for TLS Point Cloud Classification,” *PubMed Central*, 30-Nov-2018. [Online]. Available: https://www.ncbi.nlm.nih.gov/pmc/articles/PMC6308685/. [Accessed: 09-Mar-2019].

[15] Jãuregui David Villegas, Y. Tian, and R. Jiang, *Photogrammetry applications in routine bridge inspection and historic bridge documentation*. Albuquerque, NM: NMDOT Research Bureau, 2006.

[16] J. J. Sharp, “Methodologies for problem solving: An engineering approach,” *The Vocational Aspect of Education*, vol. 43, no. 1, pp. 147–157, 1991.

[17] B. Yang and I. Jahan, “Comprehensive Assessment for Post-Disaster Recovery Process in a Tourist Town,” *Sustainability*, vol. 10, no. 6, p. 1842, 2018.

[18] R. Fabio, “FROM POINT CLOUD TO SURFACE: THE MODELING AND VISUALIZATION PROBLEM,” *International Archives of the Photogrammetry, Remote Sensing and Spatial Information Sciences*, vol. XXXIV-5/W10.

[19] R. Mencl and H. Muller, “Interpolation and Approximation of Surfaces from Three–Dimensional Scattered Data Points,” tech.

[20] R. Mencl, “Reconstruction of surfaces from unorganized three-dimensional point clouds,” dissertation.

[21] H. Hoppe, T. DeRose, T. Duchamp, J. McDonald, and W. Stuetzle, “Surface Reconstruction from Unorganized Points,” tech.

[22] B. Curless and M. Levoy, “A Volumetric Method for Building Complex Models from Range Images,” tech.

[23] R. A. K. Cox, “Real-world comparisons between target-based and targetless point-cloud registration in FARO Scene, Trimble RealWorks and Autodesk Recap,” dissertation, 2015.

[24] “The PCL Registration API,” *Point Cloud Library (PCL)*. [Online]. Available: http://pointclouds.org/documentation/tutorials/registration_api.php. [Accessed: 07-Mar-2019].

[25] S. Baptista and J. Solomon, “Using Point Cloud Data to Generate a Structural Engineering Model,” rep.

[26] F. N. Catbas, R. J. Allemang, and D. L. Brown, “A Correlation Function for Spatial Locations of Scaled ...,” *ResearchGate*, 12-Dec-2012. [Online]. Available: https://www.researchgate.net/publication/253618034_A_Correlation_Function_for_Spatial_Locations_of_Scaled_Mode_Shapes_COMEF. [Accessed: 09-Mar-2019].

[27] Siemens Phenom, “Modal Assurance Criterion (MAC),” *Siemens PLM Community*, 29-Dec-2018. [Online]. Available: https://community.plm.automation.siemens.com/t5/Testing-Knowledge-Base/Modal-Assurance-Criterion-MAC/ta-p/368008. [Accessed: 07-Mar-2019].

[28] M. Pastor, M. Binda, and T. Harcarik, “Modal Assurance Criterion,” *ResearchGate*, 12-Dec-2012. [Online]. Available: https://www.researchgate.net/publication/257725890_Modal_Assurance_Criterion. [Accessed: 07-Mar-2019].

[29] C.-Z. Dong and W. Celis, “Dynamic Monitoring and Modeling of a Truss Bridge,” rep.